5-2020

Processing and Microstructural Characterization of Silicon Carbide, Silicon Nitride, and Tungsten Carbide Fibers

Christian Garcia
The University of Texas Rio Grande Valley

PROCESSING AND MICROSTRUCTURAL CHARACTERIZATION OF SILICON CARBIDE, SILICON NITRIDE, AND TUNGSTEN CARBIDE FIBERS

A Thesis

by

CHRISTIAN GARCIA

Submitted to the Graduate College of
The University of Texas Rio Grande Valley
In partial fulfillment of the requirements for the degree of

MASTER OF SCIENCE IN ENGINEERING

May 2020

Major Subject: Mechanical Engineering

PROCESSING AND MICROSTRUCTURAL CHARACTERIZATION OF SILICON CARBIDE, SILICON NITRIDE, AND TUNGSTEN CARBIDE FIBERS

A Thesis
by
CHRISTIAN GARCIA

COMMITTEE MEMBERS

Dr. Rogelio Benitez
Chair of Committee

Dr. Karen Lozano
Committee Member

Dr. Mataz Alcoutlabi
Committee Member

May 2020

ABSTRACT

Garcia, Christian, Processing and Microstructural Characterization of Silicon Carbide, Silicon Nitride, & Tungsten Carbide Fibers. Master of Science in Engineering (MSE), May 2020, 117 pp, 8 tables, 73 figures, references, 65 titles.

This research focuses on developing polymer-derived ceramic fibers. The spun micro/nanofibers were sintered into silicon carbide/silicon nitride and tungsten carbide respectively. The relationship between processing, fiber microstructure, morphology, and purity is investigated by scanning electron microscopy, Fourier transform infrared spectroscopy, energy-dispersive X-ray spectroscopy, and thermogravimetric analysis. Dynamic Mechanical Analysis was used to test the reinforcement capabilities of tungsten carbide fibers. EDS identified a near-perfect 1:1 Si-C ratio in silicon carbide fibers sintered between 1200 °C -1400 °C, Silicon carbide was confirmed by FTIR between 1000 °C – 1400 °C. Silicon Nitride peaks were noted in FTIR between 1200 °C – 1400 °C. Tungsten carbide nanofibers were confirmed by SEM, EDS, and FTIR for sintering temperatures 800 °C – 1000 °C. DMA results show an increase in mechanical properties as fiber wt % increases in the polymer-ceramic composites made.

DEDICATION

The completion of my master's studies would not have been possible without the love and support of my family. My mother, Maria Elsa Garcia, my father, Ruben Garcia Garza, my brother, Ruben Garcia Jr., and my sister, Eleni Garcia, who lovingly supported and motivated me to accomplish this degree. Thank you for your love and support.

ACKNOWLEDGMENTS

I would like to firstly thank my advisor, Dr. Benitez. Thank you for giving me the opportunity to work with you. It has turned out to be a journey full of both challenges and happiness. You have been a constant source of ideas, comments, and guidance. By working with you, I have learned how to analyze and solve complicated scientific and engineering problems. Thanks for your patience, kindness, and humor which have made me positive towards life. Thank you to my thesis committee members: Dr. Karen Lozano and Dr. Mataz Alcoutlabi, their input, comments, and guidance have on my thesis have helped increase the quality of my intellectual work.

I would also like to thank my fellow PREM colleagues, especially Dr. Padilla whose dedication to the lab and assisting the research students is unwavering. Also, I want to acknowledge Hector Arteaga for mentoring and assisting me during all machining processes.

Special thanks to my dear friend Vicente Cortes who has kept me motivated throughout my coursework and research. A friend like you comes once in a lifetime, I hope our journey together does not end here.

TABLE OF CONTENTS

Page

LIST OF TABLES

Page

LIST OF FIGURES

Page

CHAPTER I

INTRODUCTION

With technology evolving rapidly the requirement of the materials needed to realize these advancements poses a challenge. Particularly in the aerospace & energy industry the need for cheaper, lightweight, and multi-purpose materials is great. Advanced ceramics have been heavily investigated and implemented as solutions to these needs in multiple forms.

Ceramic nanofibers exhibit many excellent properties such as great corrosion resistance, high thermal stability, superior oxidation resistance, and high mechanical strength. They play a significant role in a variety of advanced applications such as catalysts, fuel cells, & aerospace parts [42, 58]. Ceramic nanofibers have been synthesized through the method of polymer derived ceramics. This method has been used to form silicon nitride, silicon carbide, & tungsten carbide fibers.

Silicon nitride, silicon carbide, and tungsten carbide have been heavily investigated for their use in a wide variety of advanced applications, but they are mainly used in composites while in their fiber form. These ceramics in nanofiber form are excellent candidates for aerospace applications due to their flexibility, mechanical properties, & potential unique electrical and shielding properties [18, 42, 58]. The properties and potential uses of these ceramics depend greatly on their processing. Thus the challenge of achieving high yield without

compromising for quality is presented. This challenge can be solved by using the Forcespinning© method as opposed to other methods such as electrospinning. Forcespinning© uses centrifugal forces to form polymer nanofibers at a rate of 1g/min [51].

The use of preceramic-polymers in Forcespinning© allows the method of polymer-derived ceramics to be implemented, allowing for high-yield and highly controlled ceramic nanofibers. The ceramic nanofibers synthesized mostly depend on the preceramic polymer and heat-treatment process which are easily adjusted to the desired ceramic material.

In this study, polyphenylmethylsiloxane, and ammonium metatungstate hydrate were used to form silica and tungsten-based ceramic fibers respectively. The process of developing the ceramic fibers was investigated and divided into several key steps: preceramic polymer solution, spinning, drying/crosslinking, and heat treatment.

CHAPTER II

LITERATURE REVIEW

2.1 Background on Ceramics

2.1.1 What are Ceramics?

Ceramics can be defined as solid compounds that are formed by applying heat, and occasionally heat and pressure, pertaining to two elements minimum provided that one of them is a non-metal or a nonmetallic elemental solid. Simply put what is neither a metal, semiconductor nor a polymer, is a ceramic. Ceramics have been used since 8,000 BC. In the form of pottery, sculpture, tiles, etc [4]. Humans taking clay mud and applying heat through a fire can be traced to the dawn of civilization. However these fired-clay articles were initially porous and could not be used to carry liquids, later it was found that by adjusting the heating and cooling rate some sands tended to form transparent, waterproof solids, known today as glass. Today ceramic engineering drives many more advanced technologies but ceramics can be generally classified as being hard, wear-resistant, brittle, and prone to thermal shock, refractory, electrically and thermally insulative, chemically stable, and oxidation-resistant.

2.1.2 Bonding & Crystal Structure in Ceramics

The arrangement of atoms in ceramics will exhibit long-range order, short-range order, or a combination of both. Solids that are long-range orders are known as crystalline solids while those that are non-periodic are amorphous, glassy, or noncrystalline solids.

Most ceramics with the exception of glasses and glass-ceramics are crystalline (long-range order). This long-range order requires atoms to be arrayed in a three-dimensional pattern, described by a unit cell that can be related to a crystal system/crystal structure. This unit cell or crystal structure can be pictured as bricks that are used to build a solid, thus the composition of the solid will depend on the bricks used. The composition of the brick will depend on the locations of atoms inside the unit cell as well as the symmetry of said atoms. The location of these atoms depends on the elements, and thus the bonds within the unit cell. These bonds can be generalized to ionic and covalent bonds or tightly and loosely packed unit cells respectively. There are 7 major crystal systems and 14 Bravais lattices, an example can be seen in figure 1.

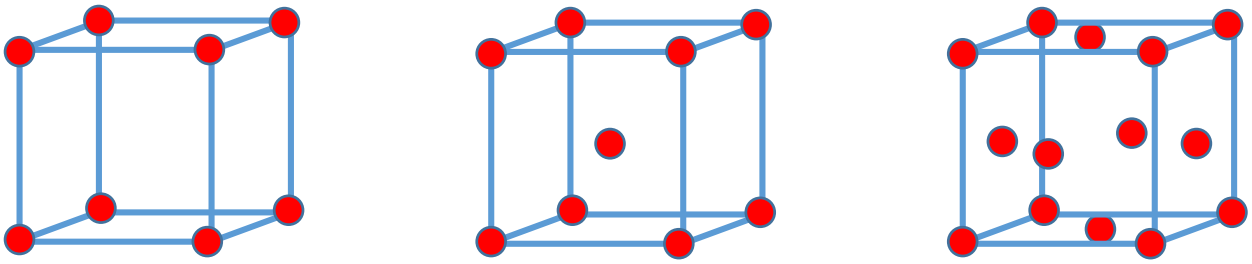

Figure 1: Cubic crystal lattices. (a) Simple (b) Body-Centered Cubic (c) Face-Centered Cubic

The chemical forces dictated by the crystal systems and lattices shown in figure 1 along with the elemental composition and heat treatment process will drive the ceramics' physical properties including melting points, thermal expansion, Young's Modulus, etc.

2.2 Advanced Ceramics

The term ’advanced ceramics’ was coined in the 1970s to designate a new category of engineering materials that were to drive new technologies into the 21st century[18]. Since then, there has been phenomenal growth in the technological advancement of these materials. A report from Grand View Research, a market intelligence platform, projected the advanced ceramics market to reach US$133.9 billion by 2025, growing at a compounded annual growth rate (CAGR) of 9.1%. [1] This growth is attributed to the increasing use of advanced ceramic materials as alternatives to metals and polymers, with key drivers being the medical, electronics, and transport industries. Advanced ceramic materials possess unique ferroelectric, dielectric, piezoelectric, pyroelectric, ferromagnetic, magnetoresistive, ionical, eletronical, superconducting, and electro-optical properties, allowing them to have a wide range of applications such as wheel balancing transducers, ultrasonic parking sensors, and fuel level sensors[58]. Biocompatible structural ceramics have been developed for orthopedic and dental implants, displaying improved chemical, wear, and mechanical properties.[25]

With evolving technologies, increased demand for advanced ceramic materials that are stronger, tougher, and more reliable has driven the interest in pursuing nanoscale technologies in the forms of composites, fibers, and advanced porous ceramics (also known as foams). Ceramic composites have seen use in high-performance brake systems[12], light-weight spacecraft structures operating at temperatures up to 1600 °C [18], furnaces, heat exchangers, and engine parts.

2.2.1-Polymer Derived Ceramics

There are key challenges that emerge when producing covalent ceramics such was WC, SiC, and Si_3N_4. Covalent bonding makes the diffusion coefficients of these materials poor, in turn, their sintering temperatures are typically high (1700-2100 °C) [36]. Because these additives are usually added and subpar sintering methods must be used – this lowers their high-temperature properties. Secondly, the high hardness and brittleness make the ceramics difficult to shape and machine. Polymer derived ceramics (PDCs) represent a novel fabrication technique in which the properties of advanced ceramics can be optimized and formed into complex shapes.

PDCs are formed from materials known as preceramic polymers which represent the inorganic/organometallic systems that provide PDCs with tailored composition and nanostructure with the proper thermal treatment (crosslinking & pyrolysis). These polymers form oxides, carbides, nitrides, & silicides upon pyrolysis.

Once the preceramic polymer is selected the transformation from polymer to ceramic can be simplified to three key steps as follows:

1. Synthesis of polymers for low molecular weight precursors which consist of structural elements as desired in the final product.

2. Thermal, chemical, or UV cross-linking of the as-synthesized precursors to obtain high molecular compounds convertible into high yield ceramics.

3. Pyrolysis of now cross-linked polymer transforming polymer into desired ceramic material as well as the formation of gaseous reaction products.

The first step is usually done by commercial companies that provide a large number of ceramic precursors. Thus this step may seem initially trivial however for high ceramic yield, desired final composition, and expected microstructure it is crucial to investigate and select the proper commercially available precursor.

2.3 Ceramic Fibers

Fibers are typically used to form a ceramic composite, however, fibers vary greatly in properties depending on their composition and morphology. Ceramic fibers have a very large aspect ratio and a very small cross-sectional area. Similar to bulk ceramics, ceramic fibers also exhibit high modulus and high-melting temperatures. Commercially available ceramic fibers, for example, typically have fiber diameters typically in the μm scale [16]. However, due to their geometry, the properties of the fibers can differ significantly from those of bulk forms of the same material. In particular, fibers have much higher strength, higher strain to failure but also greater chemical vulnerability[16, 37]. Fibers can be manufactured as fiber fabrics, flows, and short or long fibers. Fine fibers are generally bundled into so-called ‘rowings’, which consist of 500–10,000 single filaments. Bundling keeps the fibers flexible, makes them considerably easier to process and handle, and makes it possible for them to be manufactured into various fibrous forms.[19]

Ceramic fibers have been researched extensively in the past decade. One of the important applications has been the use of ceramic fibers (10–125 μm in diameter) as reinforcement of ceramic matrices to make ceramic matrix composites for high-temperature applications[37]. Improvements in fracture resistance, strength,

and creep resistance have been shown due to the incorporation of ceramic fibers into ceramic matrix composites.

Continuous ceramic fibers are commercially available in two general classes: (1) non-oxide fibers, based primarily on β-phase silicon carbide (SiC); and (2) oxide fibers, based on the alumina-silica (Al_2O_3–SiO_2) system and on α-alumina (α-Al_2O_3).[26] Ceramic fibers show high-strength and high-modulus properties in both tension and compression applications.[55]

The properties of ceramic fibers mainly depend on their composition and processing. Typically production of fine ceramic fibers first requires an organic or mineral precursor fiber, which is then heat-treated and pyrolyzed for a very short time. Ceramic fibers can also be produced by chemical vapor deposition, melt drawing, spinning, and extrusion.

2.3.1 Introduction to Silicon Nitride Fibers

Silicon nitride (Si_3N_4) has excellent mechanical properties such as Elastic modulus (320 GPa), high hardness (8-30.5 GPa)[5, 47, 49], fracture toughness (5-10 $MPa\sqrt{m}$), bend strength (500-1300 MPa). Thanks to these properties Si_3N_4 has can be used for many applications. Medical Grade Si_3N_4 has been shown to be biocompatible, stable in vivo and visible on radiographic imaging[46]. Considering that Si_3N_4's flexural strength and fracture toughness are among the highest measured values for ceramic materials [9, 25] along with the previously stated properties, make Si_3N_4 an attractive ceramic implant material.[46] Si_3N_4 is also widely used at high temperatures ranging from 1073-1500 °C due to its high-temperature mechanical properties and low coefficient of thermal expansion ($3.1 \cdot 10^{-6} K$)[49]. These high temperature applications may include heat exchangers, turbines, and automotive engine components, etc. The hardness,

wear resistivity, and low density of Si_3N_4 make it an attractive material for tribological applications[49].

Si_3N_4 fibers have gained great interests for their use as a reinforcement material for high-temperature ceramic composites[61], to increase the wear and friction properties of metal matrix composites such as Aluminum Matrix Composites (AMCs)[38], for electromagnetic interference shielding[64], biomedical applications[14], and even oil & seawater filtration[2, 62]. It is important to understand that Si_3N_4 has three phases – α,β,γ each corresponding to a unique crystal structure (trigonal, hexagonal, and cubic respectively). The α and β phases are the most common and are formed under normal pressure conditions whereas the γ phase requires high pressure during the sintering process. These three phases along with the processing, impurities, shape, and size of the fibers are what determine the chemical and physical properties of Si_3N_4 fibers and thus their potential applications.

2.3.2 Introduction to Silicon Carbide Fibers

Silicon carbide (SiC) is a non-oxide ceramic material with excellent mechanical properties in fiber form. Commercially available fibers range from 2.6 -3 GPa in tensile strength [8]. silicon carbide fibers can be used as semiconductor material but the electrical properties are heavily reliant on the impurity and crystal structure of the formed fiber [27]. The thermal properties, such as thermal conductivity of the material also vary greatly over the range of 10-70 $.1 - .7\ W\ cm^{-1}\ °C$, again this is because SiC is extremely sensitive to influences of the manufacturing method [27]. SiC fibers have seen use in a broad range of applications including abrasives, heating elements, structural materials, brake liners, turbine parts, and much more spanning the electronic, energy, healthcare, automotive, aerospace, and military industries [31].

Silicon Carbide exists in two primary phases, β and α, which are typically formed below and above 1700 °C respectively. These phases along with the processing, impurities, shape, and size of the fiber will determine the properties of the fibers.

2.3.3 Introduction to Tungsten Carbide Fibers

Pure tungsten carbide (WC) fibers have explored less compared to SiC and Si_3N_4 but WC has been heavily investigated in thin films [44] for improved tribological properties and shown promise. WC fibers have been synthesized for use in fuel cells [65] via electrospinning which also shows potential. Before this paper, WC fibers were only used to increase the mechanical and tribological properties of surfaces or matrices. WC fibers can exist in two phases (WC and W_2C), which are determined by the processing method.

2.4 Ceramic Composites

2.4.1 Introduction to Composites

A material made by combining two or more materials is a composite material. Different combinations lead to unique properties that can be better than those of the constituents taken separately. Rocks are combined with cement to make concrete, this is as strong as the rocks it contains but can be shaped easier than carving rock. While in this case, the enhanced properties of concrete are ease of fabrication and strength other chemical, physical, and processing-related properties can be enhanced/achieved by using the correct combination of materials. In general, a composite material will consist of one or more discontinuous phases distributed in a continuous phase. Further simplified to a matrix and a reinforcement, the matrix can be either a polymer, ceramic, or metal material. Polymer matrices are the most researched & easily formed however

the use of a ceramic or metal matrix can provide excellent properties and are desirable for advanced applications. Reinforcement can usually be divided into 3 major categories: Continuous long fibers, discontinuous fibers, and particles & whiskers.

Most materials are much stronger in fiber form compared to bulk form so fiber reinforcement is preferred. This is due to the sharp reduction in the number of defects in fibers compared to those in bulk form. For the same reason, polymeric fibers are much stronger since the polymer chains are aligned rather than randomly entangled in their bulk form.

Composites are desired mainly for weight reduction, corrosion resistance, and part-count reduction. Other application-specific advantages include electromagnetic transparency, toughening for impact, erosion and wear resistance, acoustic and vibration damping, enhanced fatigue life, thermal/acoustical insulation, low thermal expansion, low or high thermal conductivity, self-healing, low or high permeability, fire resistance, and fire retardancy, ablation, magnetoelectric response, and more [28].

The subclass of ceramic composites can be split up into three categories: ceramic matrix, metal matrix, and polymer matrix each of these being reinforced with ceramic fibers.

2.4.2 Silicon Nitride Ceramic Composites

As mentioned in section 2.3.1 silicon nitride has been heavily investigated for its use in composites such as those found in [16] & [17]. Titanium matrix silicon nitride composites have also been successfully synthesized for use in mechanical power transmission along with turbine blades [52]. Silicon nitride may also be formed alongside silicon carbide to form ceramic matrix composites [33].

2.4.3 Silicon Carbide Ceramic Composites

Silicon carbide has been used in metal, polymer, and ceramic matrices to form composites. SiC/graphite composite brakes are used by Porsche and SiC-based ceramic matrix composites are used by General Electric in fan blades and shrouds. The LEAP engines of the Boeing 737 Max and Airbus A320/321 Neo commercial airplanes also utilize SiC ceramic matrix composites [31].

2.4.4 Tungsten Carbide Ceramic Composites

Tungsten carbide is used primarily used to increase the strength, hardness, wear resistance of matrices either metal, polymer, or ceramic. WC has shown improvement of these properties in metal matrices such as iron and copper [23, 63] where it has been used in drill bits. WC composites have also been investigated for their use as implants in combination with Zinc [20]. WC was found to increase the hardness in structural tungsten carbide-alumina composites but decrease the electrical resistivity when sintered past 1350 °C decomposing WC into the W_2C. WC nanoparticles have been used to reinforce the polymer matrix Polytetrafluoroethylene (PTFE)[60]. The composite materials exhibited better tribological properties when the WC nanoparticle wt% increased from 10% to 20%.

2.5 Introduction to pre-ceramic polymers

Preceramic polymers, notably in the form of organo-silicon compounds (e.g., polymers based on a backbone of Si atoms containing also C, O, N, B and H atoms), have been universally accepted for the last 40 years as a tool for the production of advanced ceramics such as Si_3N_4, SiC, BN, and AlN.[7] The key advantage over conventional powder synthesis procedures stems from the capability of plastic-forming techniques (e.g., extrusion, injection molding, warm pressing, fiber spinning, etc.) to develop shaped components, later transformed into ceramic parts by heat treatment (pyrolysis).[12] The pyrolysis process decomposes the organic compounds and volatile products such as CO, H_2, CO_2, CH_2, and H_2O of the preceramic precursor leaving behind only phases with a high decomposition temperature. The atmosphere is usually composed of Argon or Nitrogen depending on the desired ceramic. The value of the ceramic yield is determined by the weight loss (amount of the released volatiles. Polymer derived ceramics also require a lower conversion temperature and can achieve bulk quantities to be added into composite materials. Various ceramic fibers such as silicon nitride and silicon carbide have been synthesized from pre-ceramic polymers.[29]

2.5.1 Synthesis of silicon nitride & silicon carbide fibers from pre-ceramic polymers

W.M. Qiao et al demonstrated that a pre-ceramic polymer - polycarbomethylsilane (PCmS) could be used to synthesize fine diameter SiC fibers (diameter 20-80 nm)[45]. PCmS was dissolved in hexane along with platelet carbon nanofiber the mixture was then dried at 80°C for 5 h in air and heat-treated at a different temperature ranging from 700 to 1400 °C for 1 h with a heating rate of 10°C/min under an argon flow of 100 ml/min to prepare PCNF/SiC composite.

The composite was calcined in air at 650°C for 2 h to remove PCNF in the mixture and isolate SiC nanofiber

In Qiao's work, the total yield of SiC was about 40 wt% based on PS weight. Above 700°C, no more weight loss was observed, indicating the formation of amorphous SiC. The pyrolysis occurred at temperatures up to 1400°C showing an increase in crystallinity with increasing temperature. The characterization techniques used will be discussed in more detail in section 2.8.

In a recent paper published in the American Ceramic Society journal[43], network-like branched Si_3N_4 nanostructures were synthesized by the thermal decomposition of a preceramic precursor, pherhydropolysilazane. The precursor was solidified at 160 °C-300 °C for .5-2 h under high-purity nitrogen (99.99 vol%). The chunk produced was then crushed into fine powder in an agate mortar. Then, the powders were loaded in a high-purity alumina crucible for thermal pyrolysis, where a ZrO2 supporter with a height of 2–20 mm was set over the powder to separate the Si wafer and preceramic powder, and a 5–20 nm Fe film was, in advance, deposited on the Si wafer as a catalyst using a magnetron sputtering system. Afterwards it was placed in a conventional horizontal tube furnace under high-purity nitrogen gas stream rate of 60 ml/min to undergo pyrolysis. The synthesized products were characterized using a field-emission scanning electron microscope (SEM), X-ray diffraction, and transmission electron microscope (TEM). Both SEM and TEM applied in this work were equipped with energy-dispersive X-ray spectroscopy (EDX).

The SEM-EDX results showed a ratio of .7562 for Si to N, very similar to the stoichiometric composition for Silicon Nitride. The SEM results also reflected a considerable variation in branch diameter, ranging from tens of nanometers to hundreds of nanometers. The

heating rate, the thickness of the Fe film, and the pyrolysis temperature of polymers strongly affect the fiber diameter. The amount of pre-ceramic polymer powder did not affect the diameter of the linear part of the nanonetwork, it did increase the overall yield of material.

In short, the key to the growth of network-like branched Si_3N_4 nanostructures were found to be the combination of plenty of polymer powder, fast heating to the highest growth temperature, and a thicker Fe catalyst film. Network-like branched Si_3N_4 nanostructures were synthesized with high yield via catalyst-assisted pyrolysis of perhydropolysilazane. The diameters of each linear part of the nanostructures ranged from tens of nanometers to hundreds of nanometers. The nanomaterials have a structure of good crystallinity.

A previous study discusses using perhydropolysilazane as a polymer precursor to form Si_3N_4 [56]. The chemical composition of the fiber was 60 wt% Si, 37 wt% N, $\geq$ 1 wt% C, and $\leq$ 3 wt% O. The resulting 10 um diameter fiber exhibited a tensile strength between 1.7-2.2 (GPa), tensile modulus 180-200 (GPa), and density of 2.5 (Mg/m^3).

Wang, P et al. used polycarbosilane (PCS) and Polyvinylpyrrolidone (PVP) as a polymer precursor for electrospinning fibers that underwent pyrolysis to transform into SiC & Si_3N_4 fibers [59]. The PCS precursor (10 wt%) was added into a homogenous solution of N, N-dimethylformamide, and chloroform with a weight ratio of 1:4 containing 4.3 wt% PVP dissolved inside. The solution was stirred for 24 hours and then transferred into a 10 ml syringe. The solution was then spun using electrospinning and the fibers were collected. The PCS/PVP fibers were then maintained under vacuum at 70°C for 24 h to burn out the solvent. The PCS/PVP nanofibers were cured in a muffle furnace from room temperature to 180 °C at a heating rate of 2 °C/ min and then to 210 °C at a heating rate of 1 °C/min and holding for 2 h in air. Finally, cured nanofibers were put in a tubular furnace for annealing from room temperature

to 250 °C at a heating rate of 2 °C/min and then to 850 °C at a heating rate of 1 °C/min . Then, the temperature of the furnace ramped to 1300 °C at a rate of 2 °C/min and maintained for 2 h in Ar. Meanwhile, cured nanofibers were annealed in N2 at 1300, 1400, and 1500 °C for 2 h.

A variety of papers used considerably more complex methods to obtain Silicon Nitride fibers. In [2] the polymer solutions (with various solvents), prepared by milling process for 24 h, containing, the ceramic powder was added to the polymer solutions, followed by milling for another 48 h to prepare stable and homogeneous suspensions. The weight ratio of the ceramic powder to the polymer solutions for the preparation of the suspension was fixed at 54% and 46%, respectively. The degassed suspension was extruded using a stainless steel tube-in orifice spinneret and discharged into an external water coagulant bath for 48 h to complete phase inversion. The HFMs were prepared at air gaps of 1, 5, 10, and 15 cm, and internal coagulant rates of 5, 10, and 15 ml·min−1 in the tube-in-orifice spinneret. After pre-drying at room temperature, the silicon nitride green fibers were sintered in a graphite furnace under N2 atmosphere at 1700°C for 4 h. NMP, DMSO, DMA, and DMF were implemented for the preparation of ceramic suspensions. The homogeneous suspension was not easily prepared by using DMF. Viscosity values of 1.325, 0.9879, and 0.251 Pa s were recorded at a shear rate of 1000 s−1 for the suspensions with NMP, DMSO, and DMA, respectively. The most compacted outer surface structure was observed in the S3 membrane, followed by the S2, which had a denser surface structure than the S1 fiber. Meaning that better fibers were formed using DMSO and DMA in this case.

Another paper, [30], uses the melt-spinning method to obtain fibers from polycarbosilane. They found that Silazane content in the Si_3N_4 fiber is reduced by heat-treatment at a higher

temperature in a N_2 gas atmosphere and the oxygen content decreases with increasing temperature.

2.5.2 Synthesis of Tungsten Carbide from preceramic salt

Tungsten carbide is not typically synthesized from preceramic polymers and is mainly used as a surface coating or thin-film [44]. However, one paper describes using a preceramic salt to synthesize WC fibers via electrospinning [65]. The preceramic salt used was ammonium metatungstate (AMT) which was combined with polyvinyl pyrrolidone (PVP) in distilled water. The electrospinning process was carried out at 40 kV and fibers were collected using a graphitic paper. The collected AMT-PVP fibers were oxidized under an oxygen flow rate of 100 mL/min at 500 °C for 3 hours and then heated at 780 °C in a 1:9 CH4/H2 mixture with a combined flow rate of 100 mL/min for 3 hours. Some WC fibers were set aside and labeled as pristine while the other WC fibers underwent additional heat treatment at 600, 850, and 900 °C under a 100 mL/min flow of NH_3. The pristine and post-treated samples were characterized by SEM, TEM, XRD, and Raman spectroscopy. Additionally, the chemical state of W elements in the WC nanofibers was measured by XPS.

2.6 Forcespinning Method for Polymer Derived Ceramics

2.6.1 Forcespinning vs Electrospinning

Electrospinning has been heavily researched for the creation of nanofibers including preceramic nanofibers. The processing effects of electrospinning are well understood and easily replicable. Electrospinning stretches a viscous polymer solution in an electric field due to the electrostatic repulsions between the surface charges along with the jet. This polymer solution is loaded into a syringe whose tip is electrified until a droplet at the tip experiences enough

electrostatic repulsion between the surface charges to overcome the surface tension of the solution and form an electrified jet of the polymer. As the polymer jet stretches the solvents evaporate leaving behind a solid fiber. Even though the process of electrospinning is well understood and easily repeatable in the creation of polymer and preceramic nanofibers, its low yield efficiency (.1g/hour) makes it unrealistic for industrial applications. Thus the challenge of finding a high-yield and highly accurate production method of preceramic polymer fibers is posed.

Recently, Forcespinning® was developed to make nanofibers from a wide range of materials[51]. This method uses centrifugal force and can use either solutions or solid materials that are the solution or melt-spun into nanofibers. The angular velocity that the spinneret experiences cause a centrifugal force, this centrifugal force drives out the liquid through an orifice where the solution becomes aligned and the solvent evaporates due to the shear force acting on it – this same shear force stretches the fiber into the nanoscale. Studies have been conducted by Padron et al and Taghavi et al to better understand the force applied and its ultimate effect on the diameter of the fibers [24].

Similar to electrospinning the Forcespinning© process requires a liquid solution with a minimal viscosity needed to form continuous fibers. The surface tension of the solution must also be overcome by the centrifugal force caused by the angular velocity of the spinneret. Once the solution exits the orifice of the spinneret the polymer solution must be continuous enough (minimal molecular weight) to stretch into fiber form. If the angular velocity of the spinneret is too high then the shear forces acting on the exiting solution may cause splatter, melt fracture, or formation beads. Important parameters in Forcespinning© thus include solution viscosity, solution surface tension, humidity during spinning, the angular speed of spinneret, size of orifice

(or needle) used, collector distance, spinning temperature, spinning time, amount of solution loaded into the spinneret per run.

The Forcespinning® method has successfully made nanofibers of polyethylene oxide, polylactic acid, bismuth, polypropylene, acrylonitrile-butadiene-styrene, polyvinylpyrrolidone, and polystyrene among others[51].

2.6.2 Active Material & Carrying Material

Typically preceramic polymers have low molecular weight [12, 22, 36] which poses an issue in the Forcespinning©(FS) process as a minimal solution molecular weight is needed to form continuous fibers. Preceramic polymers are referred to as the active material in an FS solution this is because they will provide the final fiber product with their unique properties. However, as mentioned these active materials do not have high enough molecular weight on their own to form continuous fibers. For that reason the addition of other polymers into the FS solution is necessary.

Materials used to increase the viscosity and overall molecular weight in an FS solution are referred to as carrying materials. These materials are high molecular weight polymers such as PVP and polystyrene (PS). These carrying materials are combined in a solvent with the active material to form a solution capable of undergoing the FS process.

2.6.3 Forcespinning & Treatment of a Preceramic Polymer

SiC nanofibers have been made through Forcespinning© using the polymer precursor, polycarbomethylsilane (PCmS)[48]. Polystyrene (PS)/PCmS/Toluene (15,20,25 wt% of PS with a 2:1 ratio of PS: PCmS) solutions were prepared and stirred with a magnetic stirrer for 4 hours.

The solution was then spun using the Force® method between 5000 RPM to 9000 RPM and the fibers were collected on a circular collector having 16 equally spaced polytetrafluoroethylene bars. The collected fibers were placed under UV light for 24 hours. The fibers were heat-treated at temperatures ranging from 1100-1500°C under either Nitrogen or Argon atmospheres. Fiber characterization consisted of using SEM, TGA, and XRD. The characterization results showed β-SiC nanofibers with an average diameter of 677 nm and oxygen content <5 wt%.

Here the PCmS was the active material while PS was used as the carrying material. Together these materials formed a homogenous solution and underwent the FS process to form preceramic fibers. The heat treatment process decomposed most of the carrying material and left only the high-temperature resistant phases of the active material. Characterization was used to understand how the heat treatment process affected the phases, composition, and morphology of the fibers. This same approach can be utilized to form any other ceramic fiber through FS.

2.7 Spun PVP Nanofibers

2.7.1 PVP

PVP is a good carrier for preceramic precursors and has been widely used to produce ceramic fibers. An increase in PVP content is known to be correlated to larger fiber diameters, however, a minimum PVP content is needed for the formation of continuous fibers[39, 50]. Depending on the solvents involved, PVP fibers can be smaller, more uniform, and have specific fiber forms (hollow, spiked, porous, nano bead impurities, etc). PVP is a highly amorphous polymer and can be easily dissolved in most solvents. Solvent selection depends on whether additional polymers are going to be added to the solution and the processing method of the PVP. Ideally, the solvent will be selected using the Hansen Solubility theory and Hildebrand solubility parameters [17]. The solubility of a given polymer in various solvents is generally determined

by its chemical structure. Polymers will dissolve in solvents whose solubility parameters are not too different from their own. The boiling point of the solvents must be taken into consideration as well since this will play a major role in the sintering of PVP fibers that carry ceramic precursors. If the solvents evaporate too fast or at too varied rates the fibers can rupture or be damaged during heating. On the other hand, the solvent ratios and heat treatment can be adjusted to develop specific fiber forms – this is widely used to create hollow ceramic fibers.

PVP nanofibers have successfully synthesized via Forcespinning© using various solvents such as ethanol and water [15]. The papers agree that the morphology and diameter of fibers are affected by several parameters, such as solution concentration, viscosity, surface tension, and rotational speed. The greater the concentration of the solution, the viscosity will be greater thus resulting in the greater average diameter of fibers, and vice versa. The value of viscosity also indicates the binding strength of between polymer chains, which is very important to determine whether fibers will be formed. The large surface tension leads to the formation of beads on the fibers. A solution with low viscosity indicates that the bonds in the polymer chain are not strong enough to be attracted and to form fibers. In a paper published by the University of Texas Rio Grande Valley, the average diameter of the fibers was 1.99 um after carbonization [15].

2.7.2 Dimethylformamide (DMF) Solvent

DMF has proven to be a reliable solvent for PVP, as shown in this study [17]. It was found that DMF/PVP nanofibers displayed the most uniformity and smoothest surface compared to other solvents(list the “other” solvents) used with the same amount of PVP. The solvents tested were all tested using the electrospinning method but the results are expected to apply to Forcespinning® as well. The ratio of solvent to a polymer can be determined by estimating the

desired viscosity and calculating the necessary ratio to achieve that viscosity. A minimal PVP concentration was found in this paper [39] to be higher for DMF than for Ethanol, however, DMF solutions yielded smaller fibers after the electrospinning process. For Forcespinning© the main driving forces for uniform fibers are solution homogeneity, solution viscosity, needle size, the rpm spun at, humidity, and the distance between the needles and collector[41].

2.7.3 Chloroform

Chloroform alone is not an ideal solvent for PVP as it is known to cause the formation of beads when used to form nanofibers. However, chloroform has proven to significantly decrease the fiber size of PVP nanofibers[24, 39, 40].

2.7.4 Ethanol

Ethanol provides a safer option when selecting a solvent for PVP but is found to take lower concentrations of PVP per unit of volume when compared to solvents such as DMF and Chloroform [50, 51]. However, it has been used in the synthesis of carbonized fibers via the Forcespinning© process due to its more stable boiling characteristics [15]. The major setback of ethanol, however, is that it is incapable of dissolving many preceramic polymers such as polycarbosilane and polycarbomethysilane.

2.8 Characterization of Nanofibers

Different characterization techniques used on nanofibers help determine if the desired properties were achieved. This section will briefly discuss how the literature has utilized these techniques to characterize nanofibers. More explanation on how these techniques work will be given in chapter 3.

2.8.1 Scanning Electron Microscopy (SEM)

SEM characterization is used to determine the morphology of the fiber, characteristics such as alignment, surface roughness, surface smoothness, porosity, impurities, defects, etc can be identified using the SEM. SEM images can also provide the fiber diameter of a sample when combined with a measurement tool such as imageJ, the measurement program will allow the user to measure the fibers to a statistical significance.

The effect of PVP concentration on the diameter of nanofibers was investigated using SEM analysis in [50], the images also showed the formation of beads. Similarly, the effect of concentration in fiber diameter was seen in [13] the effect of carbonization of PVP on surface morphology was also investigated. SEM images have been used for silicon nitride, silicon carbide, and tungsten carbide for similar purposes here [48, 59, 65].

2.8.2 Energy Dispersive X-Ray Spectroscopy (EDX)

EDX characterization is used to determine the elemental composition of the fiber and potential impurities. EDX can help identify differences between the surface of the fiber and the interior of the fiber. The elemental composition of the fiber is determined by the materials used and the post-spin processing of the fibers, the adjustment to these parameters can be seen using EDX.

EDX showed the effect of plasma exposure on TiO2 nanofibers on the element composition [35], here a clear correlation between plasma exposure and oxygen/carbon content is seen via EDX. EDX can also help to confirm the presence of phases such as silicon nitride by showing an atomic ratio close to the stoichiometric composition [43]. EDX/EDS was also used

to confirm the presence of silicon carbide in nanofibers while also identifying the oxygen content. [48]

2.8.3 X-Ray Diffraction (XRD)

XRD plays an important role in ceramic fibers as it is used to identify the crystal phases of materials by measuring changes in radiation intensity. It is important to note that XRD will only detect three-dimensional arrangements of atoms.

XRD is heavily used in literature and has been used in conjunction with PVP based nanofibers to identify the transformation of the active material into phases such as iron oxide, disordered carbon, zinc oxide, tungsten carbide [11, 13, 32, 65]. As well as identifying the presence of silicon carbide and silicon nitride in other carrying polymer nanofibers [48, 59]

2.8.4 Fourier Transform Infrared Spectroscopy (FTIR)

FTIR measures the vibrational energy of bonds either organic, polymeric, or inorganic. FTIR can identify the molecules within a system that can be used to identify to characterize the crosslinking process in nanofibers. FTIR can also be used to understand the preceramic fibers decomposition process as it transforms into a ceramic fiber. The confirmation of bonds through FTIR can be associated with a crystal phase and confirm the presence of ceramic phases.

The chemical structure of PVP nanofibers was traced using FTIR for stabilization, peroxidation, and carbonization showing the removal of side groups with increasing temperature as well as the addition of bonds due to oxidation [13]. FTIR was also used to identify the decomposition of PVP in these papers as well as the active material peaks [11, 32, 35]. FTIR confirmed the presence of silicon nitride, silicon carbide, and tungsten carbide in the following papers respectively [48, 59, 65].

2.8.5 Thermo Gravimetric Analysis (TGA)

TGA measures the weight change as a function of temperature and can be used to calculate the crosslink density of a material as well as its composition as a whole. TGA provides a clear visual of steps that correspond to the degradation of compounds associated which each temperature step.

TGA can be used to identify appropriate crosslinking and calcination temperatures by understanding when the active and carrying materials degrade. The appropriate calcination of Tin Oxide doped PVP fibers was identified using TGA in [34] by running the active material, carrying material, and the combined materials separately in TGA. This same process can be implemented for identifying crosslinking or sintering temperatures for new material combinations.

2.8.6 Dynamic Mechanical Analysis (DMA)

DMA is a complex characterization technique used to identify the mechanical and viscoelastic properties of composites or single materials. Often done through means of a dynamic force with relation to time, temperature, and frequency an overview of composites or single materials properties can be provided.

DMA was used to identify the effects of reinforcing the polymer matrix High-density polyethylene with carbon nanofibers as well as the effect of microwave exposure. By looking at the effects of frequency on the loss and storage modulus at specific temperatures Benitez was able to identify that 15 wt% nanofibers-reinforced composites increased in modulus after 3 minutes of microwave exposure whereas the 20 wt % nanofibers-reinforced composite exhibited a loss in storage modulus after three minutes of exposure time [6].

The effect of processing on the mechanical properties of polymer composites was determined by DMA in [3]. It was found that changing the processing temperature from 160 °C, 180 °C, and 200 °C greatly affected the mechanical properties of the material. Which initially showed an increase in value from 160 °C to 180 °C but then declined when processed at 200 °C. This is because the material "relaxes" at high temperatures which were confirmed by Differential Scanning Calorimetry.

CHAPTER III

EXPERIMENTAL TECHNIQUES

3.1 Forcespinning

Nanofibers are more easily produced through Forcespinning© at a rate of 1/gmin which is driven by a method of using centrifugal forces to transform a polymer solution into polymer nanofibers.

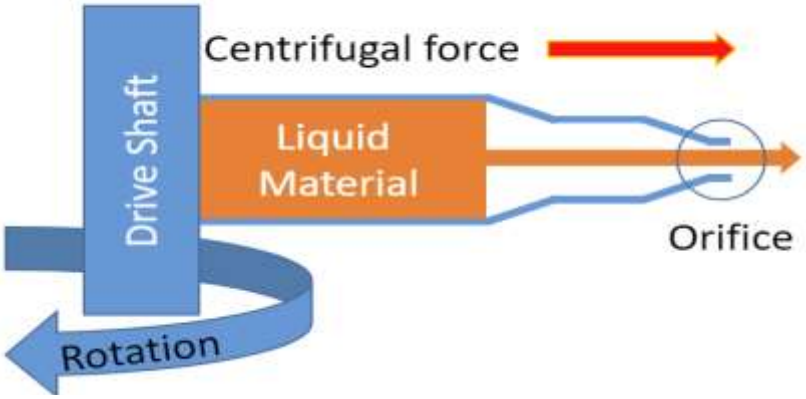

Figure 2: Forcespinning Spinneret

A liquid material, typically a polymer solution, is placed inside a spinneret which is attached to a drive shaft. As the drive shaft rotates the RPM of the spinneret increases causing a centrifugal force to push the liquid material out of the orifice of the spinneret. As mentioned

earlier the centrifugal force most overcome the viscosity of the liquid material as well as the surface tension.

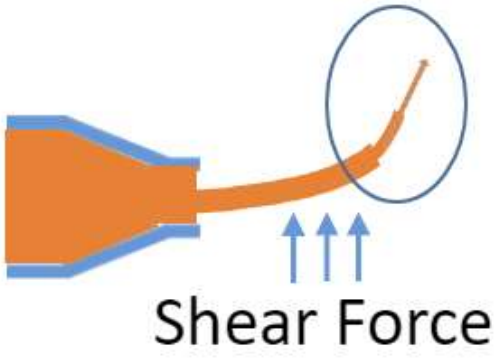

Figure 3: Forcespinning Orifice Zoom In

Once the liquid material exits the orifice of the spinneret it then experiences an initial shear force that helps to evaporate solvent as well as stretch the molecular chain to the nanoscale. The inertial force of the spinning fiber also helps to stretch the fiber itself into the nanoscale. Recall that if the angular velocity of the spinneret is too high then the shear forces acting on the exiting solution may cause splatter, melt fracture, or formation beads. Important parameters in Forcespinning© thus include solution viscosity, solution surface tension, humidity during spinning, the angular speed of spinneret, size of orifice (or needle) used, collector distance, spinning temperature, spinning time, amount of solution loaded into the spinneret per run.

As the solution exits the spinneret and transforms into nanofibers the nanofibers are collected on "collectors" that are placed in a circular formation equidistantly around the spinneret. Note that the fibers must be long enough to reach the collectors if they are to be collected, depending on the conditions the collectors may be moved closer or further to properly collect fibers – this is due to the fact that the liquid material needs to properly be dried and

stretched before being collected hence if the bars are too close short fibers or even no fibers may be collected.

The amount of solution, as well as its viscosity, will determine the spinning parameters utilized. For example, if 1.5ml of a highly viscous solution is placed inside the spinneret it will need to be spun at a higher rpm or longer time compared to 1 ml of a less viscous solution. The RPM can range from 1000-10000 RPM and time input from 10 seconds – typically within 10 minutes. Once the fibers are settled on the collectors they need to be manually collected on a fiber mat. Collection varies depending on the fiber, some fibers may require to be spun and collected in an inert gas atmosphere such as Nitrogen[48]. Other fibers may require the same alignment thus the fibers must all be collected in the same direction. It is all necessary to understand how the fibers form on the collectors as fibers deposited towards the end of the spinning time will have a larger diameter than the fibers that were initially deposited due to the decrease in the inertial force of the liquid material inside the spinneret as the amount of liquid material lessens due to it exiting the spinneret.

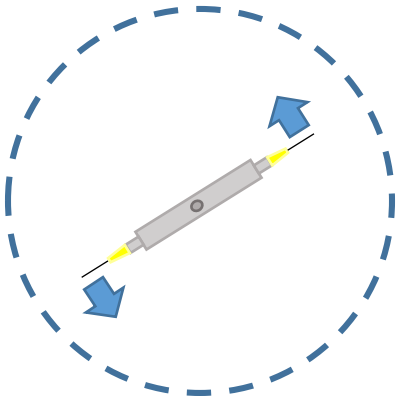

Figure 4*:* Spinneret with Collectors

Figure 4 shows the spinneret in the middle of collectors. As seen in the image the spinneret rotates and the liquid exits the spinneret through the orifice which is depicted as 30

gauge needles the liquid solution then transforms into a fiber and is deposited in the surrounding collectors.

3.2 Tube Furnace Heat Treatment

Tube furnaces are furnaces with controllable heating rates, heating times, as well as heating atmospheres. This work utilizes two different tube furnaces but each presents the same functionality. The tube furnaces were either ran under gas flow or in atmospheric conditions. Figure 5 depicts a simplified figure of how the tube furnace works.

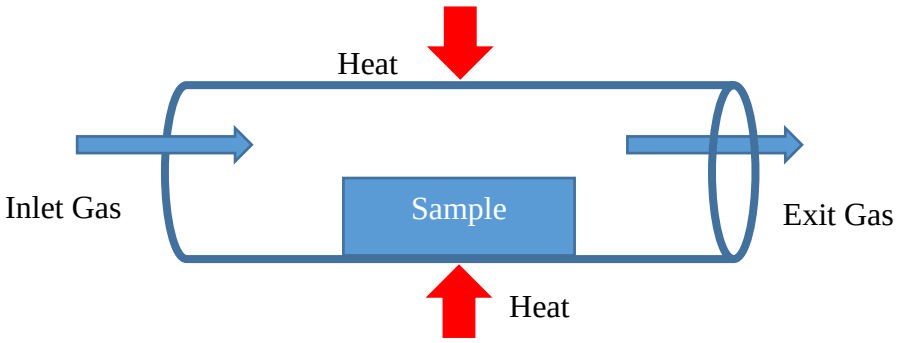

Figure 5: Tube Furnace with Flowing Gas

The tube furnace is used to heat treat samples at specified conditions, inert gases are used to prevent the oxidation of materials as well as stabilize materials during heat treatment. It is possible for the gas in the tube furnace to react with the sample and introduce new phases in the sample. Figure 5 shows a sample placed in the middle of the furnace such that it is heated uniformly to the programmed temperature. The inlet gases used in this research were nitrogen and argon, argon was used to stabilize and prevent oxidation whereas nitrogen was used for stabilization, prevention of oxidation, and chemical vapor deposition. The outlet gas is composed of the inlet gas as well as volatiles released by the sample during heat treatment.

Figure 6: Small Programmable Tube Furnace

Figure 6 depicts the small tube furnace used during the research. Here you can see a quartz tube surrounded by a heating element so that it is evenly heated. The sample is placed in the center of the tube furnace and an inert gas well enter from the left valve and exit out the right valve both circled in red.

Figure 7: Small Programmable Tube Furnace Control Panel

Figure 7 depicts the control panel of the small tube furnace which is used to set the heating program of the tube furnace. In order to program the furnace, the power must be on.

Heating programs are made by setting temperatures and times it will take to get to that set temperature. Initially, the furnace will ask for a starting temperature or C0 which would be room

temperature, so 23 °C. Then the furnace will ask for the first time input or t1 which indicates the time it will take to get to the second program temperature.

Table 1: Dwelling Heating Program

C0	23°C
T1	77 min
C1	100°C
T2	120 min
C2	100°C

Table 2: Ramping and cooling Heating Program

C0	23°C
T1	77 min
C1	100°C
T2	100 min
C2	300°C
T3	139 min
C3	23°C

Table 1 starts at 23°C and heats up to 100°C at 1°C/min then holds at 100°C for 120 min. Table 2 reaches 100°C at 1°C/min but instead of dwelling at 100°C the furnace heats up to 300°C at 2°C/min then cools back down room temperature at ~ 2°C/min.

3.3 Characterization Techniques Explained

Materials can be characterized through a variety of ways, the more characterization techniques used the more certain you can be of materials properties. FTIR can be used to identify molecules in a system that can be confirmed as a crystal phase with XRD. TGA can identify the wt% of materials in your sample which can be confirmed by EDX. For this project SEM, EDX, TGA, FTIR, and DMA were used.

3.3.1 Scanning Electron Microscopy & Energy Dispersive X-Ray Spectroscopy

As mentioned in section 2.8.1 the SEM characterization technique is used to determine the morphology of the fiber, characteristics such as alignment, surface roughness, surface smoothness, porosity, impurities, defects, etc. While EDX is used to detect the elements present in a material. SEM is necessary as a nanofiber's topography is not visible by traditional microscope tools. For comparison, a human hair is approximately 50,000 nm while a nanofiber is about 1,000 times smaller. The SEM tool allows for characterization at the micron and nanoscale. The SEM & EDX tools work in conjunction with one another.

The SEM is a microscope that uses an electron beam to scan the surface of a sample, which is sometimes coated with metal atoms, to study the details of its topography. It contains 8 main components: the electron gun, electron beam, anode, lenses, backscattered electron detector, secondary electron detector, stage, and specimen. Before using the SEM sample is placed inside the SEM and a vacuum is pulled in the sample chamber. Electrons shoot out of the top a column accelerating through an anode and initial condenser lens. An objective lens and two apertures are used to adjust the acceleration and direction of the beam focusing the beam onto the sample in the chamber below. As electrons come in contact with the sample itself has

its own electrons displaced generating both secondary electrons and backscattered electrons. X-rays are also produced which can be recorded to detect the elements present allowing for EDX analysis. All the signals are collected by independent detectors and sent to software which then formulates an image based off the signals, the x-ray detectors send their recorded signals to a separate software which is used for EDX analysis.

Figure 8 was taken from "A Beginners' Guide to Scanning Electron Microscopy" [57].

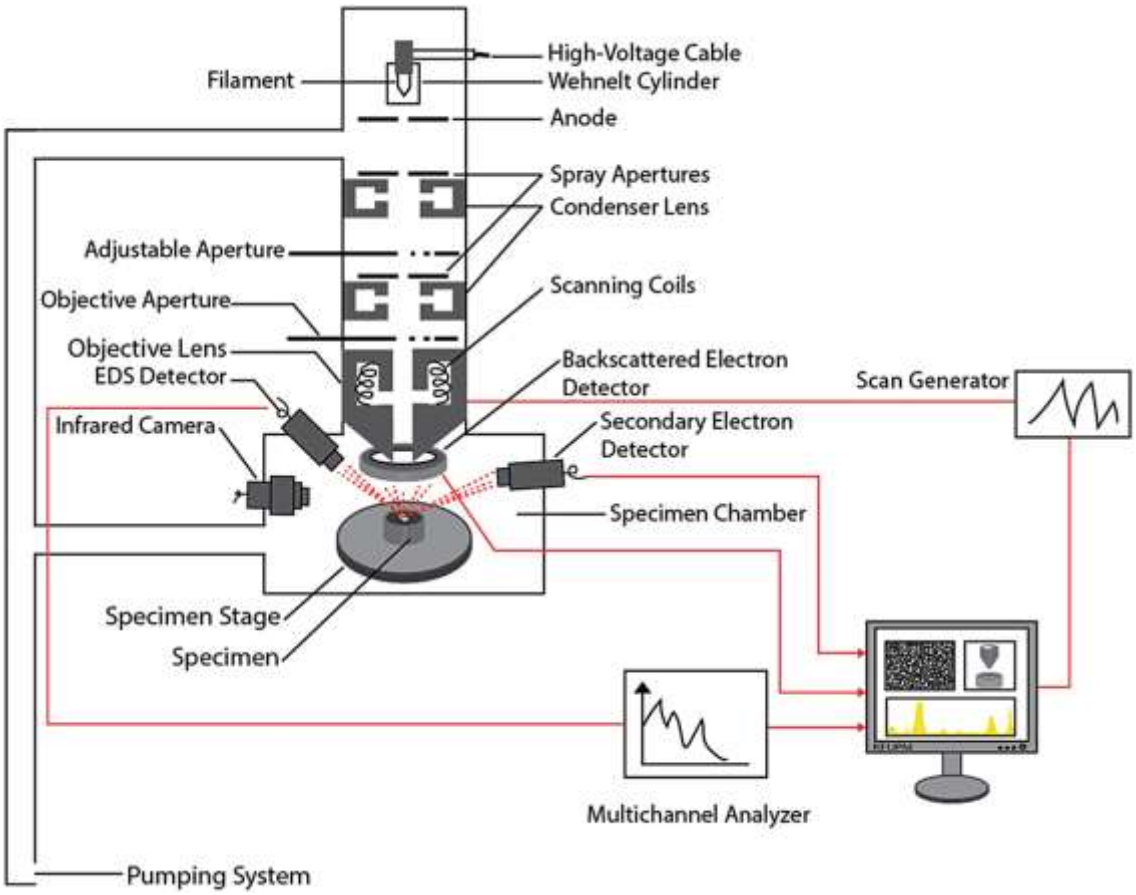

Figure 8: SEM & EDX Schematic

As seen in the figure a high voltage is shot through a filament to produce electrons then is focused by lenses and apertures onto the sample. The independent detectors then send the signals to the appropriate software to generate images and data. The minimum voltage used is typically 1 kV for SEM images however the minimum voltage for EDX is usually higher as a

minimum amount of x-ray signals are required to generate the EDX data with confidence – this minimum voltage depends on the stability and conductivity of the sample inside the chamber.

The quality of SEM images depends on the set magnification, focus, aperture, voltage, stability & conductivity of the sample. Samples that have poor conductivity must be sputtered, sputtering is the process of transferring material from a "target" onto the surface of the sample by generating a plasma from the target material. The target material deposited onto the surface of the SEM sample is usually gold. The gold promotes electrons to bounce off the surface of the sample. The degree of sputtering ranges depending on the SEM sample but the layer of material generated by sputtering is always in the nanoscale, however, if sputtering occurs long enough the target material will be detected by EDX analysis.

3.3.2 Thermo Gravimetric Analysis (TGA)

TGA is a thermal analysis method which measures the mass changes in a sample during heating. Different heating programs can be implemented to investigate different characteristics of a material, for example, if one would like to know the weight percentage of a specific compound in a material a heating run can be done past that compound's decomposition temperature and then the weight loss of the sample due to the decomposition of the compound can be recorded. For example, if a compound consists of 3 compounds – A, B, & C and the thermal decomposition of these compounds are known the weight percentage of the compounds can be derived from the TGA. Assume A decomposes at 300°C, B at 650°C, and C at 1200°C.

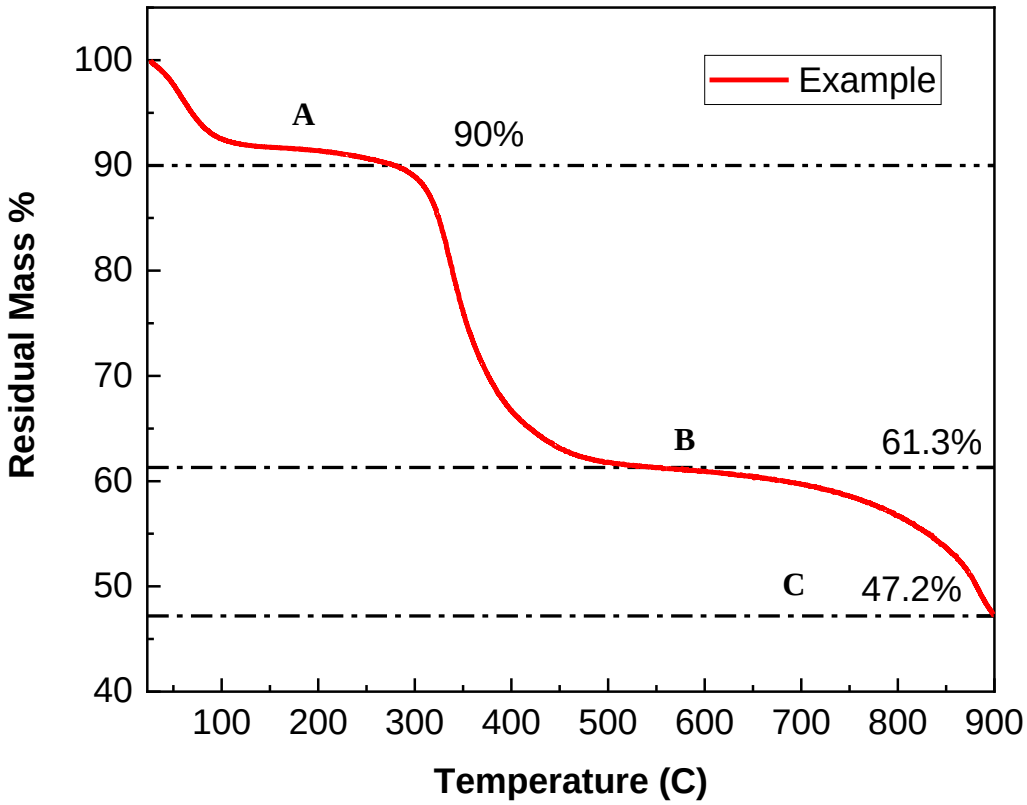

Figure 9: TGA Example

Referring to figure 9 we can see that we have an initial weight loss of ~ 10% before A starts to decompose, this can be due to impurities in the material or volatiles such as water. Between 300°C and 550°C, a change of 28.7 % of the total mass is seen (90%-61.3%) this means that compound A makes up for 28.7% of the mass of the material. Similarly, we can calculate the mass percentage of compound B to be 14.1 % (61.3%-47.2%) then we are left with only compound C which makes up 47.2 % of the material.

The changes of mass in a sample don't only reflect decomposition but also depict oxidation, absorption, sublimation, vaporization, desorption, reduction. TGA may also be used to investigate the effects of crosslinking and heat treatments on the thermal properties of a

material by analyzing how the TGA curve is effected by different crosslinking or heat treatment parameters.

3.3.3 Fourier Transform Infrared Spectroscopy (FTIR)

FTIR is a characterization technique that belongs to the family of spectroscopy. Spectroscopy is the branch of science concerned with the investigation and measurement of spectra produced when matter interacts or emits electromagnetic radiation. Techniques include Raman Spectroscopy, X-Ray Diffraction (XRD), Nuclear Magnetic Resonance (NMR), and FTIR. Which use similar concepts but are unique in their measurement techniques.

FTIR studies the interaction between matter and infrared radiation. Infrared radiation is electromagnetic radiation (light) with a longer wavelength than visible light. This longer wavelength means the light will carry less energy and have a smaller wavenumber. Infrared light passes through a sample for example water.

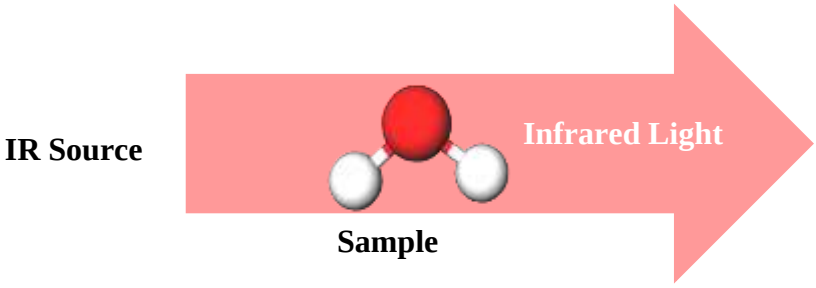

Figure 10: FTIR Absorption Example

When infrared light passes through the water molecule the light can trigger vibrations of specific molecular bonds (absorption). These vibrations include symmetric stretching, anti-

symmetric stretching, deformation, rocking, wagging, and twisting. The energy absorbed by the molecule will be consumed and thus missing from the original IR beam.

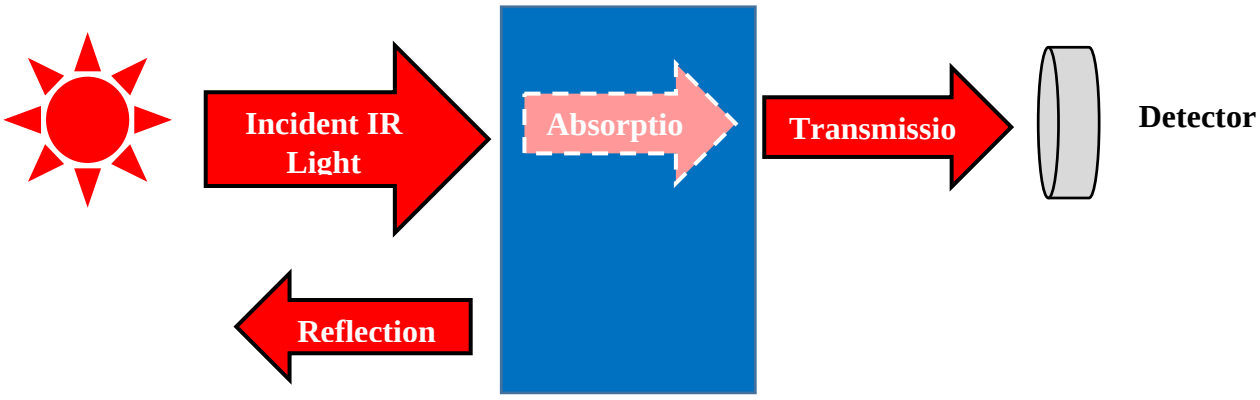

Figure 11: Infrared Spectrum Measurement

Thus an IR light source is directed to a sample having some of it reflected but the larger portion passing through the sample. Specific parts will be absorbed by the sample material and the IR light that passes through will be transmitted to a detector which in turn produces an electron signal that can be interpreted by software. Improved FTIR advances on these principles by using a Michelson interferometer

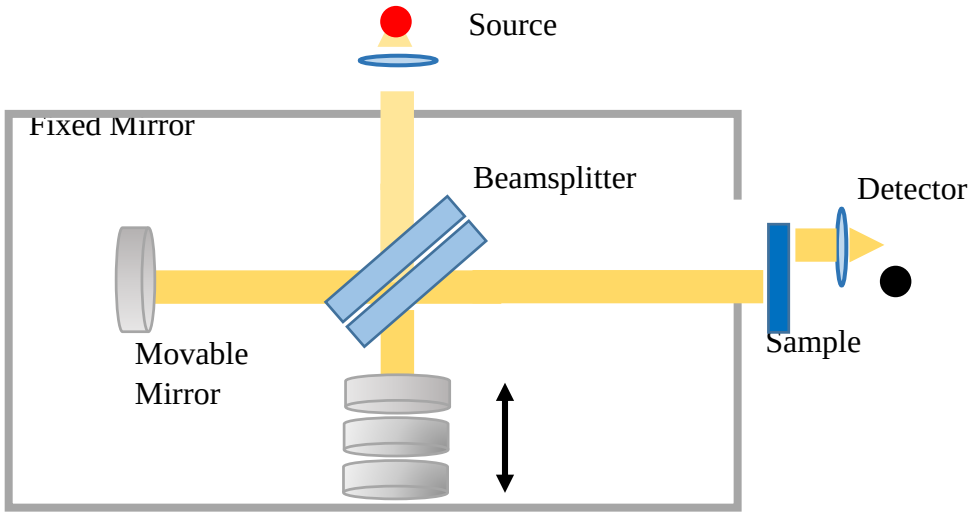

Figure 12: Michelson Interferometer

Figure 12 shows a Michelson interferometer in action, a source shoots out an IR beam which is then split towards two mirrors, a fixed mirror, and a moveable mirror. These mirrors reflect the beam back through the splitter and into the sample. The infrared light that passes through the sample is then detected by a detector. This allows for the spectra information of all wavelengths to be acquired simultaneously.

Before performing FTIR an initial background test must be done without any sample this raw single-channel background is then mathematically Fourier transformed in a light intensity vs wavenumber plot. Using the single-channel reference spectrum we can insert the sample into the beam path and repeat the analysis, the Fourier transformation will yield another single channel but this time it is the sample spectrum. The FTIR equipment will automatically divide the sample spectrum by the reference spectrum providing the sample's transmission vs wavenumber plot. This FTIR spectrum is essentially a chemical footprint of the sample. The spectrum can be used to identify and verify known and unknown characteristics of the sample

3.3.4 Dynamic Mechanical Analysis

DMA is a material characterization technique that provides information on the viscoelastic mechanical properties of a material as well as thermal properties such as identifying the glassy or transition regions of material. DMA is often used to study the performance of a material under specific conditions under dynamic loads, either oscillating stresses or strains, the temperature and frequency conditions can be changed throughout the entirety of one test allowing for a multitude of information to be derived from one test specimen. DMA is considered to be more sensitive for detecting transitions (Tg, Tm) than other techniques such as Differential Scanning Calorimetry.

Assuming sinusoidal oscillating stress is applied during DMA the sample would respond with a sinusoidal oscillation with similar frequency as applied so long as the sample stays within its elastic limits. If the material responds to the applied oscillating stress perfectly elastically the resulting strain wave is in-phase (storage or elastic response). A viscous material responds with an out-of-phase strain wave (loss or viscous response). A Hookean solid would respond with a phase angle of 0 degrees while a Newtonian liquid would have a phase angle of 90 degrees, a viscoelastic material would fall in between the two extremes.

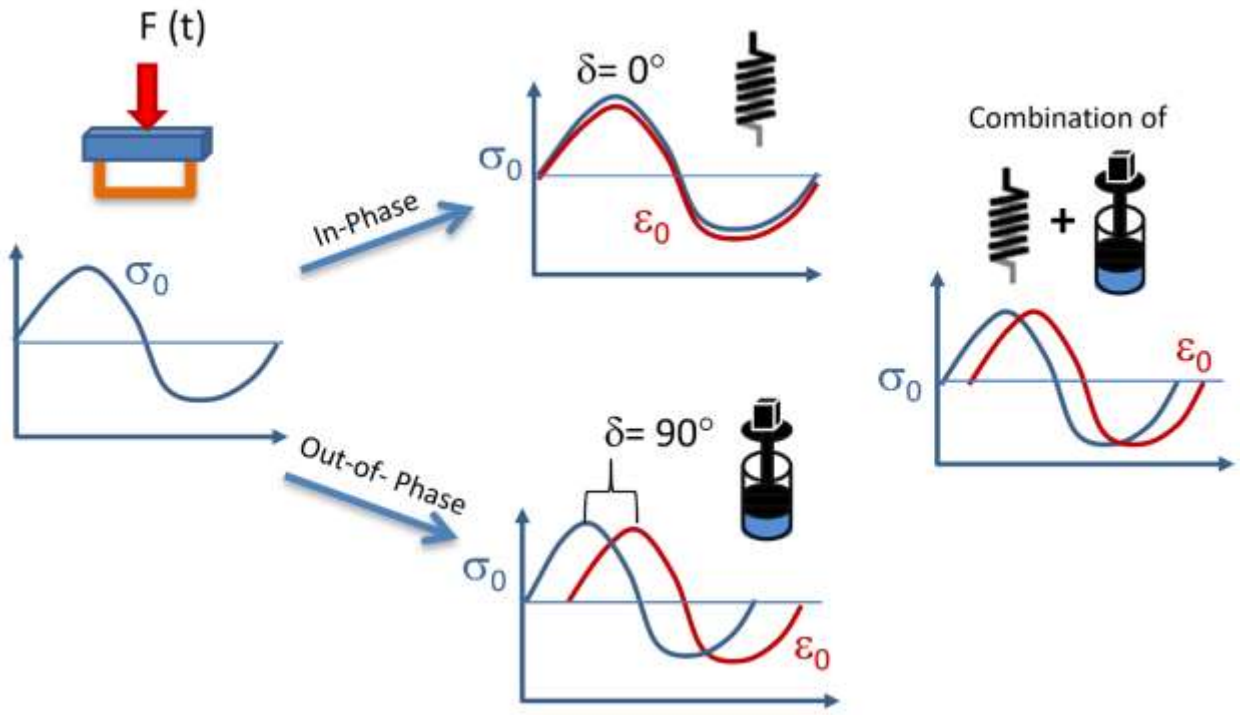

Figure 13: Dynamic Mechanical Analysis

Any point on the stress curve can be described by:

$$\sigma(t) = \sigma_0 \sin(\omega t)$$

Here σ_0 is the maximum stress and ω is the frequency of oscillation. Deriving this equation provides the rate of stress in terms of time:

$$d\sigma/dt = \omega\sigma_0\cos(\omega t)$$

Recall that the two extremes are a purely elastic and purely viscous response. By investigating the two extremes we can understand the behavior for material in between. A material that is spring-like or exhibits a Hookean limit response responds elastically to the oscillating stress. Thus the strain at any time is:

$$\varepsilon(t) = \varepsilon_0\sin(\omega t)$$

ε_0 is the maximum amplitude of strain and ω is the frequency of oscillation.

For a viscous response, the stress is proportional to the strain rate which is the first derivative of the strain.

$$\frac{d\varepsilon}{dt} = \omega\varepsilon_0\cos(\omega t) = \varepsilon_0\sin(\omega t + \frac{\pi}{2})$$

Additionally multiplying by the materials viscosity results in:

$$\sigma = \eta\frac{d\varepsilon}{dt} = \omega\eta\varepsilon_0\cos(\omega t) = \sigma_0\sin(\omega t + \frac{\pi}{2})$$

Thus the behavior of a viscoelastic material will lie between the two limits meaning the difference between applied stress and resultant strain is an angle, δ:

$$\varepsilon(t) = \varepsilon_0\sin(\omega t + \delta)$$

The equation can be rewritten as:

$$\varepsilon(t) = \varepsilon_0\sin(\omega t)\cos(\delta) + \varepsilon_0\cos(\omega t)\,sin(\delta) = \varepsilon'\sin(\omega t) + \varepsilon"cos(\omega t)$$

$$\sigma(t) = \varepsilon_0 E^*\,[\sin(\omega t)\cos(\delta) + \cos(\omega t)\,sin(\delta)] = \varepsilon_0\sin(\omega t)E' + \varepsilon_0 cos(\omega t)E"$$

Here $\varepsilon_0 \cos(\delta)$ and $\varepsilon_0 \sin(\delta)$ are the "in" and "out" of phase strain (ε',ε"), E^* is the ratio of maximum stress to maximum strain while $\sigma_0 \cos(\delta)/\varepsilon_0$ and $\sigma_0 \sin(\delta)/\varepsilon_0$ are the storage and loss modulus (E', E"). Also known as the elastic (storage) and viscous (loss) modulus. The sum of the vectors of the loss and storage modulus gives the complex strain and modulus

$$\varepsilon^* = \varepsilon' + i\varepsilon"$$

$$E^* = E' + iE"$$

The ratio of the loss to storage modulus is the phase angle and is called damping:

$$\tan(\delta) = E"/E'$$

By understanding these concepts the DMA plots can be interpreted. DMA effectively measures the loss and storage modulus across multiple frequencies and temperatures. In polymers, the modulus decreases when transitioning from glassy to rubbery as seen below.

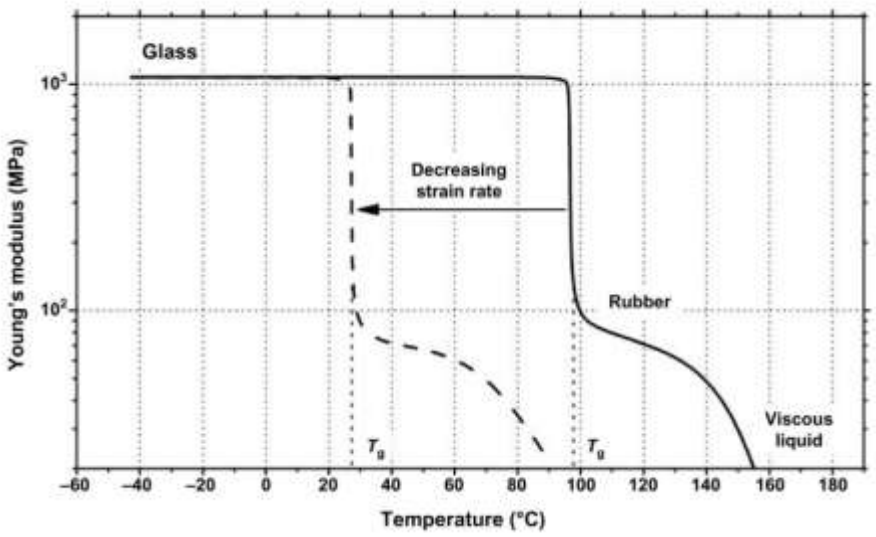

Figure 14: DMA TG Transition

Figures 14 and 15 are from [54]. DMA tests are complex in nature and offer a variety of testing setups. The proper DMA setup and type of test must be selected by an educated operator.

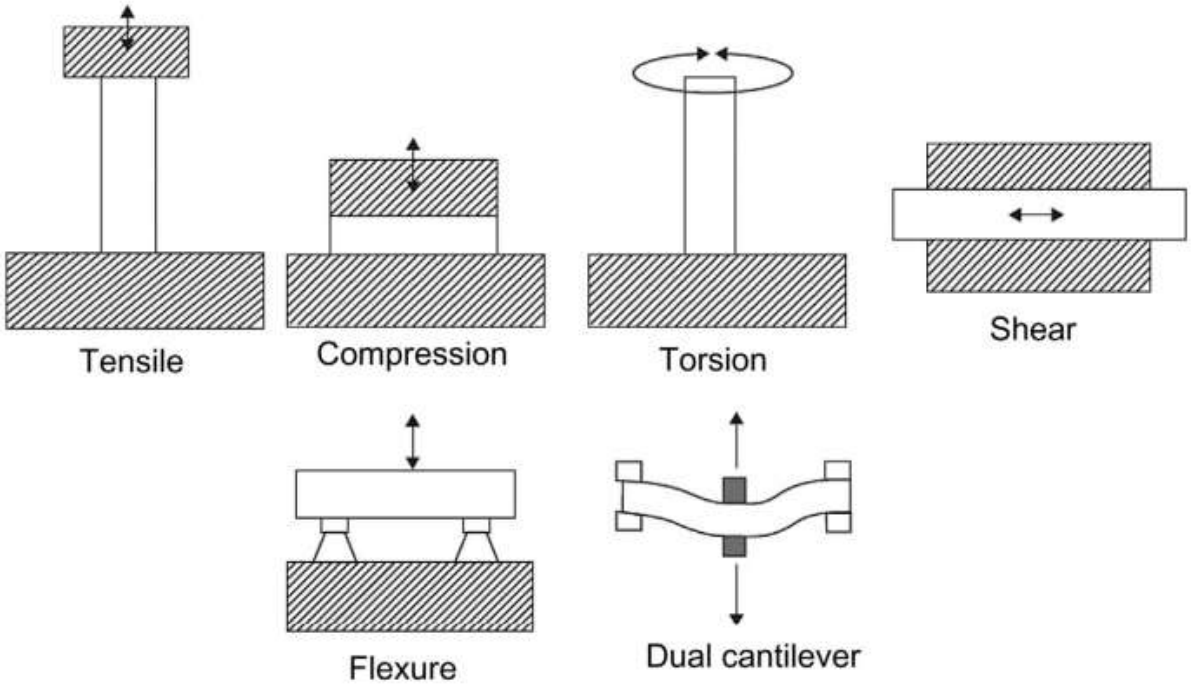

Figure 15: DMA Sample Setup

This research utilizes samples tested in tensile mode, the samples were made from a mold for consistency. It is critical that the geometry of the sample is symmetrical and satisfies the parameters of the DMA equipment. Again the by changing the frequency and stress a multitude of properties can be derived from using the DMA.

CHAPTER IV

METHODOLOGY

Silicon carbide, silicon nitride, and tungsten carbide nanofibers were synthesized using the same methodology but with adjusted parameters with respect to each fiber. Ceramic nanofiber production can be simplified into 5 steps, solution preparation, solution spinning, drying/crosslinking, nitridation/carbonization, and characterization. Additionally, polymer-ceramic composites were made from tungsten carbide. All safety guidelines for handling nanomaterials were used. Proper training and was done before conducting any of the following methods. The appropriate personal protective equipment must be worn at all times.

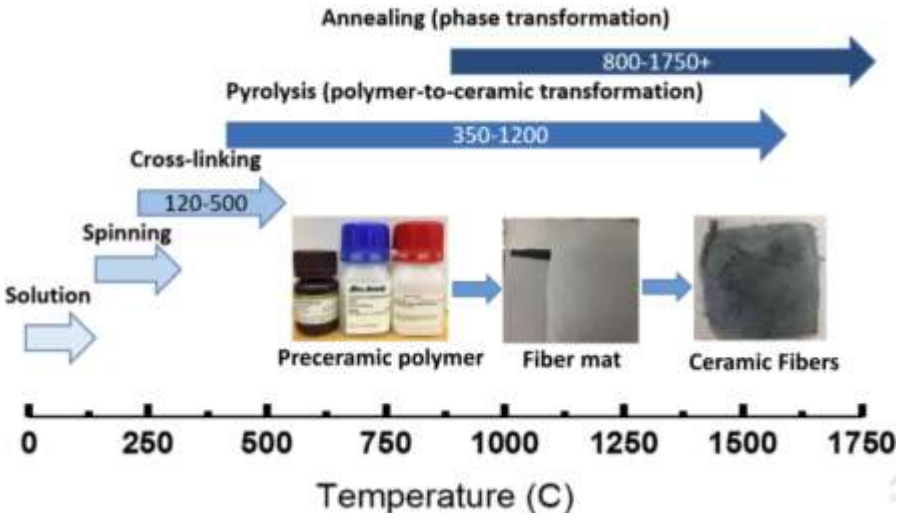

Figure 16: Methodology Overview

4.1 Solution Synthesis

Recall that the solutions for preceramic nanofibers consist of active material, carrying material, and an appropriate solvent to combine the active and carrying material into a homogenous solution with the appropriate viscosity for spinning.

4.1.1 Polycarbomethylsilane Solution One

Solution one was synthesized using polycarbomethylsilane (PCmS) as the active material, PVP as the carrying material, and chloroform & N, N-Dimethylformamide (DMF) as the solvents. PVP was added into a 20 ml scintillation vial then the solvents were added and the solution was stirred using a .5" magnetic bar for one day at 700 RPM then active material was added and stirred the same way as before. The following amounts were used:

Table 3: Solution One PCmS

Name	Supplier	Amount	Wt %
PVP	**Sigma-Aldrich**	**2.62 g**	**26**
Chloroform	**Sigma-Aldrich**	**5.65 ml**	**38**
DMF	**Alfa-Aeser**	**2.25 ml**	**23**
PCmS	**Sigma-Aldrich**	**1.28 g**	**13**

4.1.2 Polycarbomethylsilane Solution Two

Solution two was synthesized similarly to solution one but a different supplier for PCmS was used. Solution two was made using polycarbomethylsilane (PCmS) as the active material, PVP as the carrying material, and chloroform & N, N-Dimethylformamide (DMF) as the solvents. PCmS was added into a 20 ml scintillation vial then the half the solvents were added

and the solution was stirred using a .5” magnetic bar for one day at 700 RPM then carrying material along with the other half of the solvents were added and stirred the same way as before. The following amounts were used:

Table 4: Solution 2 PCmS

Name	**Supplier**	**Amount**	**Wt %**
PVP	**Sigma-Aldrich**	**2.62 g**	**26**
Chloroform	**Sigma-Aldrich**	**5.65 ml**	**38**
DMF	**Alfa-Aeser**	**2.25 ml**	**23**
PCmS	**BOC Sciences**	**1.28 g**	**13**

4.1.3 Polyphenymethylsiloxane Solution

Solution three was made using polyphenylmethylsiloxane (PPS) as the active material, PVP as the carrying material, and ethanol as the solvent. PPS was added into a 20 ml scintillation vial then the half the solvents were added and the solution was stirred using a .5” magnetic bar for one day at 700 RPM then the carrying material along with the other half of the solvent was added and stirred the same way as before. The following amounts were used:

Table 5: Solution 3 PPS

Name	Supplier	Amount	WT %
PVP	**Sigma-Aldrich**	**1.6 g**	**15.5**
Ethanol	**Decon**	**10 ml**	**76.2**
PPS	**Alfa-Aeser**	**.778 ml**	**8.3**

4.1.4 Ammonium Metatungstate Hydrate Solution

Solution four was made using Ammonium Metatungstate Hydrate (AMT) as the active material, PVP as the carrying material, and deionized water as the solvent. AMT was added into a 20 ml scintillation vial then the half the solvents were added and the solution was stirred using a .5" magnetic bar for one day at 700 RPM then the carrying material along with the other half of the solvent was added and stirred the same way as before. The following amounts were used:

Table 6: Solution 4 AMT

Name	Supplier	Amount	Wt%
PVP	**Sigma-Aldrich**	**1.5 g**	**11.3**
DI Water	**Decon**	**10 ml**	**75.5**
AMT	**Alfa-Aeser**	**1.75 g**	**13.2**

4.2 Forcespinning

4.2.1 Solution 1 & 2 PCmS

After each solution is made the must be spun within 3 days of synthesis ensuring solution integrity. Solutions one and two were heated before spinning in a silicon oil bath of 80°C for 30 minutes. Once the spinning process began the solutions were left stirring in a Colepolymer 8890 Ultrasonic Cleaner in between runs. These steps were taken to lower the viscosity of the solution allowing it to be spun. Prior to spinning the Forcespinning© machine must also be prepped along with the collectors. The machines used were the Cyclone L1000M from Fiberio Technology Corp. The lab facilities had two of the same machine labeled cyclone 1 and cyclone 2 respectively. For PCmS only cyclone 1 was used. The interior of cyclone 1 was covered with foil paper to and then a donut-shaped collector with eight bars was set around the center of the machine. Prior to placing the collectors inside the stainless steel spinneret was inserted into the center of the machine. The collectors themselves were covered with aluminum foil and the bars were set to the fifth space available on the donut. Spinning parameters ranged from 6000-8000 RPM depending on several things: viscosity of the solution, relative humidity in the lab, the temperature in the lab, the amount of time spun (6-10 min).

For each spinning cycle, 1-1.5 mL of solution was injected into the stainless steel spinneret inside cyclone 1 using a 3 mL syringe with a 10 gauge needle attached. Once the solution was placed inside 25 gauge needles were attached to both sides of the spinneret. Both doors of cyclone 1 were closed then locked and the spinning run began. After the run was complete the machine was opened and the fibers were collected on a 4”x4” cardboard mat that was covered in aluminum foil. After each run new solution needs to be placed into the spinneret and new 25 gauge needles must be attached while the old ones must be discarded.

4.2.2 Solution 3 PPS

After the PPS solution is made it must be used within 7 days to preserve solution integrity. The PPS solution was spun at room temperature and follows the same process as spinning solutions one and two except cyclones 1 & 2 were both used and 30 gauge needles were used instead of 25 gauge needles. The solution was spun between 5000-7000 RPM and for 10 seconds – 2 minutes depending on the viscosity of the solution, relative humidity in the lab, the temperature in the lab. The collection of the fibers is the same as for solutions 1 & 2.

4.2.3 Solution 4 AMT

After the AMT solution is made it must be used within 7 days to preserve solution integrity. The AMT solution was spun and collected the same way as the PPS solution except the RPM ranged from 5000-8000 RPM and the spinning times ranged from 1 minute – 4 minutes depending on the viscosity of the solution, relative humidity in the lab, temperature in the lab.

4.3 Crosslinking & Pyrolysis

4.3.1 PCmS Fibers

For PCmS only solution three yielded fibers. Fibers were dried at 110 °C under nitrogen for 24 hours. The fibers were then heat-treated from room temperature to 250 °C at 2°C/min under 20 mL/min nitrogen flow and dwelled at 250 °C under nitrogen flow to undergo the crosslinking process. The fibers were then heated from 250 °C to 850 °C at 1 °C/min. Once at 850 °C the fibers were taken to 1300 °C at 2 °C/min and held at 1300 °C for 120 min before being cooled to 50 °C at 2 °C/min. All this was done under 20 mL/min of nitrogen flow.

4.3.2 PPS Fibers

The PPS fibers were dried at 120 °C under a nitrogen atmosphere for 24 hours. After the drying process several crosslinking temperatures were used each starting from room temperature then being ramped up at 5 °C/min to the set crosslinking temperature of either 120 °C, 170 °C 220 °C, 270 °C, 320 °C and held at that crosslinking temperature for 120 minutes. All processes were done under 20 mL/min nitrogen flow. After the fibers were crosslinked they were taken from room temperature to 800 °C at 1°C/min and stabilized for 120 min before being ramped to either 1000 °C, 1100 °C, 1200 °C, 1300 °C, 1400 °C at 2 °C/min and then dwelled at the temperature it was ramped up to. After dwelling the fibers were cooled to room temperature at 2 °C/min. All Processes were done under 20 mL/min of nitrogen.

4.3.3 AMT Fibers

The AMT fibers were dried and crosslinked simultaneously by heating from room temperature to 280 °C at 5 °C/min then dwelling at 280 °C for 120 min before cooling to room temperature at 3°C/min under atmospheric conditions (no inert gas). The fibers were then carbonized by being heated from room temperature to either 600 °C, 700 °C, 800 °C, 900 °C, 1000 °C at 5 °C/min dwelling for either 60 min or 120 min (total10 different heat treatments) before being cooled to room temperature at 5 °C/min, all under argon flow.

4.4 WC Composite

WC composites were made by crushing WC fibers heat-treated at 900 °C and 1000 °C with dwell times of 120 min into powder form. The fibers were combined with ultrahigh molecular high weight polyethylene at 3, 5, 7 weight percentages of fibers. The mixtures were tumbled for 3 days then placed into a mold and hot-pressed at 180 °C under two tons using a 15-ton Specac manual hydraulic press. The temperature was kept at 180 °C for two minutes then the mold was allowed to cool to room temperature under two tons. Once at room temperature, the pressure was relieved and the composites were removed from the mold after one day.

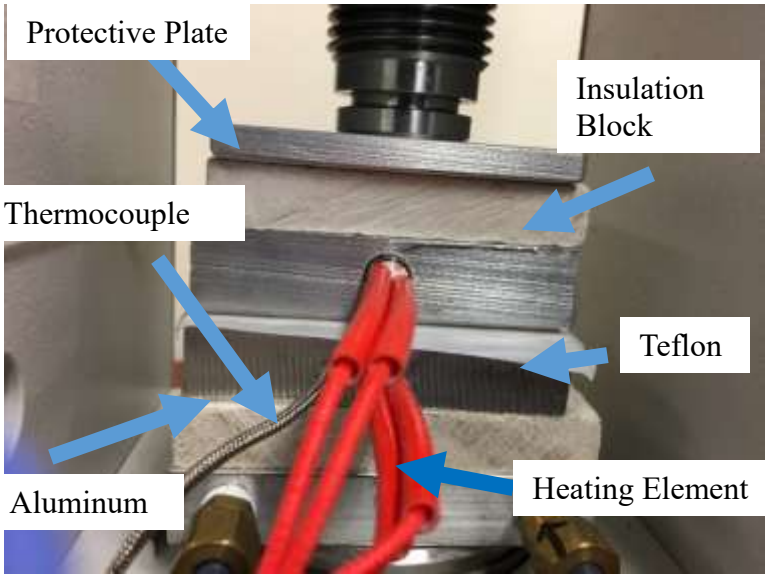

Figure 17: Hot Press Set up

As seen in figure one the mold is placed between two aluminum hot plates which each have a heating element running through them. These heating elements are connected and series and controlled by a temperature controller which is regulated by the thermocouple.

4.5 Characterization

4.5.1 Scanning Electron Microscopy (SEM)

PPS, & AMT fibers were characterized using SEM. The morphology and average diameter of the fibers were investigated using a Zeiss Sigma VP SEM operated using line average, n = 100 and voltages between 1 kV- 7 kV depending on the magnification and sample. Images were taken at 250 and 2000 magnification, additional magnifications were used to investigate points of interest. ImageJ was used to measure the diameters of the fibers from the SEM images taken at 2000 magnification.

4.5.2 Energy Dispersive X-Ray Spectroscopy (EDS)

The element composition of AMT & PPS fibers was analyzed using the EDAX Octane Super EDS combined with APEX software. The EDS was operated in conjunction with the SEM, a line average of n=100 was used under 5 kV – 7 kV while selecting EDS analysis locations. The element composition of the image area and impurities were analyzed at 250 magnification. At 2000 magnification the element composition of the image area, as well as the composition of individual or bundles of fibers, were analyzed. Additionally, the points of interest were investigated.

4.5.3 Thermo Gravimetric Analysis (TGA)

Thermal analysis was performed on AMT & PPS fibers using the TG 209 F3 Tarsus. Crosslinking mechanisms, thermal stability, and fiber uniformity were investigated using the TGA. A calibration run was performed weekly on a blank crucible prior to all tests. Every run

consisted of a ~ 10 mg (+/- .01 mg) sample which was heated from room temperature to 900°C at 10°C/min under a 20 mL/min nitrogen flow for both the purge and protective gas.

4.5.4 Fourier Transform Infrared Spectroscopy (FTIR)

FTIR was performed on heat-treated and untreated AMT & PPS fibers using a Bruker© Invenio FTIR spectrometer operating at 70 spectra/s with 16 cm^{-1} resolution. Prior/after each run the lenses were cleaned using deionized water and kimtech wipes. Once the machine was cleaned the OPUS software was opened and a background channel test was performed in 42 scans from 80 cm^{-1} to 4000 cm^{-1}. Next, sample single-channel tests for all samples were performed using the same parameters, unloading test data in between runs and cleaning the lenses between runs too. Samples of ~ 1 cm x 1 cm were used, additionally, since the test is nondestructive some samples were reused for TGA.

4.5.5 Dynamic Mechanical Analysis (DMA)

DMA was performed on UHMWPE/WC rectangular composites using the DMA 242 E Artemis under tensile mode. The composite sample was clamped as seen in figure 18.

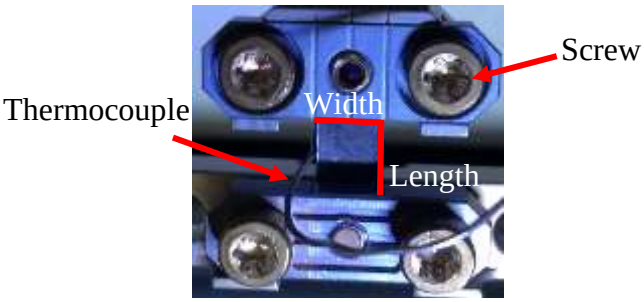

Figure 18: DMA Sample Configuration

Samples ranging from 4.68-4.83 mm in width and 1.63 mm of thickness were placed into the clamps and the four holding screws were torqued to .12 Newtons. The length between the clamps was adjusted to ~ 5 mm allowing for a minimum of 1.5 mm of sample to be clamped on the top and bottom clamps. The thermocouple was then placed next to the sample prior to testing.

A dynamic test with a targeted amplitude of 1 μm was performed using an isothermal step function from 25 °C-120 °C at a heating rate of 2 °C/min. Data was recorded in 5 °C increments (19 segments) at .1, .333, 1, 3.33, 10, 33.3, 100 Hz. The temperature was stabilized for 5 minutes at every isothermal step prior to data acquisition. Additionally, a control was done at 3.33 Hz from 25 °C-120 °C at a heating rate of 2 °C/min under the same dynamic conditions.

CHAPTER V

RESULTS AND DISCUSSION

5.1 Crosslinking Mechanisms

Prior to pyrolysis, preceramic fibers must become infusible by undergoing crosslinking. Different active materials and carrying materials have their own unique optimal crosslinking conditions. This is dependent on the composition of both the active material & carrying material, as well as the volatility of the solvents used. The optimal conditions for AMT & PVP fibers were found in the literature and thus weren't investigated in this work. However, the crosslinking mechanisms of PPS and PVP were investigated as this is the first study done using PPS and PVP to form preceramic fibers.

5.1.1 PPS TGA Analysis

Preceramic fibers are composed of polymer materials that contain the necessary elements needed to form the desired ceramic fiber. The properties of polymers can thus be taken advantage of prior to ceramic conversion. The crosslinking temperature of PVP with preceramic polymers ranged from 120 °C to 280 °C in the literature. For PPS it was discovered that crosslinking at 320 °C yielded the highest residual mass when heated to 900°C as seen in figure 19.

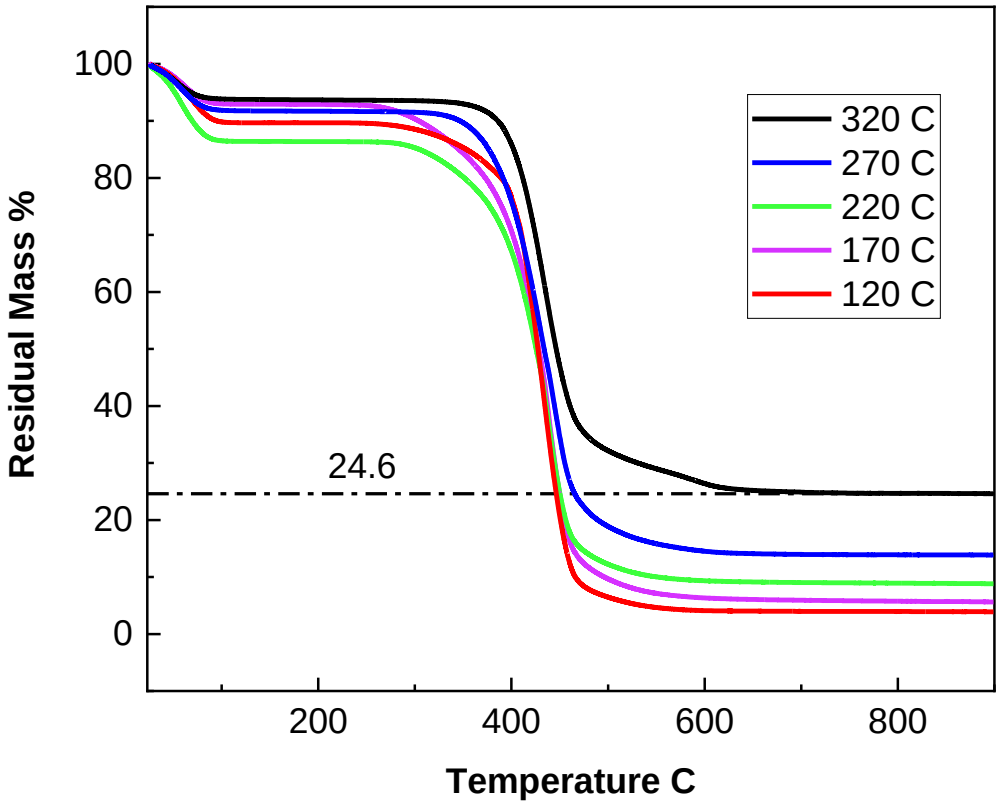

Figure 19: TGA of PPS Crosslinking Mechanisms

Initially, all crosslinked fibers experience weight loss prior to the decomposition temperature of PVP, 380 °C. The fibers crosslinked at 220 °C showed the highest initial mass loss of ~12% but had the second-highest residual mass overall. This could be due to improper handling of the sample in which it was exposed to air post crosslinking. Ignoring the 220 °C sample a positive correlation between increasing temperature and residual mass can be seen throughout the TG plot. A shift in the second weight loss is seen in all samples with the highest temperatures being seen in the 270 °C & 320 °C samples. All samples stabilize by 700 °C with the best performing sample, 320 °C, having 24.6% residual mass. For all runs only the 270 °C and 320 °C yielded fibers, the other samples fused. Thus the best crosslinking temperature is 320 °C as it has the highest yield of infusible fibers.

5.1.2 PPS FTIR Analysis

FTIR was used to understand which molecules are present in each crosslinking temperature. An investigation into which molecules were weakened, strengthened, missing, or formed can be correlated to thermal performance. This information can then be used to explain

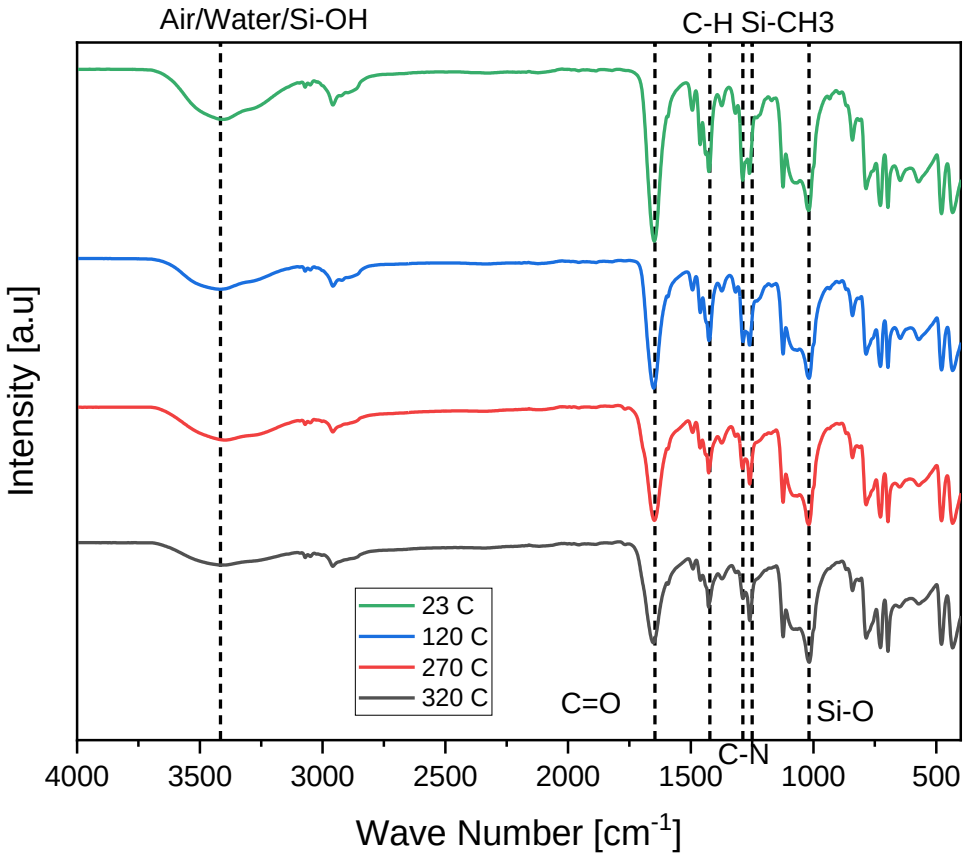

Figure 20: PPS Fibers Entire FTIR

the phenomena seen in the TGA as well as help predict crosslinking temperatures for new preceramic fibers.

Figure 20 shows the FTIR for untreated fibers and fibers treated a 120, 270, and 320 °C. The valley at 3425 cm^{-1} represents OH stretching of the Si-OH end groups in PPS but can also indicate the presence of water. As the temperature increases from 23 °C to 120 °C water is removed from the system reflected by a rise in the valley, however, the valley continues to rise

with increasing temperature indicating the removal of OH for the Si-OH side groups freeing the Si to bond to other elements. At 1653cm^{-1} a valley indicating C=O stretching of the carbonyl group in PVP is seen, this valley rises as temperature increases indicating the removal of oxygen from the sample. The valley at 1422 cm^{-1} represents the bend deformation of the C-H branch in PVP which rises with increasing temperature meaning that the bond is being replaced. The symmetric deformation of CH_3 in the PPS side group Si-CH_3 is indicated at 1281 cm^{-1} This valley rises with increasing temperature indicating less CH_3 in the sample. C-N wagilling of the N-CH_2 side group decreases initially between 23 °C and 120 °C but then stabilizes at higher temperatures as seen in the valley at 1277 cm^{-1}. Stretching of linear Si-O in the Si-O-Si structure of PPS at 1016 cm^{-1} remains unchanged throughout temperature increase.

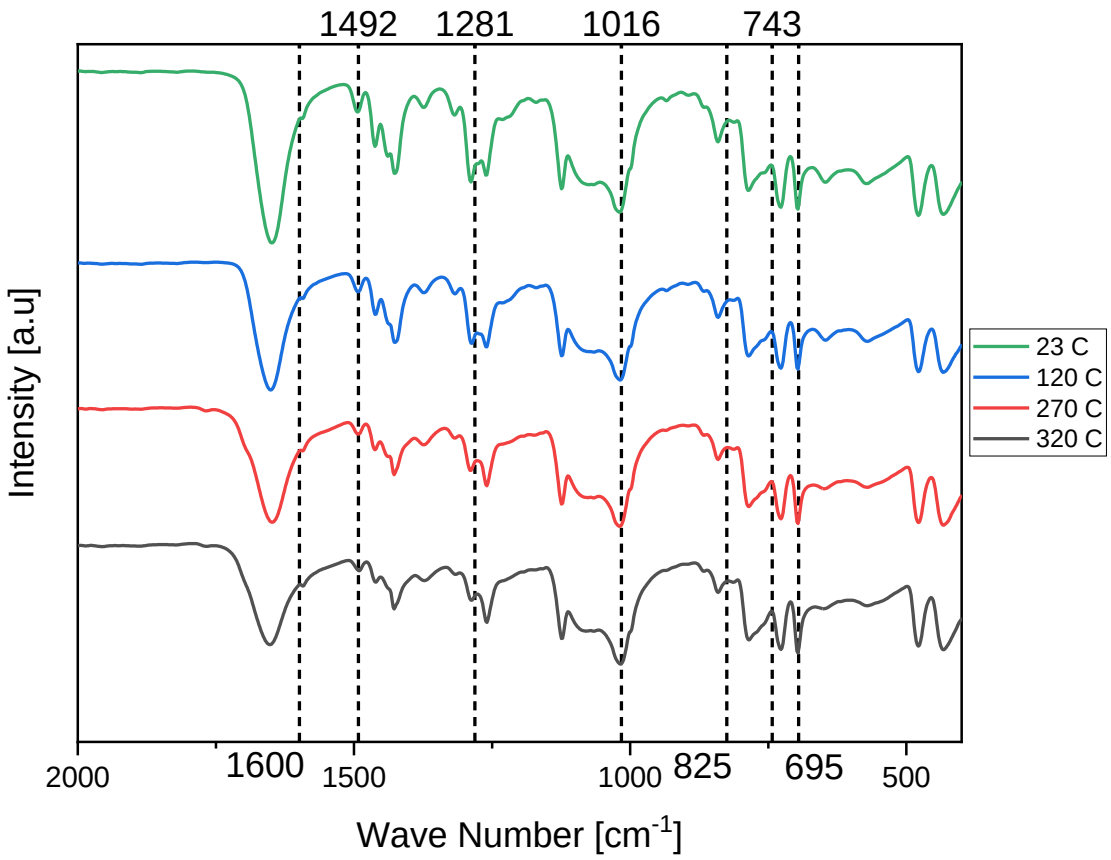

Figure 21: FTIR of PPS Fibers - PPS bonds

Figure 21 takes a closer look at the bonds in PPS between 2000 cm^{-1} and 500 cm^{-1}. As expected the C=C ring stretching remained constant through increasing temperature as seen at 1600 cm^{-1} and 1492 cm^{-1}. When zoomed in the expected symmetric deformation of CH_3 in the PPS side group Si-CH_3 is not at 1281 cm^{-1} but instead closer to 1285 cm^{-1}. Si-C stretching vibrations remain constant as seen at 825 cm^{-1}. C-H stretching vibrations of the phenyl ring in PPS remains constant as seen at 743 cm^{-1} and 690 cm^{-1}

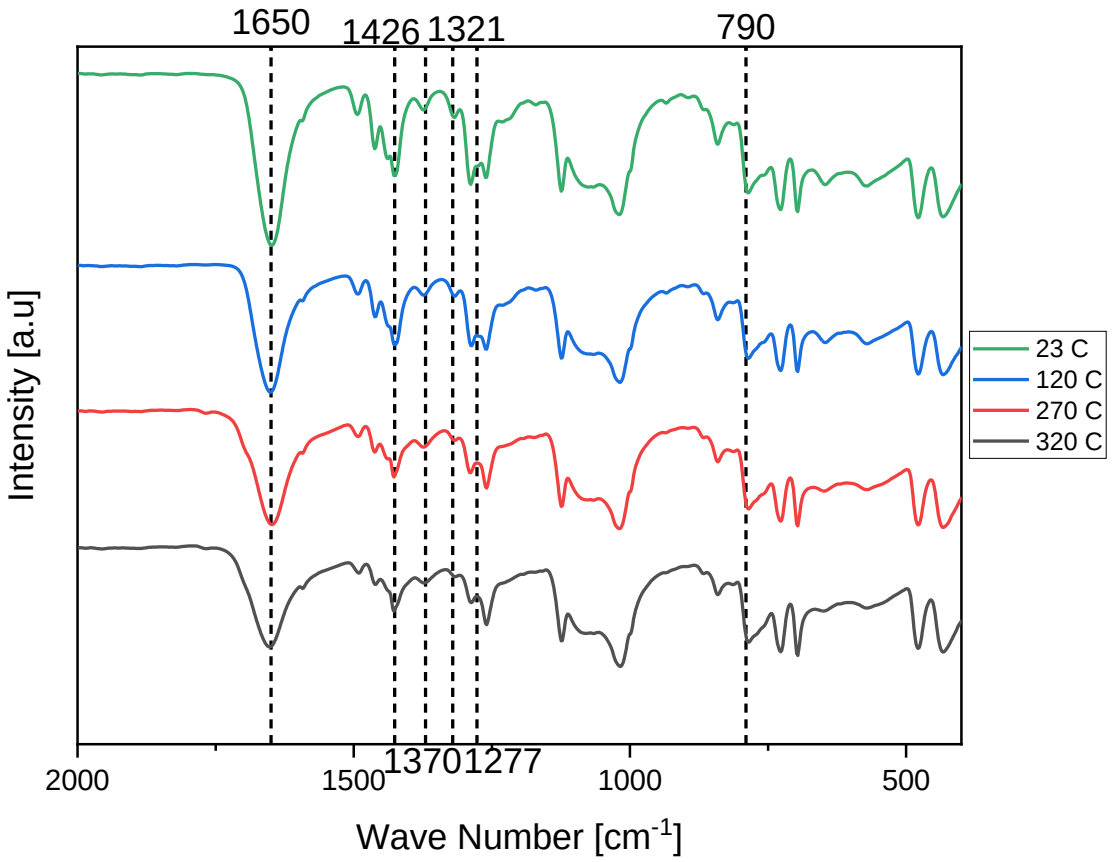

Figure 22: FTIR of PPS Fibers - PVP bonds

Figure 22 is the same as figure 21 but the PVP bonds are marked instead. The peaks and valleys between 1468 cm^{-1}1426 cm^{-1}represent C-H_2 scissoring which decreases in magnitude with increasing temperature. At 1370 cm^{-1} the C-C bond vibration in the PVP ring remains constant with increasing temperature. C-H_2 wagging at 1321 cm^{-1} decreases with increasing temperature. Between 790 cm^{-1} and 720 cm^{-1} C-H_2 deformation is present, which decreases with increasing temperature.

5.2 SEM & EDS Analysis of Ceramic Fibers

After the pyrolysis of preceramic fibers, the morphology and composition of the fibers must be investigated to ensure that the fibers have completed the pyrolysis process and are composed of the appropriate element ratios that reflect the desired ceramic. The diameter of the fibers may also be investigated and associated with the pyrolysis process – as unwanted material leaves the fibers during the pyrolysis process the fibers should decrease in size. The surface and interior of the fibers should also be analyzed to check for porosity, a characteristic property of ceramics.

This section will investigate the morphology and element composition of post pyrolysis PPS & AMT fibers in separate subsections.

5.2.1 PPS Fibers – SEM/EDS 2000 Magnification

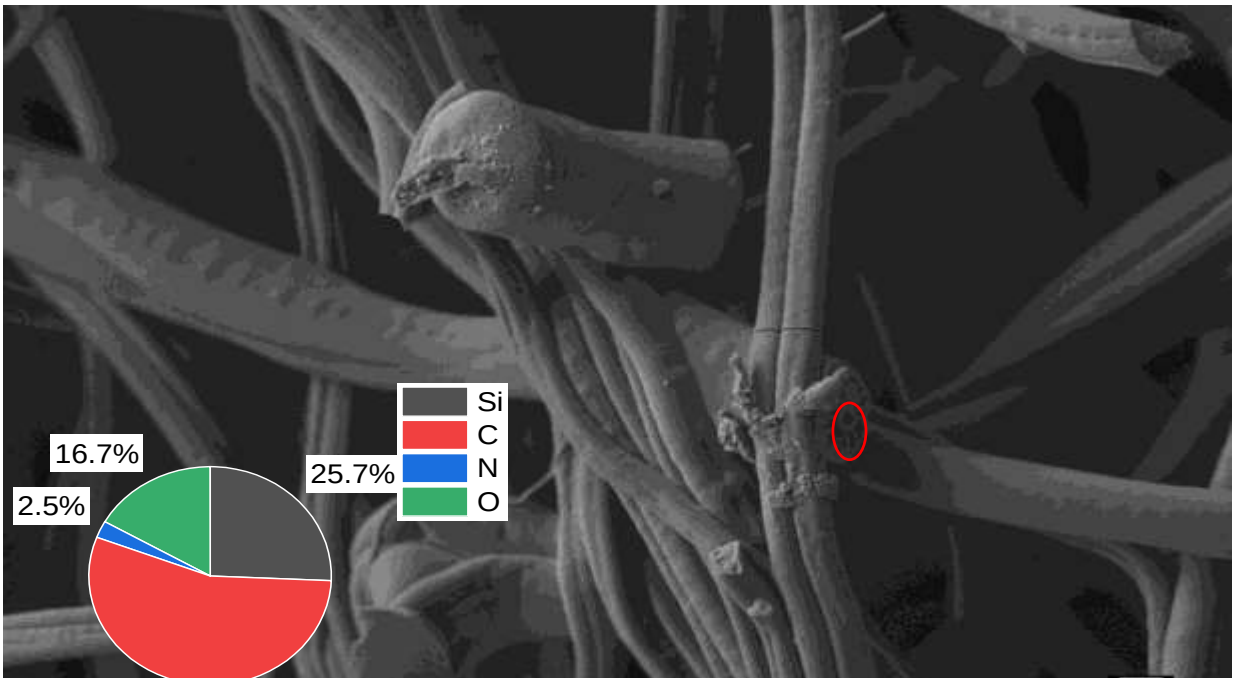

Figure 23: PPS Fibers 1000 °C SEM & EDS

Figure 23 shows PPS fibers at 2000 magnification that were heat-treated to 1000 °C. All the fibers are seen in this image range on the macro scale. The surface of the fibers are generally smooth but there is some roughness seen throughout the fibers. Towards the middle of the image, there is a large fiber with a smaller hollow fiber inside which is composed of the following atomic percentages: 70.84 % Si, 29.06 % C, .04 % N, and .06% O indicating completion of pyrolysis for SiC. The element composition of the material seen in the entire image is shown in figure 23, fibers mainly consist of carbon and silicon but there is a considerable presence of oxygen in the material. The nitrogen content is almost negligible indicating little to no presence of silicon nitride in the system, as expected since the formation silicon nitride typically occurs at temperatures above 1300 °C. Brittle fractures are also seen throughout the image which are confirmed by the semi-brittle behavior of the material during handling.

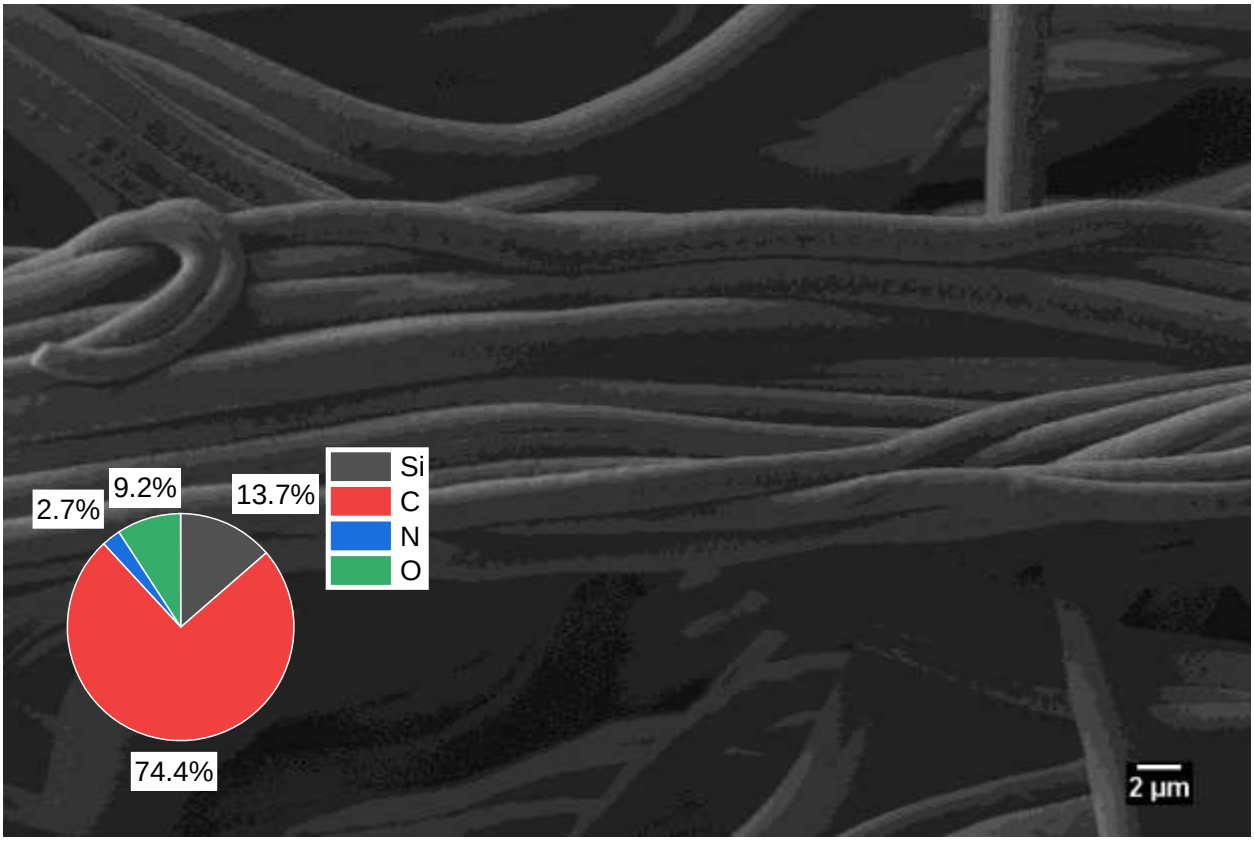

Figure 24: PPS Fibers 1100 °C SEM & EDS

SEM & EDS analysis was performed at 2000 magnification on fibers heat-treated at 1100 °C. No hollow fibers or porous fibers are visible and the fibers are fairly consistent in smoothness throughout. All fibers range in the microscale and consist of the same elemental composition which can be seen in figure 24. Again carbon is the dominant element in the system while the nitrogen content remains negligible. Oxygen content decreased by over 6% in the system getting closer to the ideal 0% of oxygen in the system. There is no evidence of brittle behavior in this image which could be due to the bundling of fibers seen in the image.

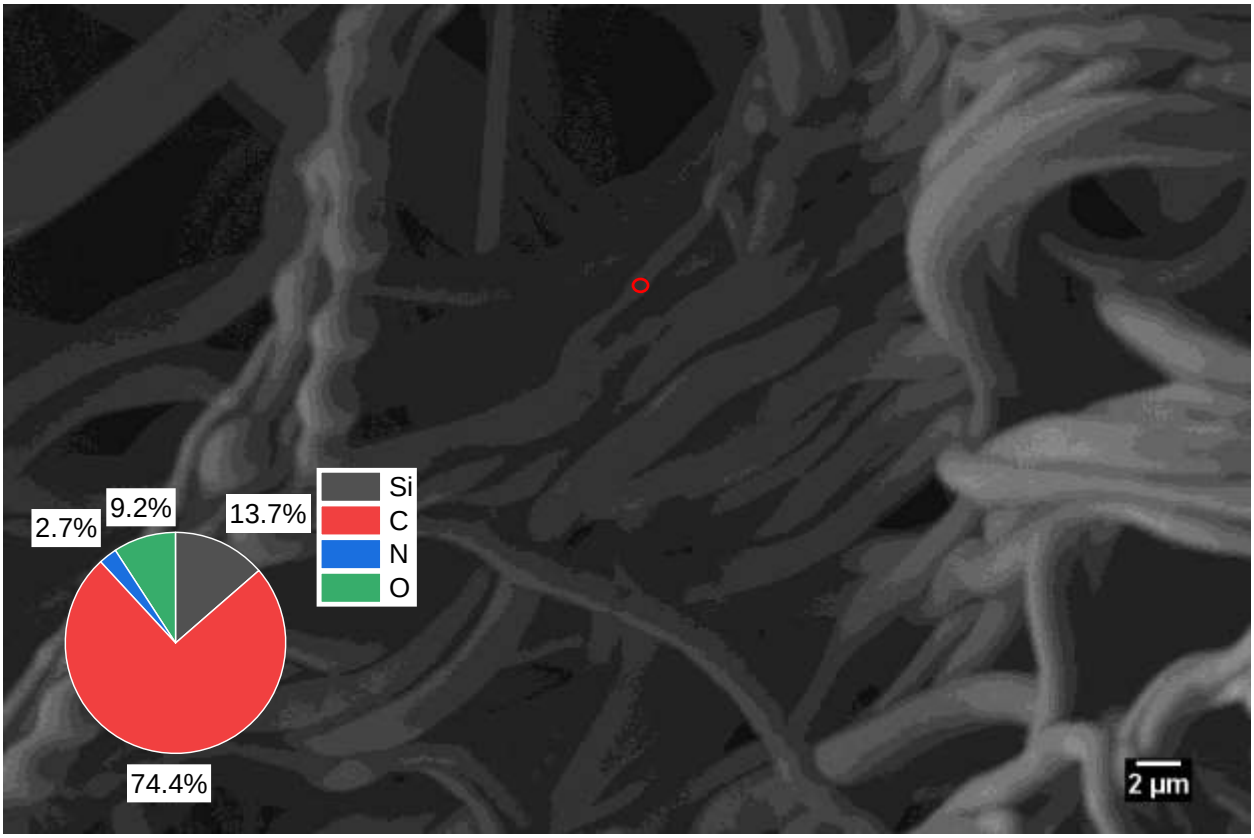

Figure 25: PPS Fibers 1200 °C SEM & EDS

The PPS fibers in figure 25 were heat-treated to 1200 °C and SEM & EDS analysis was done at 2000 magnification. Again there are no visible hollow or porous fibers. The fibers are mostly microscale with the exception of some fibers in the back being nanoscale. EDS done on the smaller, nanoscale, fibers reflected a better Si:C ratio. One nanofiber circled in red had 0 oxygen and was composted of 52% C and 48% Si. The material seen in the image was composed of mainly carbon and silicon as seen in figure 29. Again the fibers had negligible nitrogen in the system and some residual oxygen.

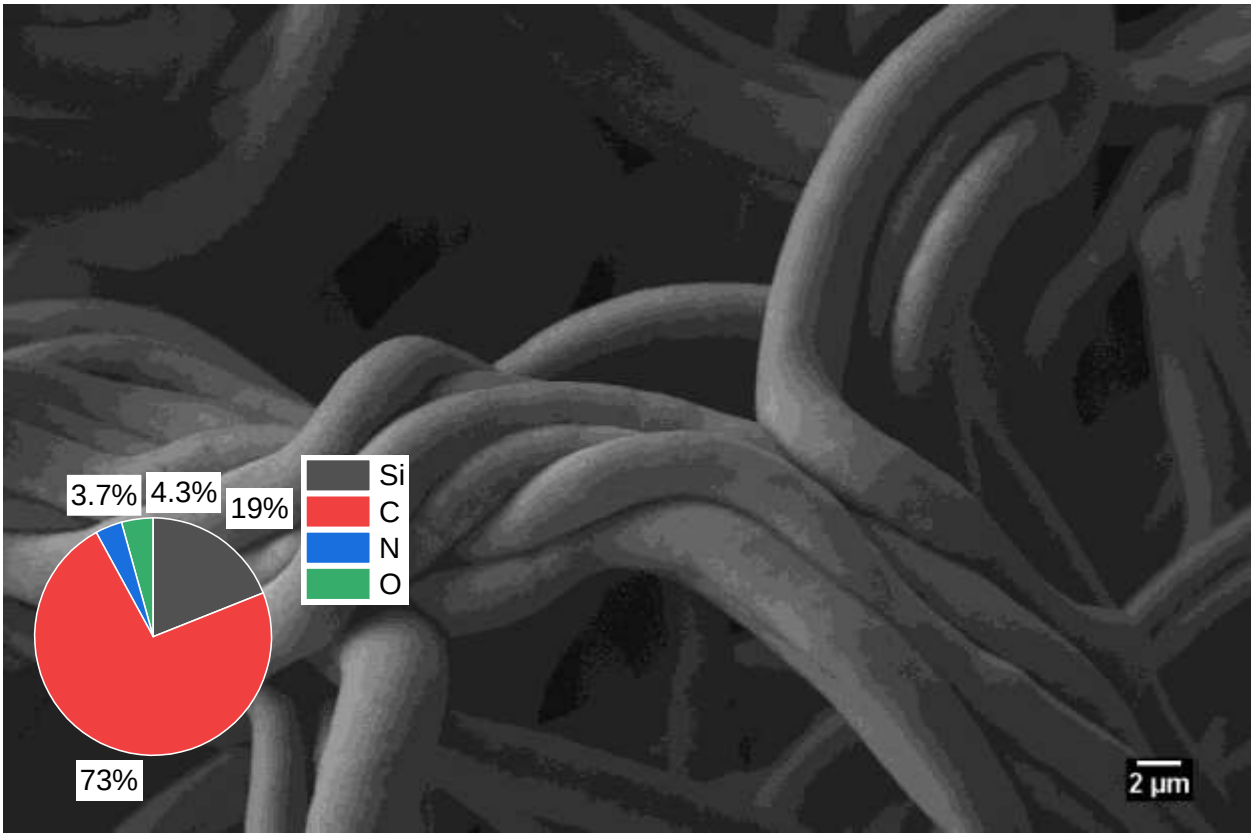

Figure 26: PPS Fibers 1300 °C SEM & EDS

PPS fibers heat-treated to 1300 °C were analyzed using SEM & EDS at 2000 magnification. All visible fibers appear smooth and are in the microscale. Several fibers were analyzed using EDS and reflected similar compositions when compared to the composition of the entire area of the material. Again, carbon is the main component in the system followed by silicon as shown in figure 26. Compared to the previous fibers the oxygen content is reduced by more than half. The nitrogen content in the system also increases by 1% suggesting the formation of silicon nitride. Another image taken at the same magnitude had visible fiber interiors (see appendix) the fiber interior was found to be composed of 40%, .5%, and 59.5% carbon, oxygen, and silicon respectively.

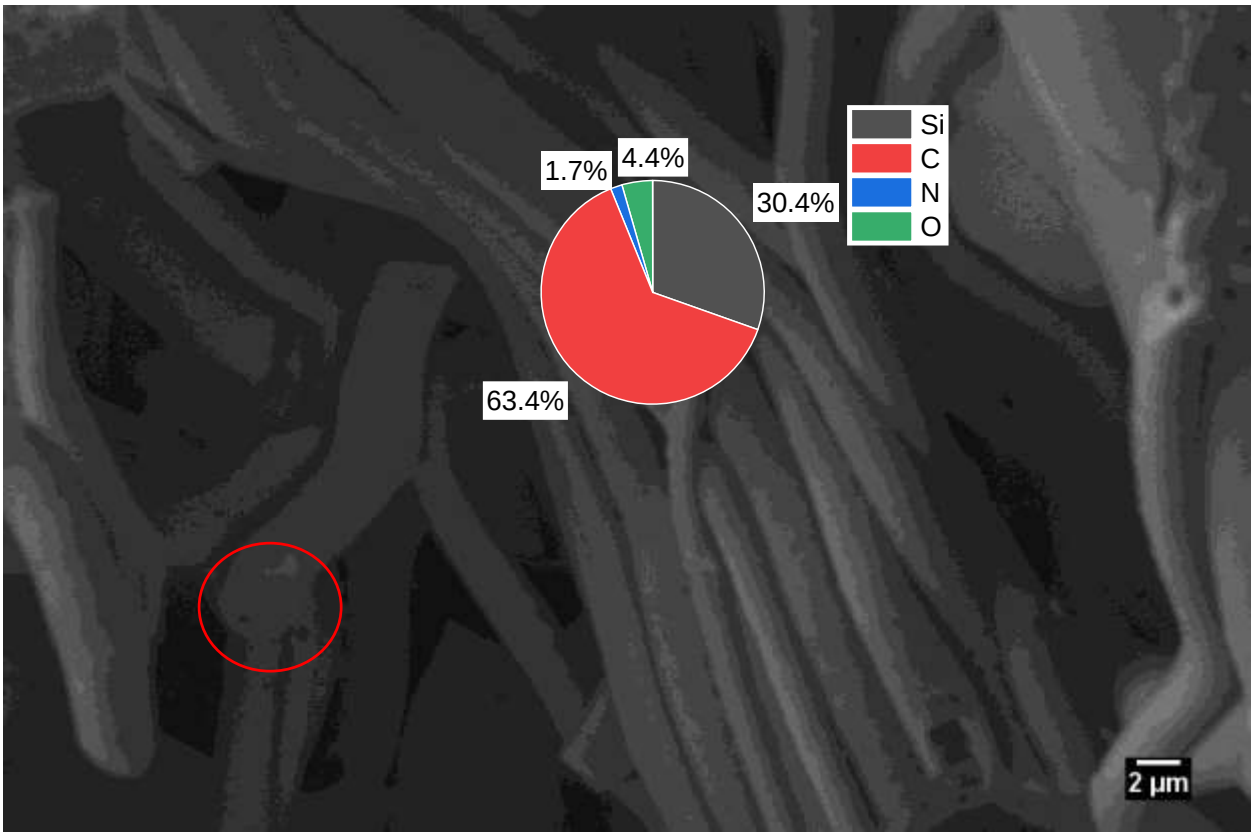

Figure 27: PPS Fibers 1400 °C SEM & EDS

PPS fibers treated at 1400 °C at 2000 magnification showed smoothness under the SEM while also exhibiting brittle behaviors as breaks in the fibers are seen. Fibers range from the microscale to the nanoscale, the larger fibers contain a higher percentage of carbon as confirmed by the EDS. Two fiber interiors were analyzed using EDS, circled in red, large fiber and small fiber. The larger fiber's interior composition consisted of 40% carbon and 60% silicon, a much higher silicon content than the surface of the fiber. The smaller fiber's hollow interior consisted of 48% carbon and 52 % silicon, a nearly perfect 1:1 ratio silicon carbide fiber.

EDS of the entire image showed that the carbon made up the majority of the material followed by silicon. The oxygen content is very low as a whole and no oxygen presence is detected for most fibers

5.2.2 PPS Fibers – SEM/EDS 250 Magnification

The surface of post-treated PPS fibers was analyzed at 250 magnification using SEM & EDS in conjunction. No visible beads or impurities were seen in any sample, however, the fusing of fibers is clearly seen. There are also considerably larger abnormalities of fibers throughout the samples. The fibers mainly occur in bundles, very rarely were individual fibers seen. The EDS results reflected a similar percent composition for the entire surface of every sample.

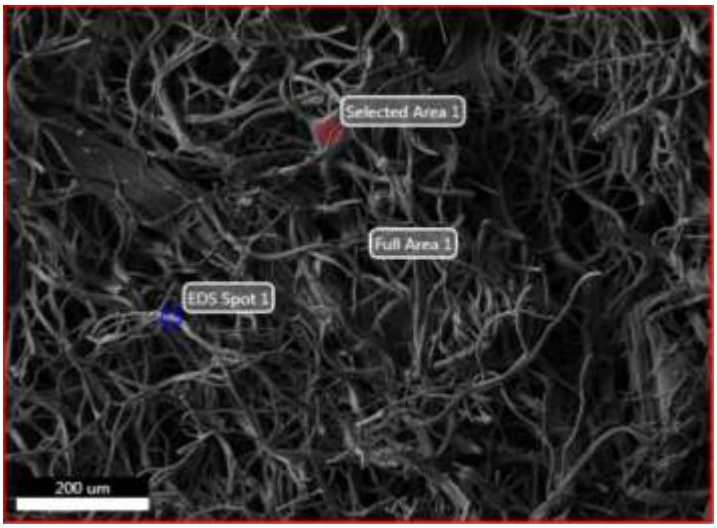

Figure 28: PPS Fibers 1000 C Surface EDS & SEM

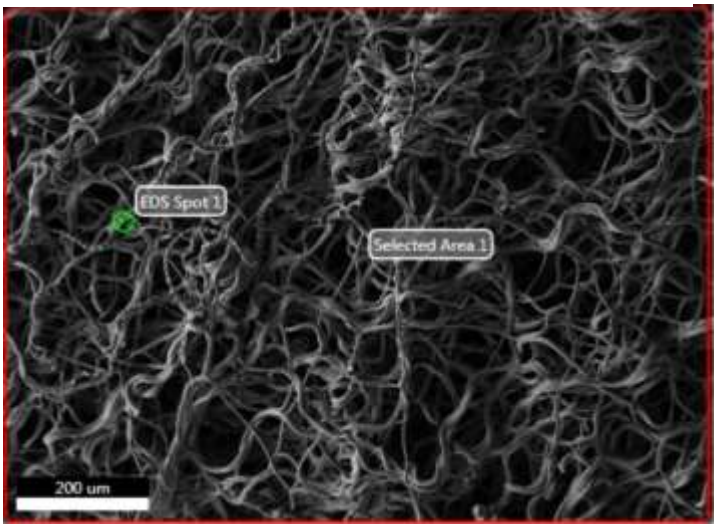

Figure 29: PPS Fibers 1100 °C Surface EDS & SEM

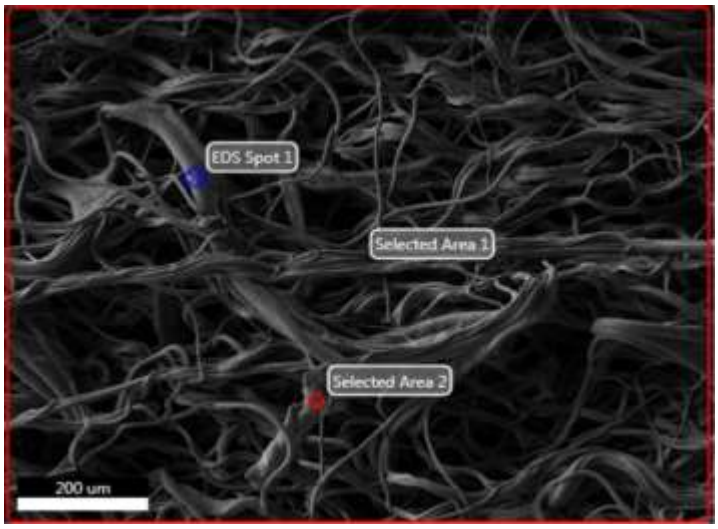

Figure 30: PPS Fibers 1200 °C Surface EDS & SEM

No significant changes in composition occurred between the samples the only exception being selected area 3 in figure 34 which was 100 % SiC at a 1:1 Si-C ratio. The composition of the entire area of the other fibers can be found in the appendix.

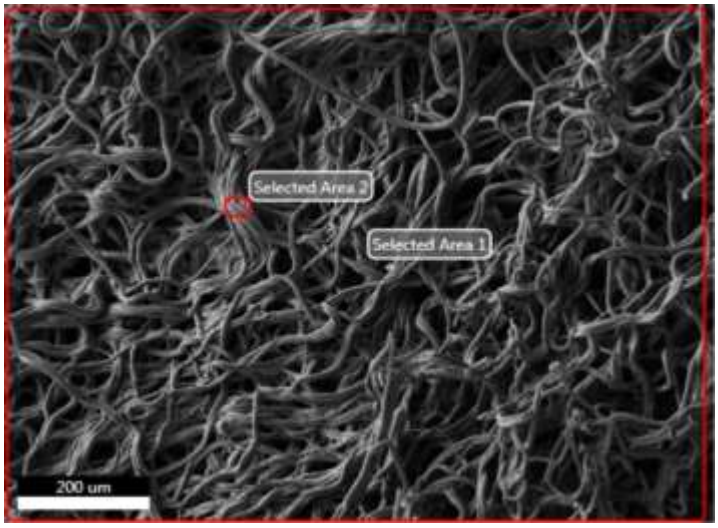

Figure 31: PPS Fibers 1300 °C Surface EDS & SEM

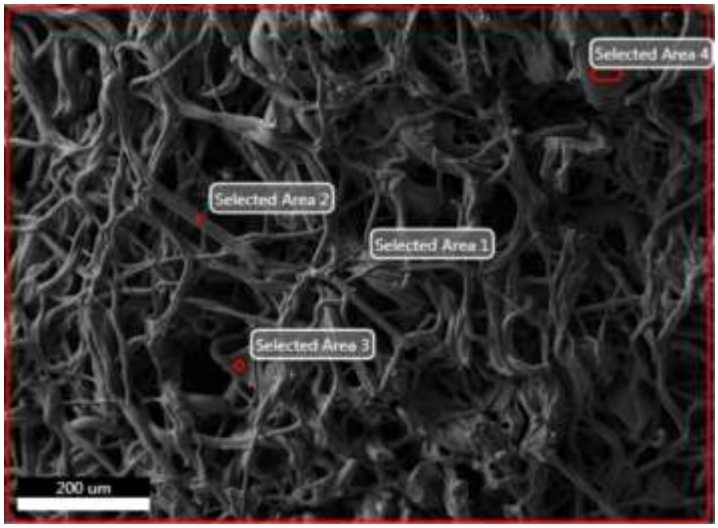

Figure 32: PPS Fibers 1400 °C Surface EDS & SEM

5.2.3 Fibers Si-C Ratio Overview

Using the average EDS data at 2000 magnification (including entire image) the Si-C ratios were compared. The highest values were seen for the 1000 °C and 1400°C samples.

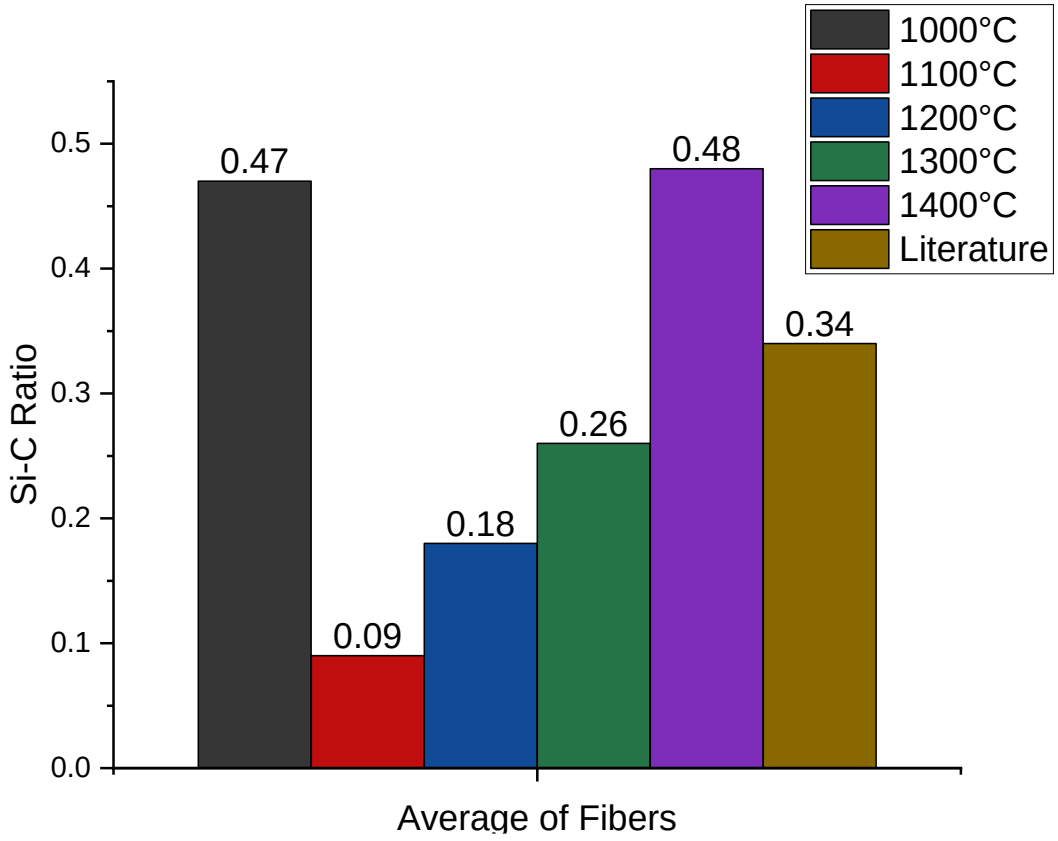

Figure 33: Si-C Average Ratios

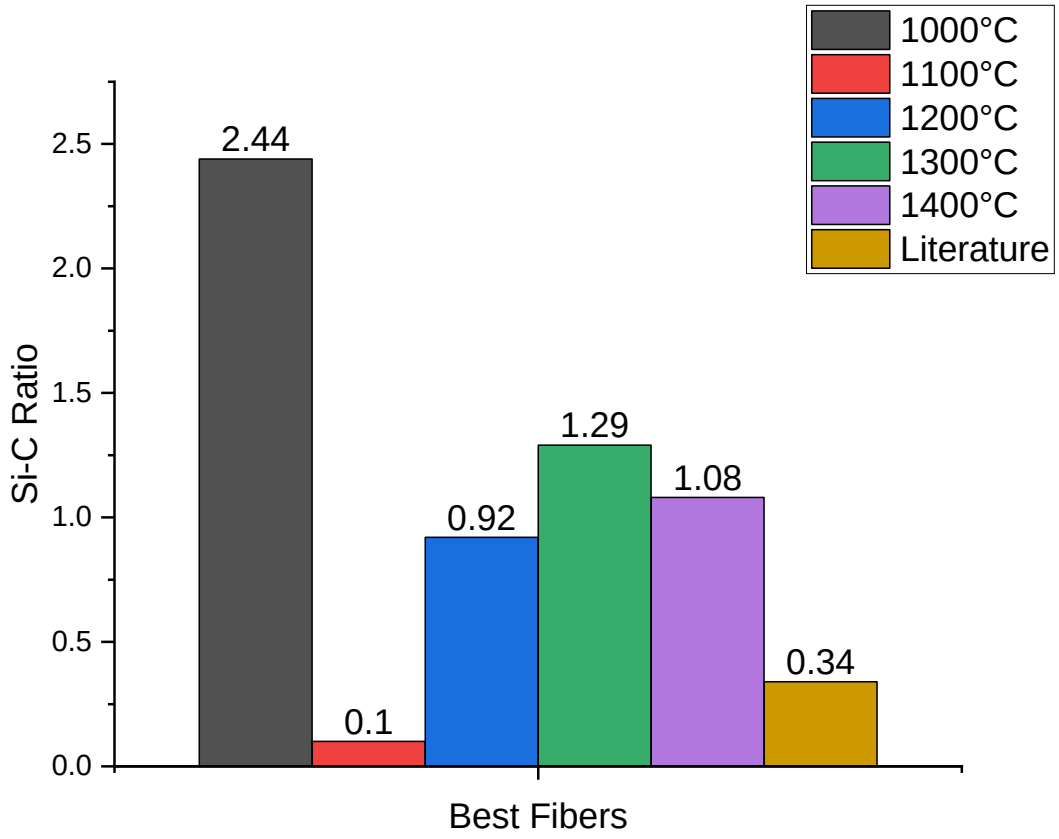

Figure 34: Si-C Best Fibers' Ratios

EDS data of fibers with the highest silicon content at 2000 magnification (including entire image) the Si-C ratios were compared. All fibers besides the 1100 °C sample had higher values than the previously force spun Si-C nanofibers. Additionally, these same fibers had oxygen content and the smallest diameters.

5.2.4 AMT Fibers – 60 min dwell time SEM/EDS 2000 Magnification

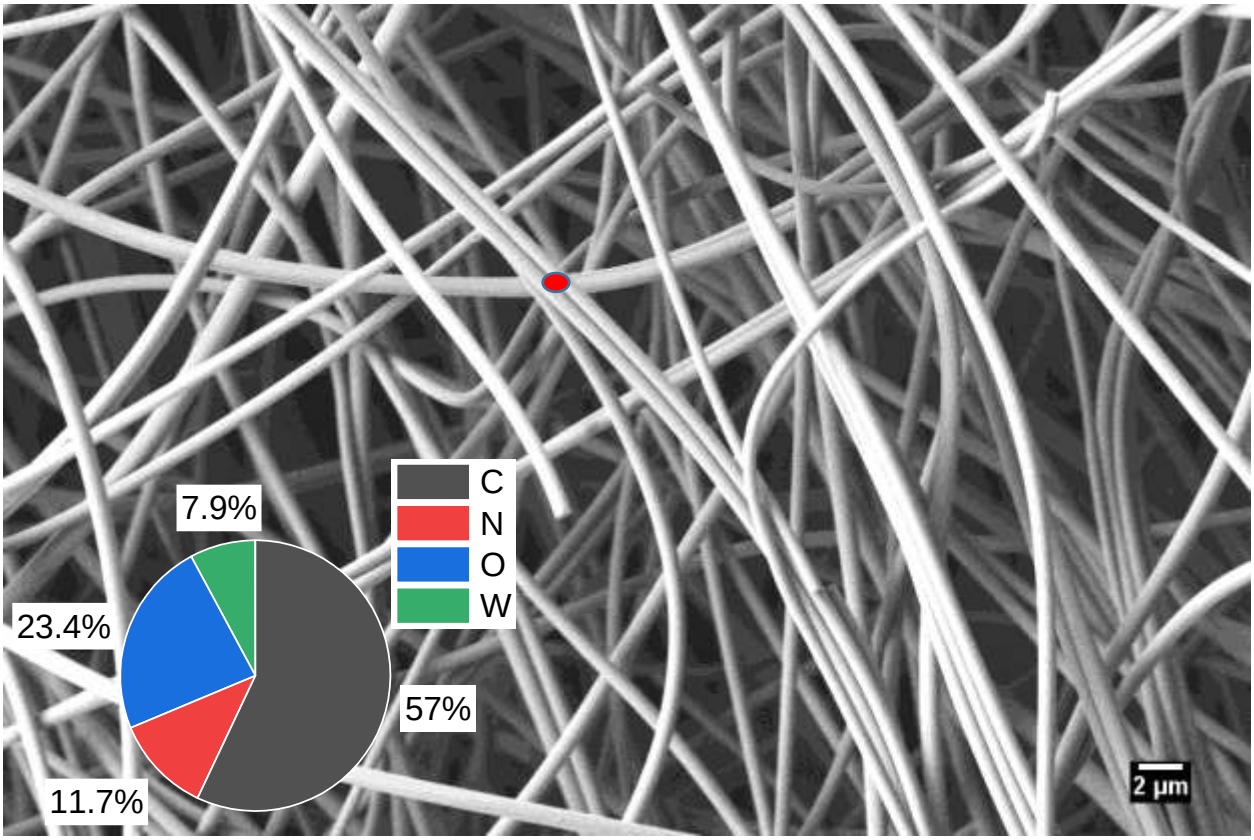

Figure 35: AMT Fibers 600 °C 60 min SEM & EDS

Figure 35 shows AMT fibers heat-treated at 600 °C for 60 minutes at 2000 magnification. The fibers ranged from 400 nm to 1300 nm in diameter with a uniform distribution (see appendix). The surfaces of the fibers are smooth with no visible defects. The EDS results of the area in red are seen in figure 35. These fibers are composed mainly of carbon while oxygen and nitrogen are more present than tungsten. Suggesting that the formation of tungsten carbide has not begun, ideally, tungsten carbide fibers will be composed of 50 % carbon and 50 % tungsten. The presence of nitrogen in the system indicates that the PVP component of the fiber has not fully decomposed while the oxygen content suggests that there are still W=O and C=O bonds from the AMT and PVP respectively.

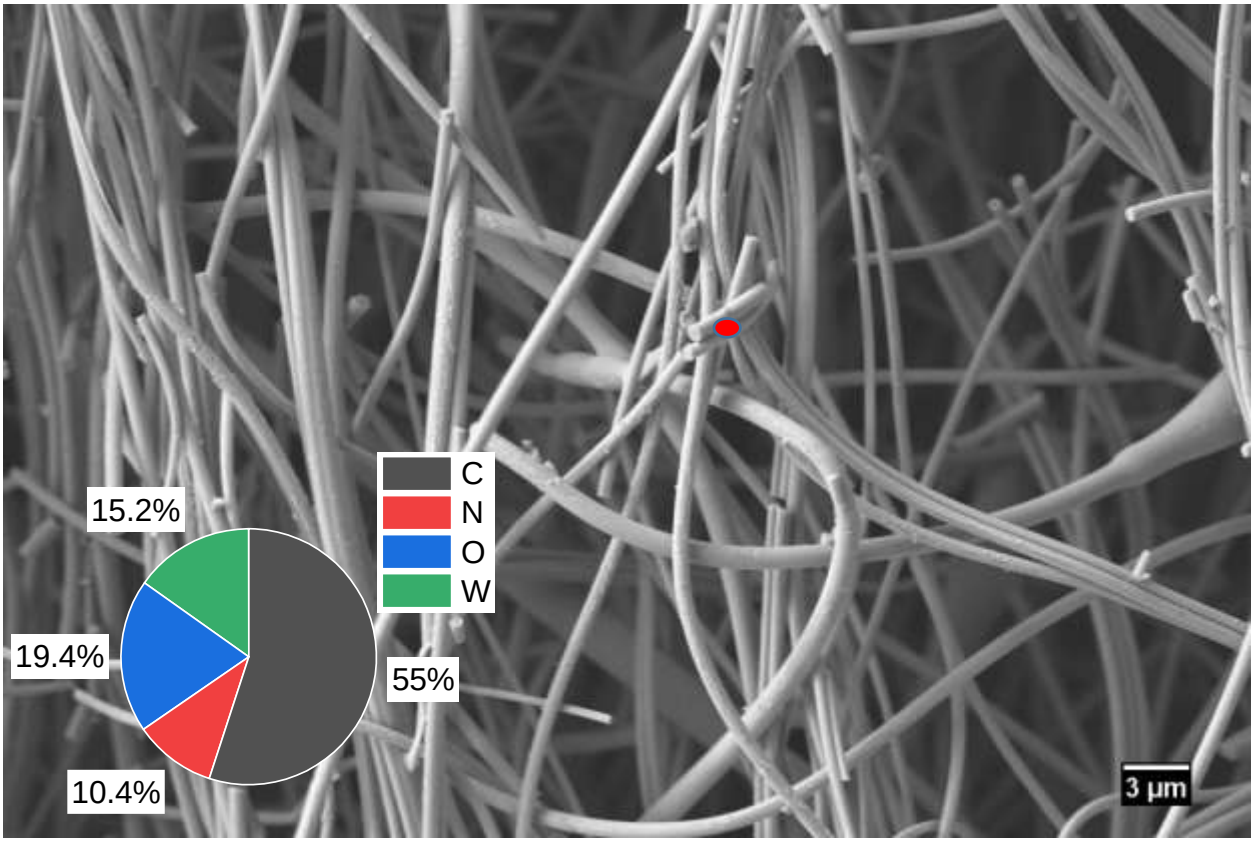

Figure 36: AMT Fibers 700 °C 60 min SEM & EDS

The red area in figure 36 EDS results are reflected by the pie graph seen in the figure. The presence of tungsten is almost doubled compared to figure 35 due to a decrease in all other components in the system. Fiber diameters range from 200 nm to 1600 nm with a uniform distribution (see appendix). As preceramic fibers transform into ceramic fibers it is expected that the fiber diameter decreases in size by 50 %. Thus, fibers with nitrogen and oxygen present should be larger than fibers that have only tungsten and carbon present. Pyrolysis time also plays an important role in ceramic transformation thus a longer pyrolysis time was also investigated for every heat treatment temperature to confirm the dominant factors in successful preceramic to ceramic transformation. Again it is expected that W=O and C=O bonds are still present from the AMT & PVP respectively. The movement of nitrogen molecules should also be detectable in this sample.

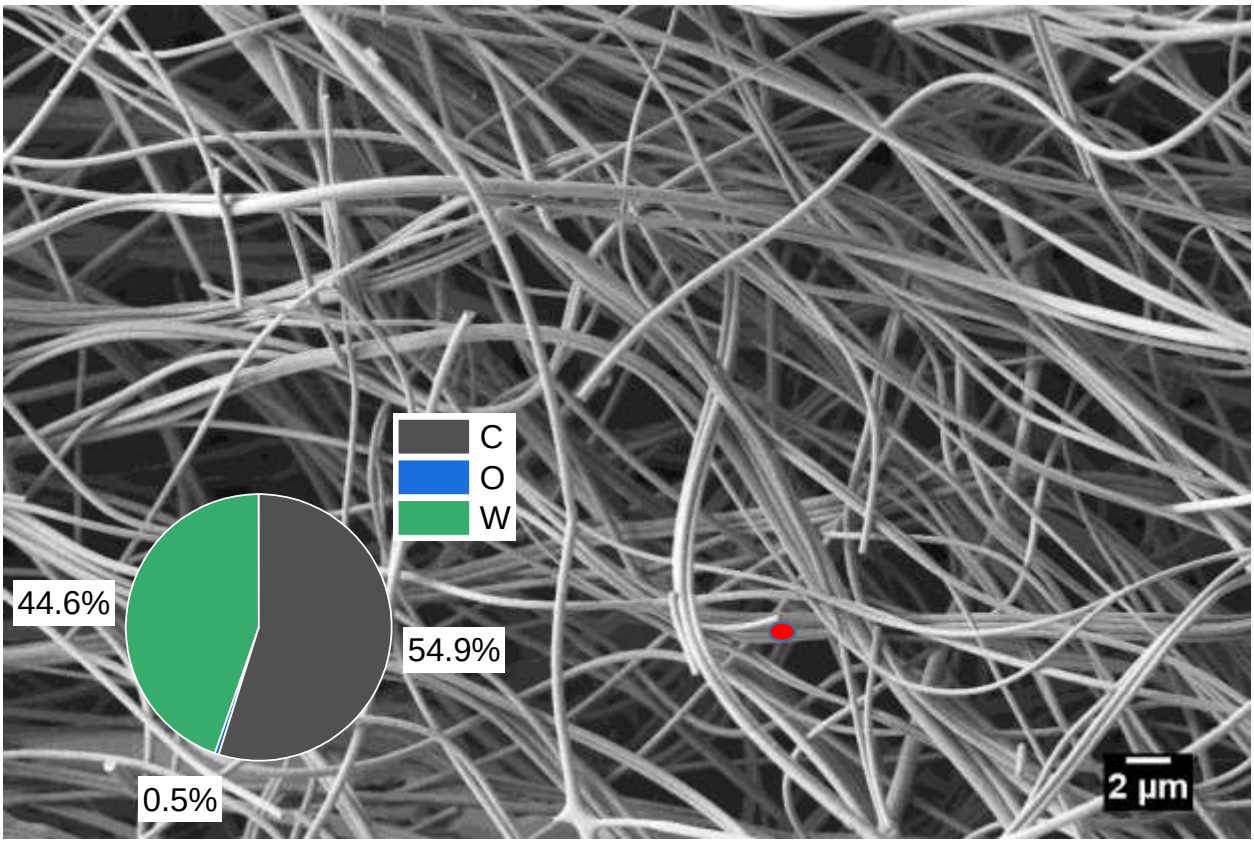

Figure 37: AMT Fibers 800 °C 60 min SEM & EDS

The composition of the fibers indicated by the red circle consists of mainly carbon and tungsten, a negligible amount of oxygen was also detected. The composition of fibers suggests that PVP is decomposed and that the fiber is composed of tungsten carbide. Suggesting that preceramic to the ceramic transformation of nanofibers occurs starting at 800 °C. SEM results show that the fiber diameter ranges from 100 nm to 700 nm with a uniform distribution (see appendix) also suggesting the transformation of fibers into ceramics. No visible beads or impurities can be seen in the SEM image however there are some short or broken fibers scattered throughout the image. There is also one branchlike structure that appears towards the bottom of the image. Again the dwelling time (pyrolysis time) plays an important factor in phase transformation thus it necessary to investigate a longer dwell time than 60 minutes.

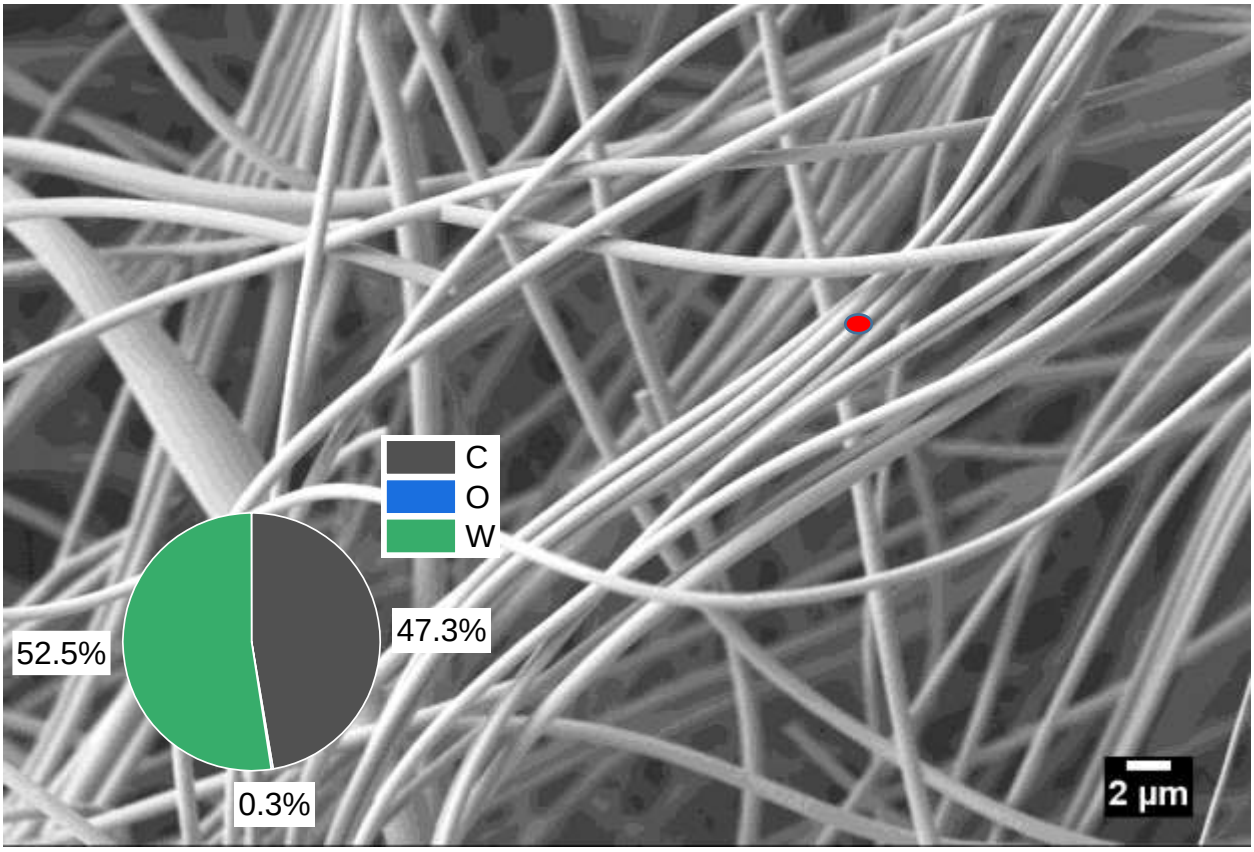

Figure 38: AMT Fibers 900 °C 60 min SEM & EDS

The EDS of the fibers marked in red shows a closer 1:1 ratio between tungsten and carbon compared to figure 37. The oxygen content of the fibers is also slightly lower, suggesting that 900 °C could promote a better transformation of preceramic to ceramic fibers. The fibers range from 400 nm to 1300 nm with a uniform distribution (see appendix), which on average were higher than those seen in figure 37. It is unexpected that fibers in figure 38 would have a larger fiber diameter compared to those in figure 37 as a direct inverse correlation is expected between temperature and fiber diameter. Eventually, the effect of temperature on fiber diameter should level out as there would no longer be material to decompose and preceramic to ceramic transformation. These results indicate that the initial preceramic fibers for this sample were larger than those seen in figure 37, which is due to the Forcespinning© process.

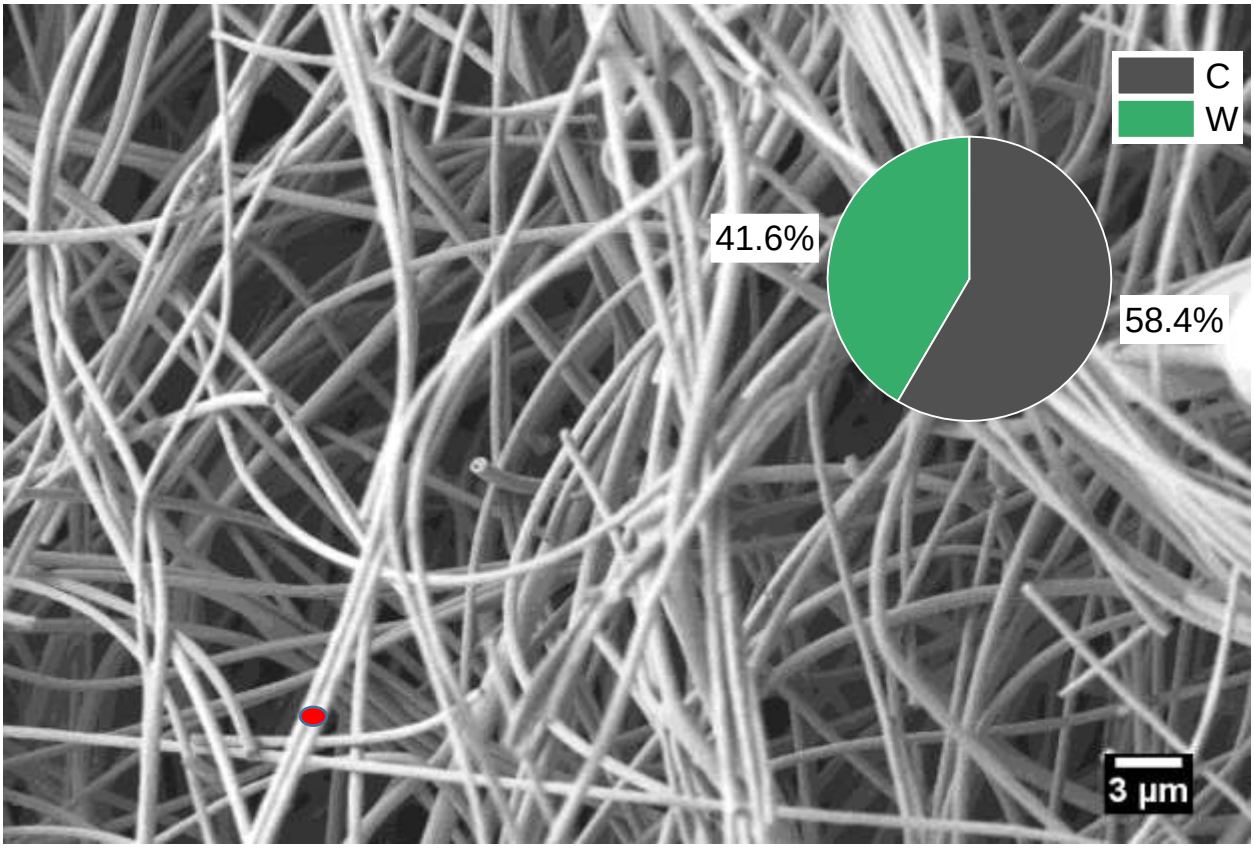

Figure 39: AMT Fibers 1000 °C 60 min SEM & EDS

Figure 39 reflects no oxygen presence in the fibers circled in red as well as a higher carbon composition when compared to figure 38. Fibers show some surface roughness and hollow fibers can be seen scattered throughout the image. The diameter of the fibers ranges from 200 nm to 800 nm with a uniform distribution (see appendix).

EDS results from figure 39 suggests that there is no improvement in the tungsten to carbon ratio in the fibers when increasing from 900 °C to 1000 °C. The amount of tungsten carbide present in the sample can't be confirmed by EDS thus additional characterization techniques such as FTIR and XRD should be implemented to confirm the phases in the material especially for the samples heat-treated between 800 °C to 1000 °C which is where the preceramic to ceramic transformation is suggested by EDS.

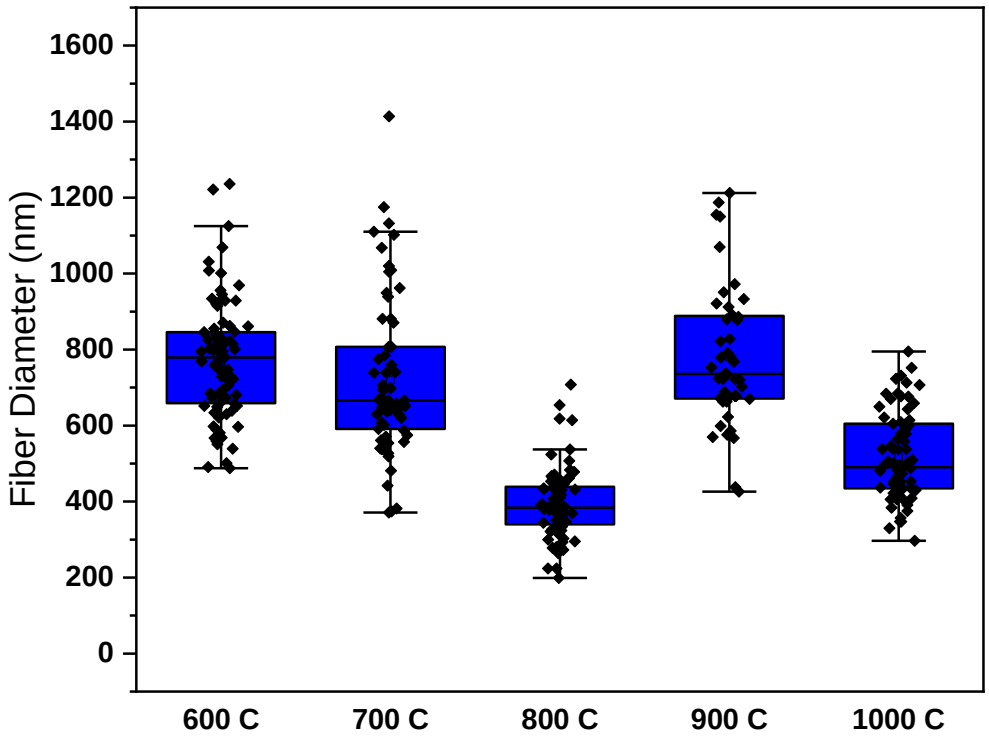

Figure 40: Fiber Distribution 60 min Dwell Time

Figure 40 shows the fiber diameter distribution for all samples that were heat-treated for 60 minutes. As mentioned the fiber diameter should decrease with increasing temperature however the average diameter changes from 774. 720, 393, 781, to 517 nm from left to right respectively. Also, the distribution of fiber diameters should tighten as temperature and dwell time increases.

5.2.5 AMT Fibers –120 min dwell time SEM/EDS 2000 Magnification

The same approach as discussed in section 5.2.4 was applied to fibers heat-treated for 120 minutes, twice as much as the 60 minutes dwell time. In theory, an increase in dwell time should promote more phase transformation at temperatures where it occurs. Longer dwell times should also narrow the fiber diameter distribution. SEM & EDS analysis was conducted on all samples but the focus will now be on samples heat-treated from 800 °C to 1000 °C.

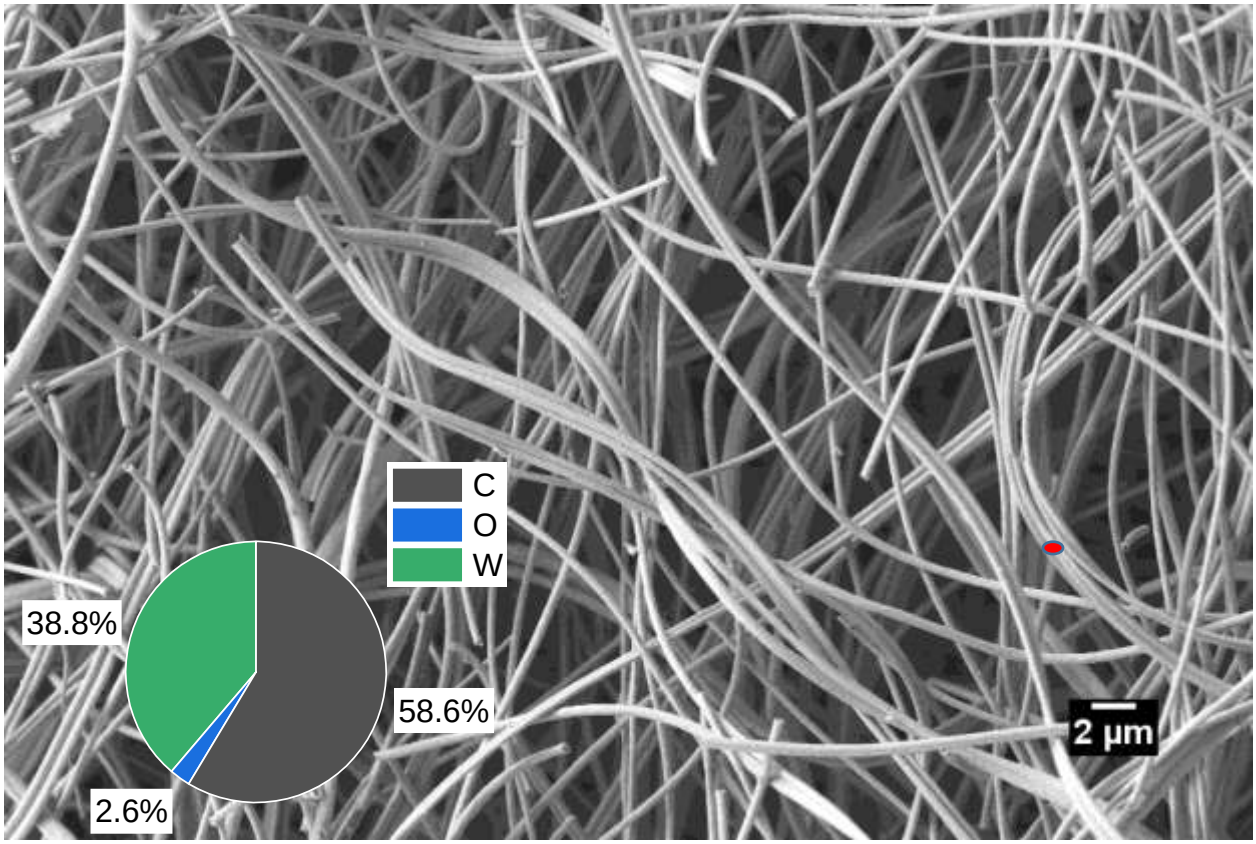

Figure 41: AMT Fibers 800 °C 120 min SEM & EDS

Figure 41 suggests that the dwell time does not affect the elemental composition of the nanofibers as the atomic percentages shown in the figure are similar to the fibers dwelled for 60 minutes. Also, the overall fiber diameter remained the same, ranging from 200 nm to 700 nm with a uniform distribution (see appendix). The surface of the fibers appears smooth and short fibers can be seen scattered throughout the image.

Hollow fibers are also visible and frequent throughout the image which could be attributed to the orientation of the fibers in the sample and is not necessarily an effect of dwell time. FTIR and XRD can be conducted to investigate the effect of dwell temperature more.

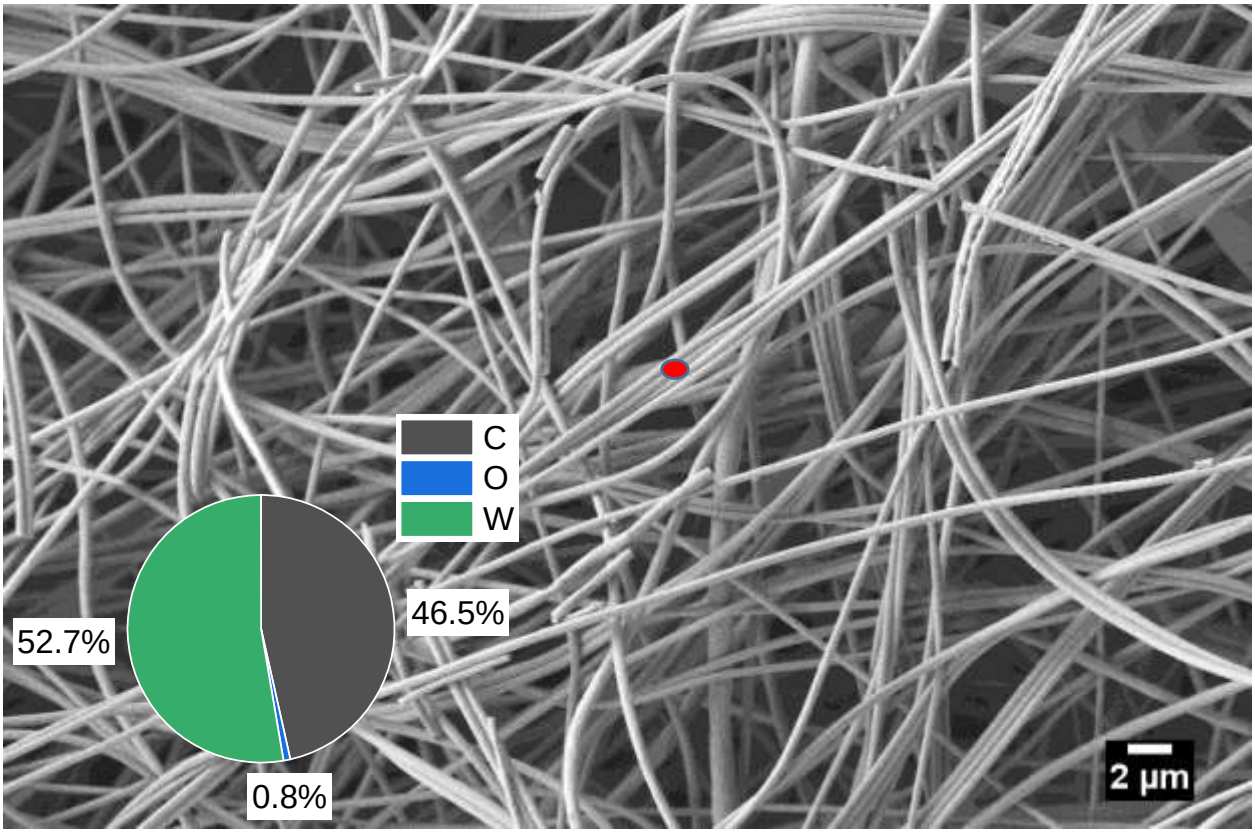

Figure 42: AMT Fibers 900 °C 120 min SEM & EDS

Fibers seen in figure 42 appear predominantly smooth but fibers with rough surfaces can be seen throughout the image as well as short fibers. The composition of the selected fibers circled in red is similar to the fibers that were dwelled for 60 minutes suggesting that additional characterization techniques must be used to investigate the effect of dwell time further.

The fibers range from 200 nm to 700 nm in size with a uniform distribution (see appendix).

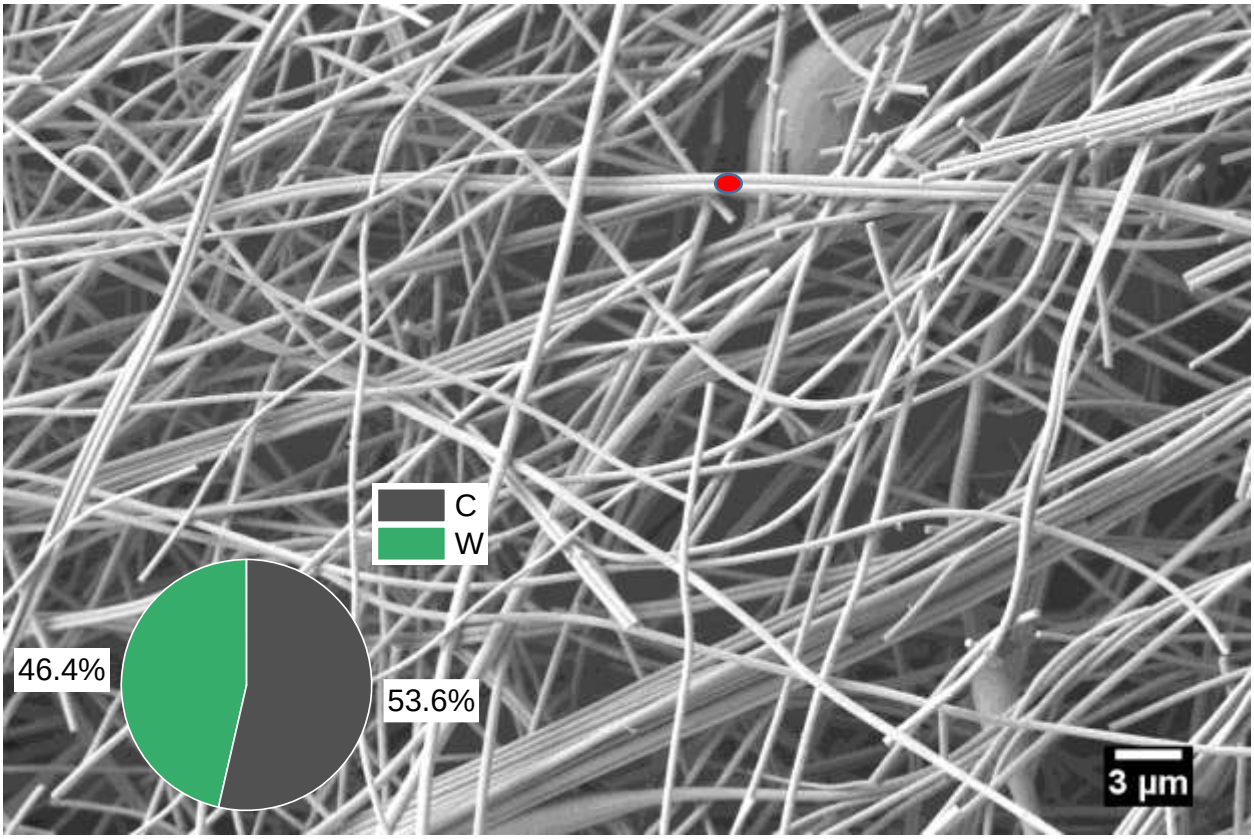

Figure 43: AMT Fibers 1000 °C 120 min SEM & EDS

Figure 43 shows a similar composition for the fibers selected in the image when compared to the 60 minute dwell time. The fibers are generally smooth with some debris being seen on the surface scattered throughout, note that all debris was found to be consistent with fiber composition or had a higher tungsten content. A bead can also be seen in the image which mainly consists of carbon, beads are undesirable in the fibers as they can serve as point defects in a composite matrix as well as prevent proper wetting between fibers and a matrix.

The fiber diameter of the fibers ranged from 100 nm to 600 nm having a uniform distribution (see appendix). Short fibers (lengthwise) are seen scattered throughout the image, longer fibers are better for composite applications, as discussed in the literature review.

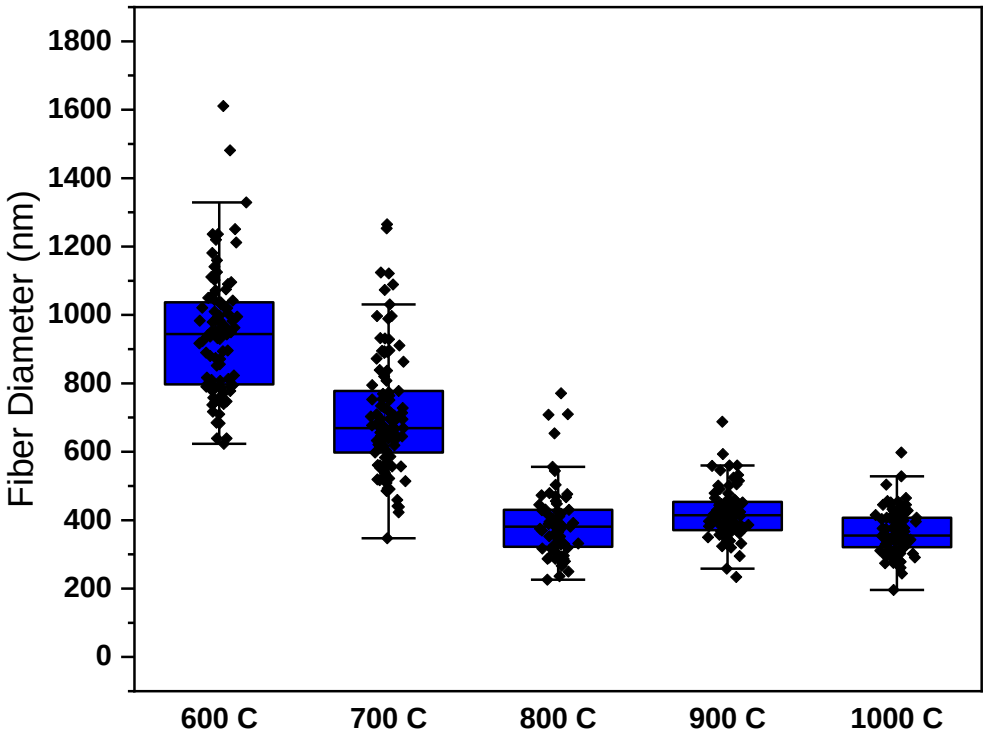

Figure 44: Fiber Distribution 120 min dwell time

Figure 44 shows the fiber diameter distribution for all samples dwelled for 120 minutes at their respective temperatures. An inverse correlation between temperature and fiber diameter is seen as the average fiber diameter changes from 945, 707, 393, 420, 365 nm from left to right.

The fiber diameter distribution is also more closely packed with increasing temperature and dwell time when compared to figure 44.

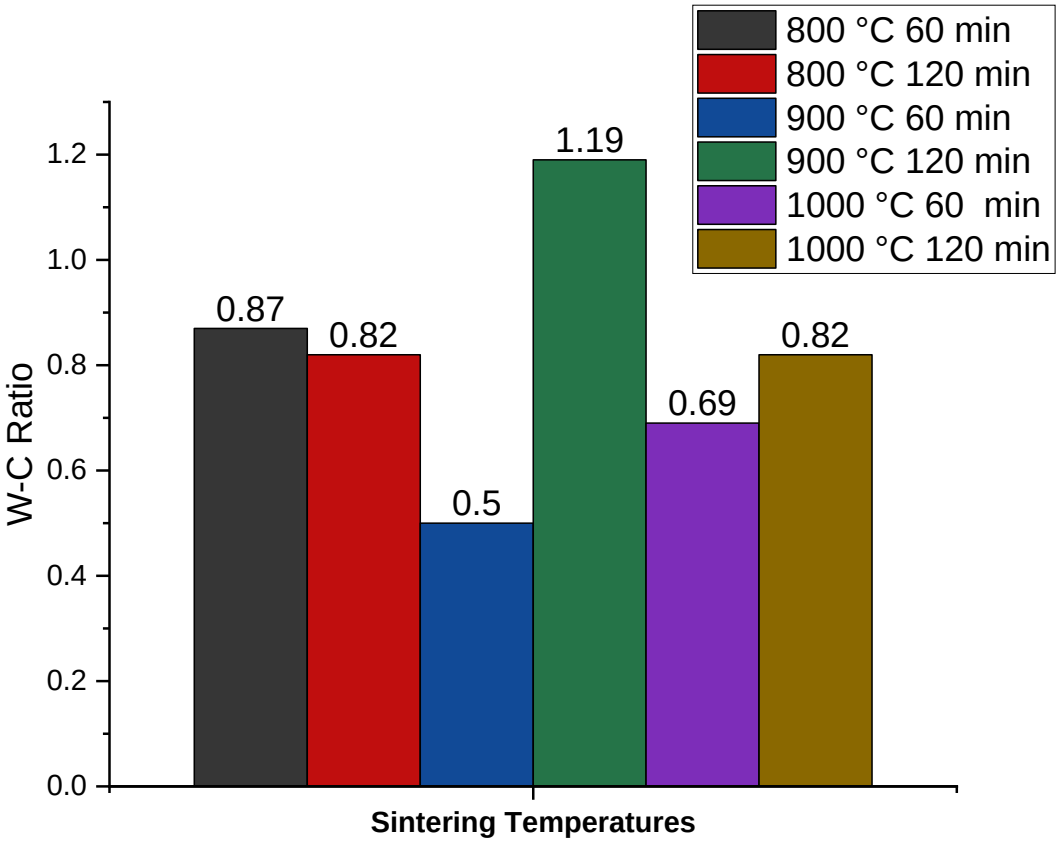

Figure 45: W-C Ratios of AMT Fibers

The W-C ratio of the entire are of the images seen in this section are shown in figure 45 for various heat treatment temperatures and dwell times, a ratio closer to 1 is desired as that reflects the WC ceramic. On average the fibers dwelled for 120 minutes time exhibit better results than those only dwelled for 60 minutes. Again the fibers heat-treated at 900 °C for 60 minutes appear to be an outlier, which can be attributed to the nature of Forcespinning©. As explained in chapter 3 fiber diameter increases during the spinning process as there is less solution to drive an inertia force however that does not explain the W-C ratio. One explanation is the solution not being completely homogenous which allowed the heavier homogenous part of the solution to travel through the syringe first, forming smaller fibers with a higher amount of

AMT while the solution exiting later during the spinning process was composed mainly of PVP forming larger fibers with less AMT.

5.2.6 AMT Fibers – SEM/EDS 250 Magnification

The surface of AMT fibers was analyzed after heat treatment for various temperatures and dwell times to identify impurities, beads, and imperfections in the samples. It is especially important to understand to what degree these items occur since they will influence the DMA

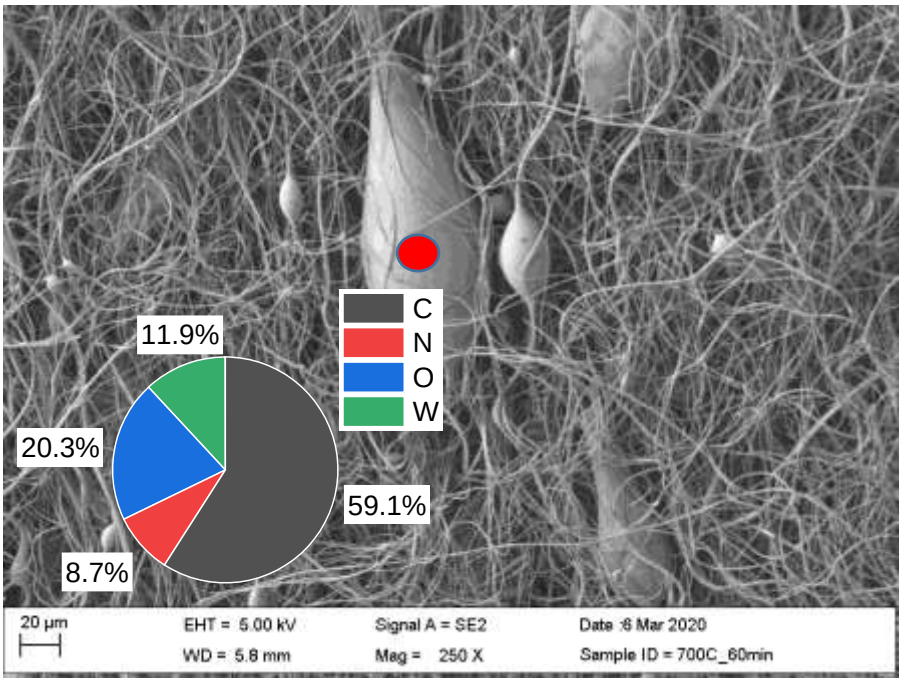

Figure 46: AMT Fibers 700 °C 60 min Surface SEM & EDS

composite properties. Ideally, no impurities, beads, or imperfections in the sample would allow the nanofibers to combine perfectly into the UHMWPE matrix. However, the SEM results show beads and imperfections with high carbon content in every sample as seen in the following figures as marked by the red circles:

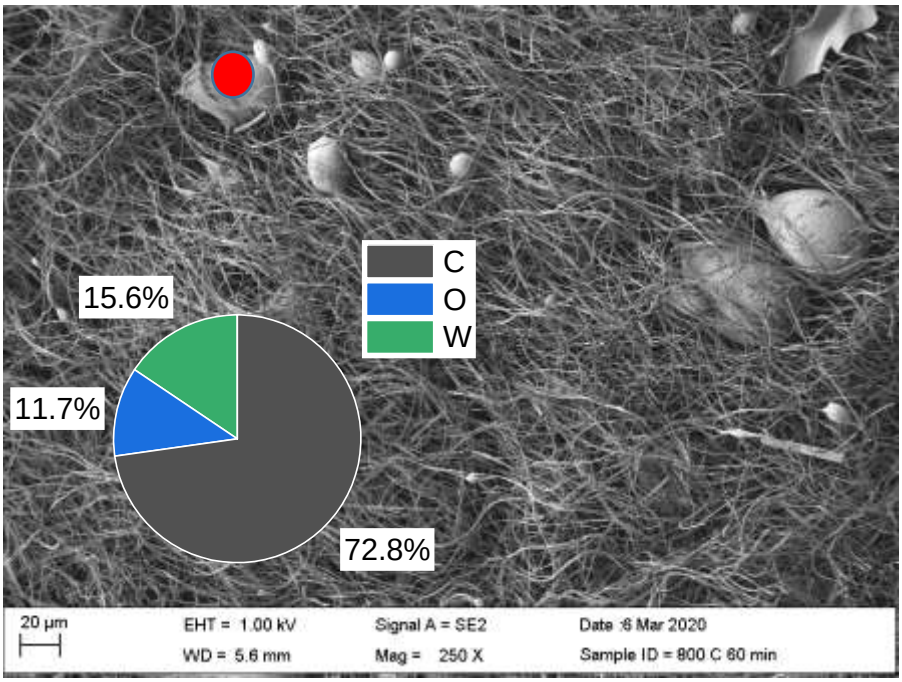

Figure 47: AMT Fibers 800 °C 60 min Surface SEM & EDS

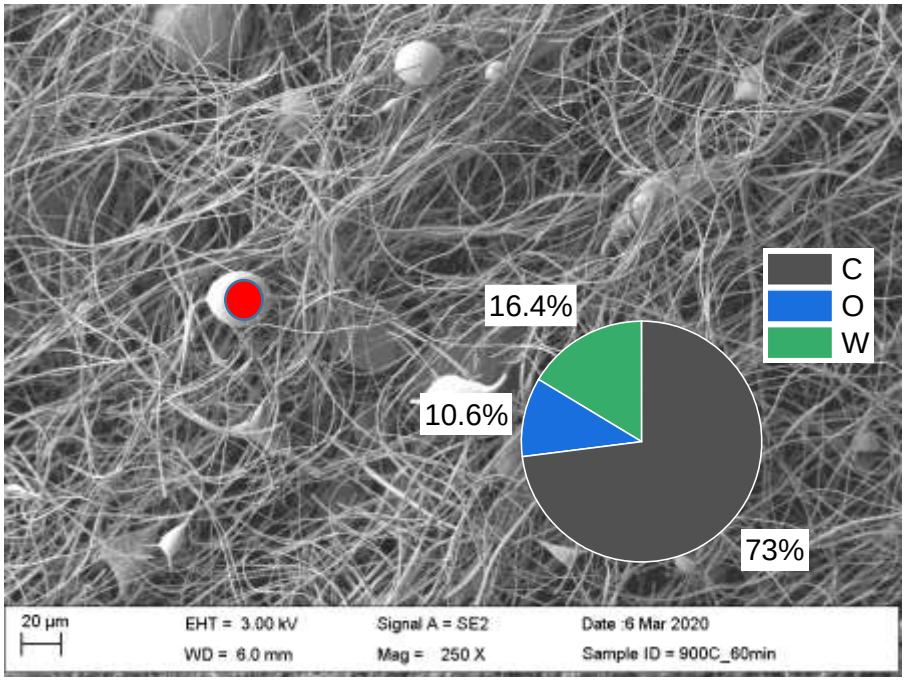

Figure 48: AMT Fibers 900°C 60 min Surface SEM & EDS

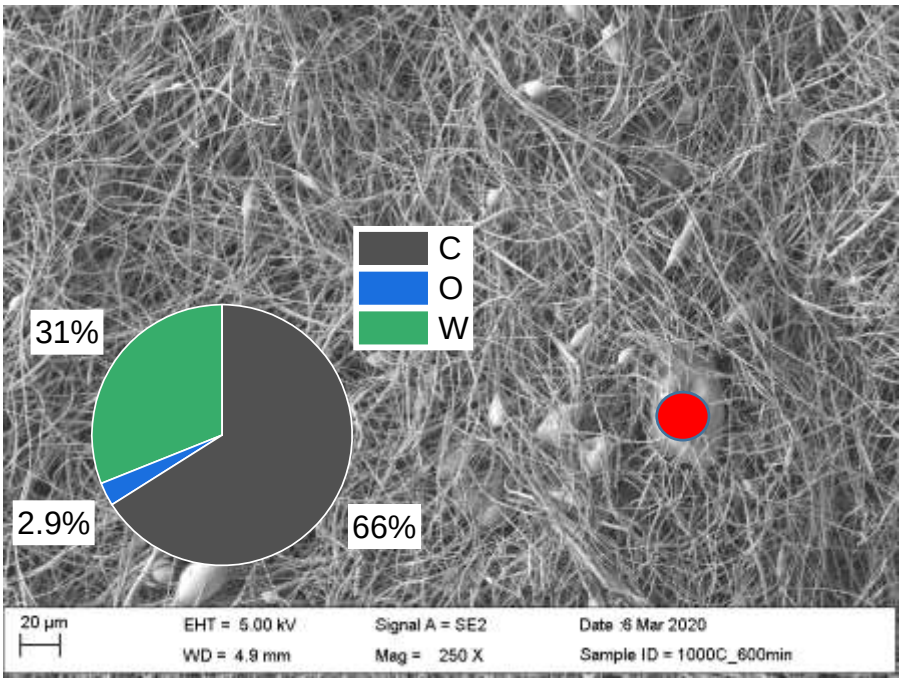

Figure 49: AMT Fibers 1000 °C 60 min Surface SEM & EDS

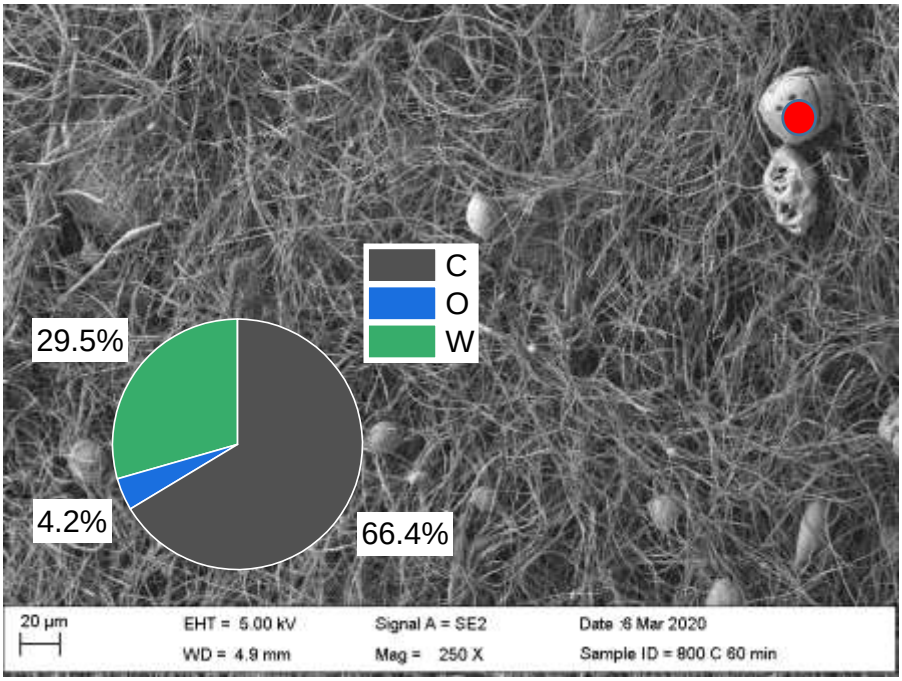

Figure 50: AMT Fibers 800 C 120 min Surface SEM & EDS

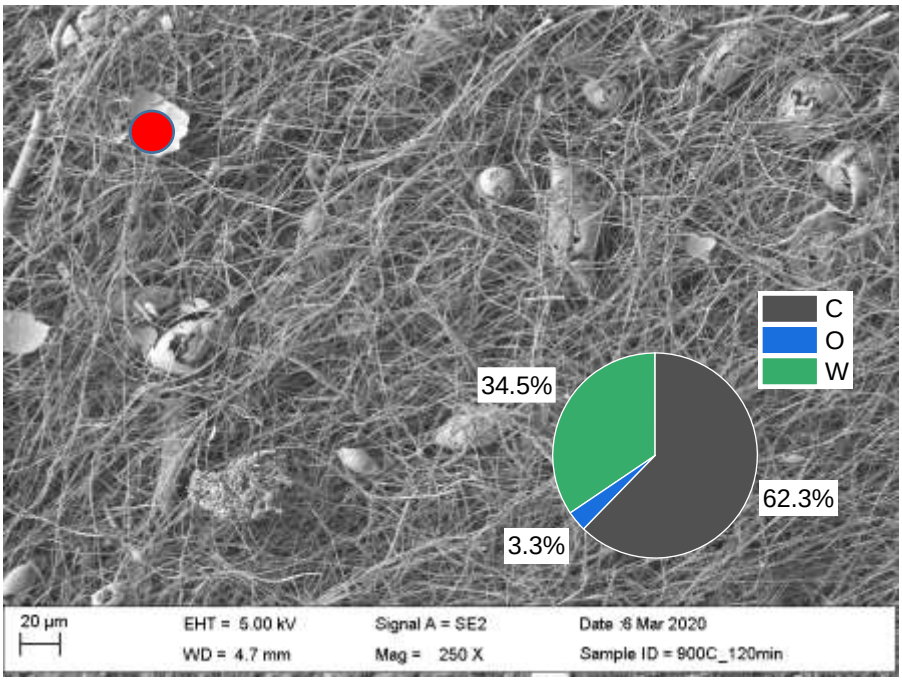

Figure 51: AMT Fibers 900 C 120 min Surface SEM & EDS

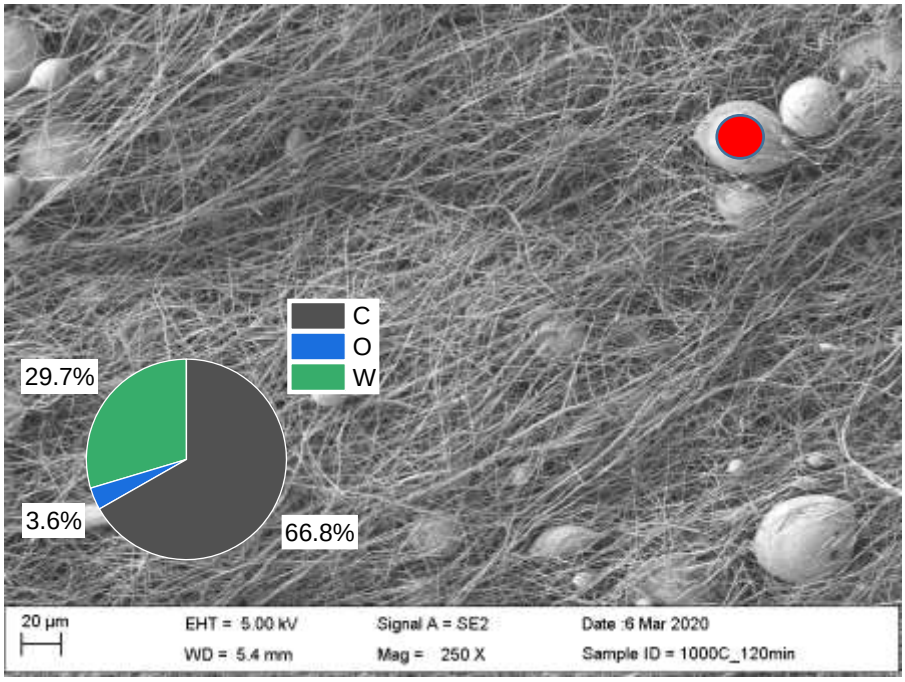

Figure 52: AMT Fibers 1000°C 120 min Surface EDS & SEM

In temperatures before 800 °C, the beads and impurities consist of nitrogen as well as carbon, oxygen, and tungsten. While after 800 °C the composition of the beads remains similar

regardless of temperature or dwell time. Beads are consistent throughout the samples and are in the microscale sometimes exceeding 20 μm, these beads are mainly composed of carbon and are similar in composition throughout the sample. The presence of these beads is impurities that are likely to lower the performance of any formed composite samples.

5.3 FTIR of Treated PPS & AMT Fibers

The properties of the produced fibers depend on their ceramic phase and overall composition. Silicon carbide exists in two primary phases β and α which are typically formed at below and above 1700°C respectively while silicon nitride has three phases – α,β,γ each corresponding to a unique crystal structure (trigonal, hexagonal, and cubic respectively). Tungsten carbide fibers can exist in two phases, WC and W_2C. Each of these respective phases has a unique chemical footprint which may be reflected in FTIR. Thus the FTIR analysis should indicate the presence or absence of these ceramic components in the fibers.

However, studies have shown that ceramic phases may sometimes be missing from the FTIR but confirmed through other spectra characterization techniques such as XRD and Raman Spectroscopy [59]. Recall from the EDS analysis that PPS fibers consist of mainly carbon and secondly silicon followed by oxygen than nitrogen. For those reasons it is expected that the dominant peaks be reflective of carbon bonds. Other points of interest in PPS are those that reflect Si-C and Si-N bonds.

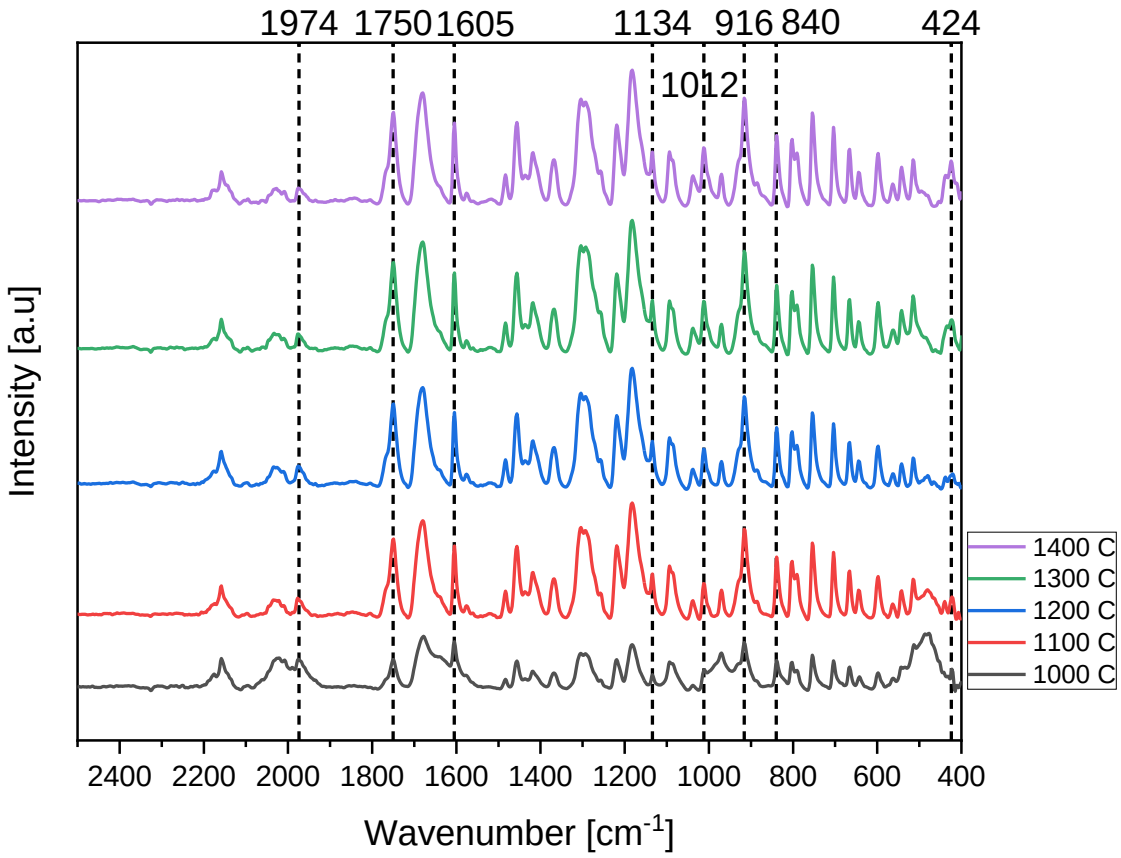

Figure 53: FTIR of Heat Treated PPS Fibers

FTIR analysis of treated PPS fibers showed a large number of peaks, for now, the peaks marked will be the focus of discussion. As temperature increases the intensity of most peaks increases as well, indicating an increase in bonds. At 1974 cm^{-1} Si-C-N is depicted and remains stable throughout the heat treatments. 1750 cm^{-1} and 1605 cm^{-1} represent C=O and C=C vibrations, respectively, each of these increasing with temperature. The peak at 1134 cm^{-1} represents the lower orbital of Si_3N_4 which increases in intensity between 1000 °C and 1200 °C before stabilizing. 1012 cm^{-1} signifies Si-O or Si-O_2 which increases in intensity with temperature. Si-N-Si bonds are depicted by the peak at 916 cm^{-1} which increases in intensity before stabilizing between 1300 °C and 1400°C. Peaks between 754 cm^{-1} and 1000 cm^{-1} also, indicate Si-C stretching as seen in the peak at 840 cm^{-1} which increases in intensity with

temperature before stabilizing between 1300 °C and 1400°C. Si-N wagging of Si_3N_4 is seen 424 cm^{-1} whose peak can be seen at 1300 °C and 1400°C.

FTIR analysis suggests that the transformation process peaks at 1300 °C with no distinguishable changes at 1400 °C. Literature suggests that at 1500 °C the β phase of Si_3N_4 will start to appear so the assumed phase of all the Si_3N_4 present is in the α phase. The presence of Si_3N_4 is strongest at 1300 °C and 1400°C, which is expected. Carbon and oxygen bonds increase in intensity with increasing temperature as well, either bonded to each other or with some silicon. Overall FTIR suggests a composite ceramic of multiple ceramic phases in combination with carbon which is similar to a study done before on polymer-derived ceramic fibers [59].

Further analysis needs to be done to confirm the identity of the rest of the peaks as the literature read so far cannot confirm the peaks, however, the peaks are iterations of Si, C, N, O bonds with some harmonics throughout. For that reason, the use of XRD, XPS, and Raman Spectroscopy is highly recommended to confirm the ceramic and carbon phases present in the samples.

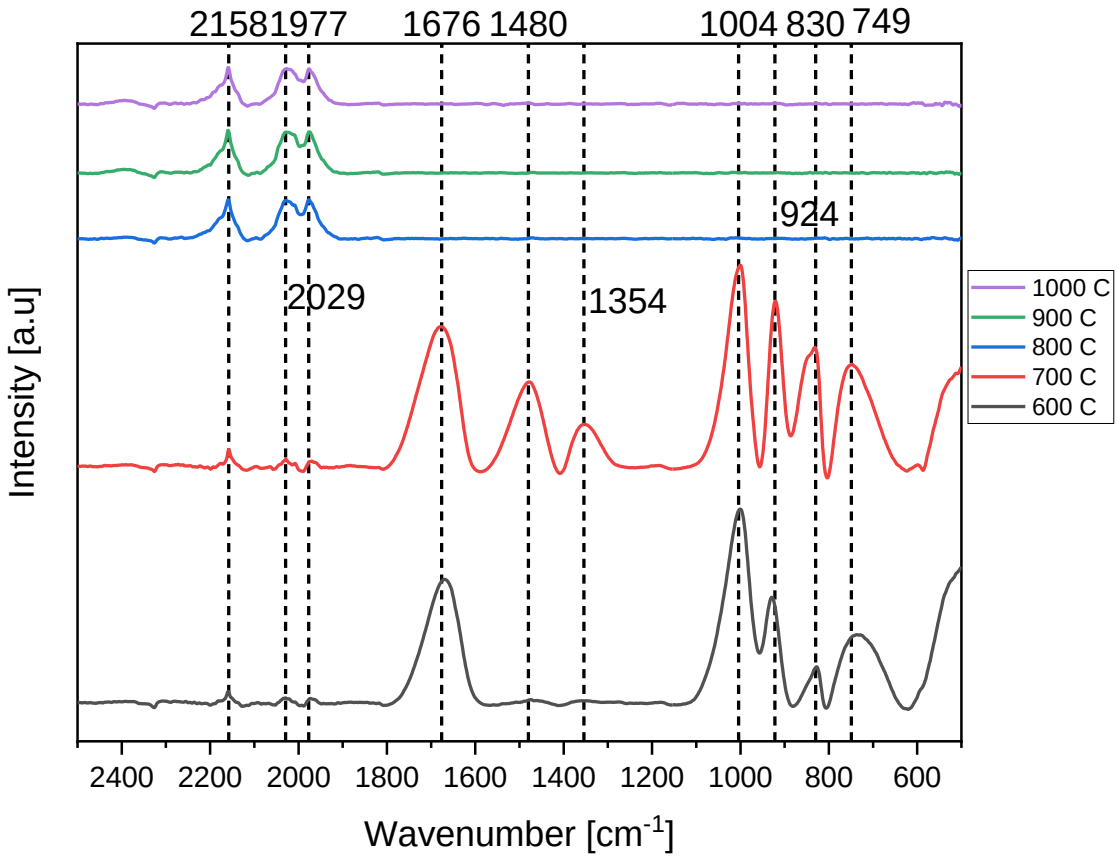

Figure 54: FTIR of Heat Treated AMT Fibers – 120 min Dwell Time

FTIR of AMT heat-treated fibers with 120 min dwell time are shown in figure 54. The FTIR of fibers dwelled at 60 minutes and 120 minutes were the same for all samples (see appendix). The peaks at 2158, 2029, and 1977 cm^{-1} grow significantly in intensity between 700 °C and 800 °C suggesting a transformation process between the temperatures. There is currently no literature on FTIR for W-C vibrations in nanofibers so W-C vibrations of either the cubic or hexagonal structure of WC were assigned to those three peaks. XRD needs to be used to confirm the assumption. C=O vibrations of the PVP carbonyl group is seen at 1676 cm^{-1} which disappears at 800 °C. The two peaks at 1480 and 1354 cm^{-1} are only intense at 700 °C, these peaks were assigned C=C stretching and N-O stretching respectively, indicating carbonization

and oxidation of PVP. The peak pairs at 1004 & 924 cm^{-1} and 830 & 739 cm^{-1} were assigned W=O, W-O vibrations respectively [53].

5.4 DMA of AMT Fiber Composites

Prior to DMA testing the composite samples the ground nanofibers were analyzed using SEM to check for impurities such as beads. Figure 55 shows a surface image taken at 250

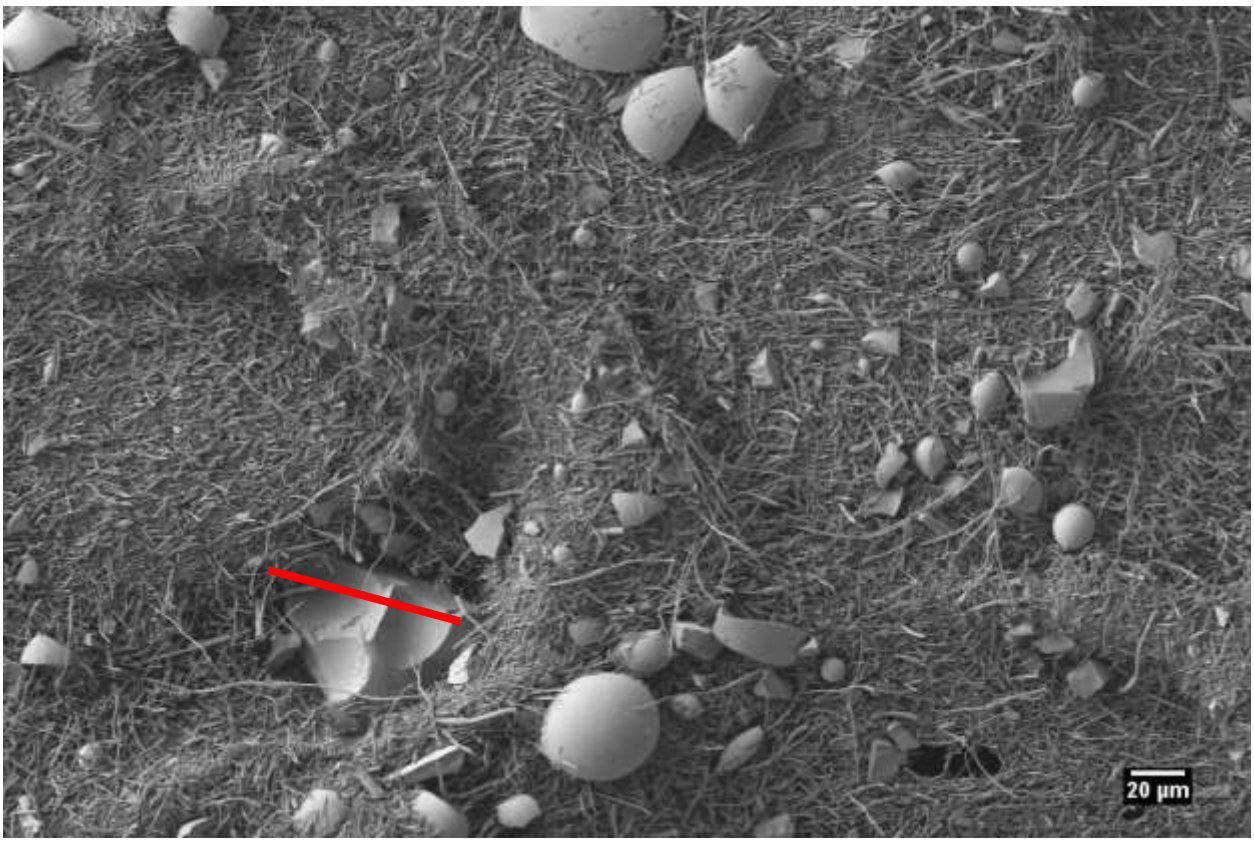

Figure 55: AMT Grinded Fibers 800°C 120 min Surface SEM

magnification of ground fibers. More beads are present compared to the SEM images seen in section 5.2, this is due to particle dynamics, meaning that during mixing larger particles will tend to settle at the surface. Particles as large as 70 µm are seen (marked by a red bar).

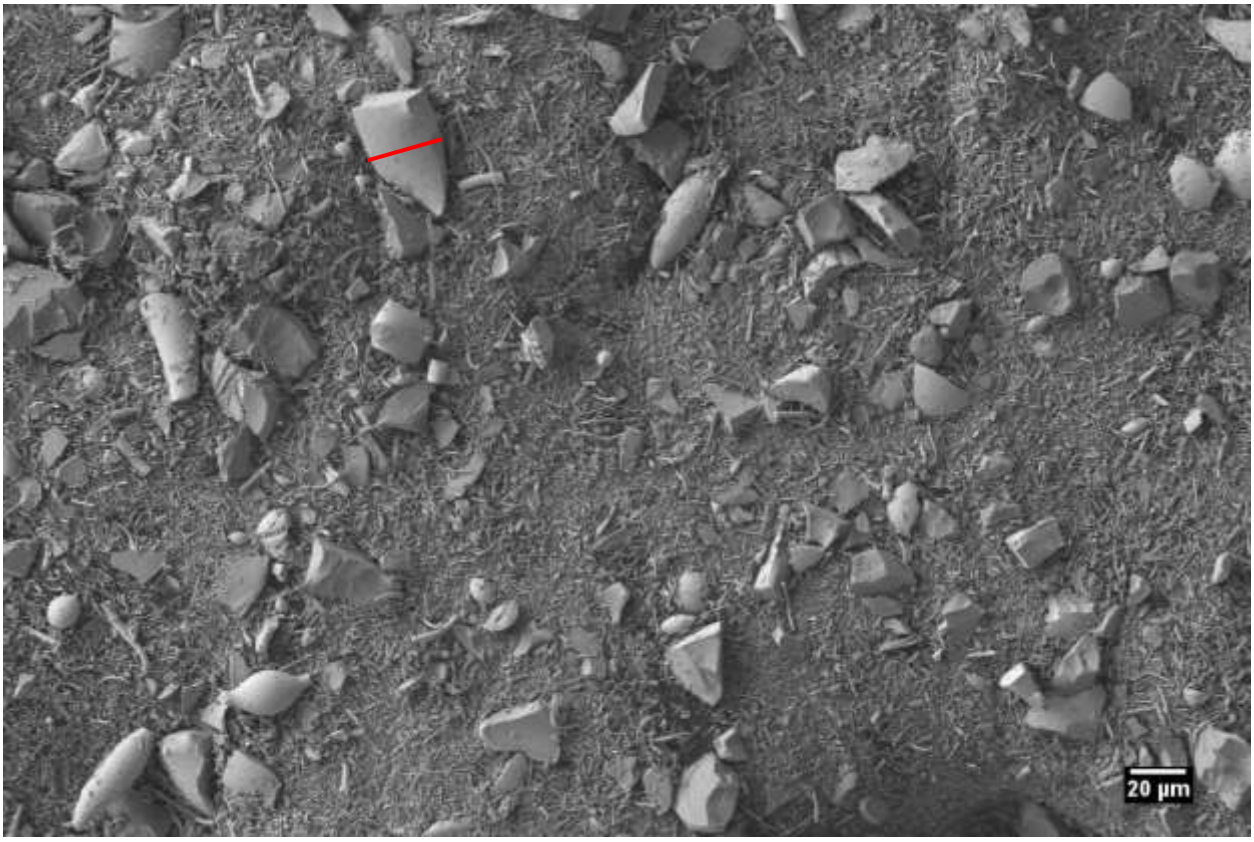

Figure 56: AMT Grinded Fibers 900°C 120 min Surface SEM

Figure 54 depicts the SEM image taken at 250 magnification of ground AMT fibers that were heat-treated at 900 °C for 120 minutes. Again, grinding the fibers brings all the large particles to the surface, the particle in this image was 27 µm in length (marked by a red line). EDS analysis was also conducted on the particles, which are ground beads, showing a similar composition to the beads seen in section 5.2. SEM images and EDS analysis were also conducted at 2000 magnification which shows the same results seen in section 5.2 but with more beads.

It is expected that the large particles well reduce the wettability of the composite by causing gaps between the nanofibers and the UHMWPE which will reduce the strength of the composite material [10]. Ideally, these beads would be sieved out using a -425 mesh sieve.

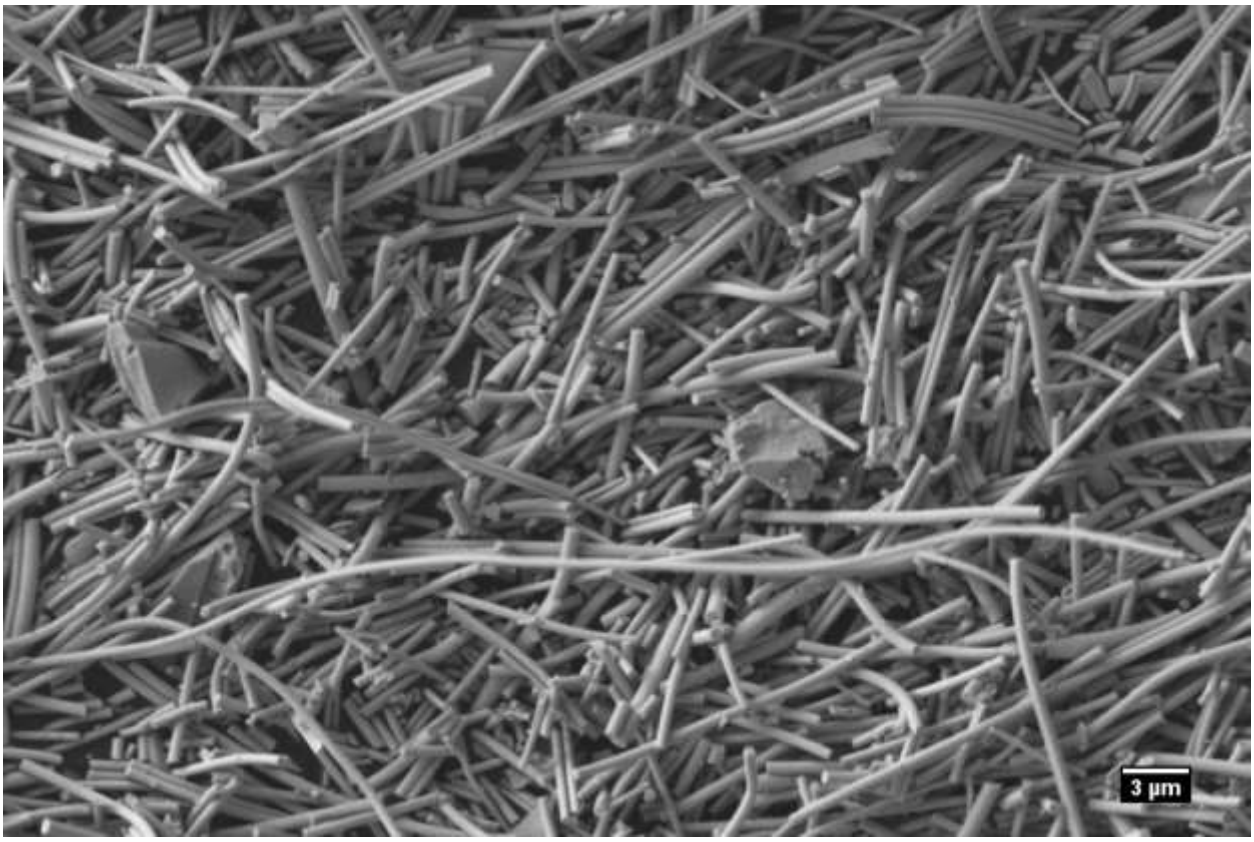

Figure 57: Ground 800 °C 120 min AMT Fibers

Figure 57 is an image of fibers that were ground using a motor and pestle for 30 minutes and then tumbled for 3 days (only fibers present). The diameter and composition of the fibers were the same as the unground fibers. However the length of the fibers decreases and ranges from 1 µm to 33 µm, suggesting poor processing.

Figure 58: Ground 900 °C 120 min AMT Fibers

Similar to figure 57, figure 58 is an image of fibers that were ground using a motor and pestle for 30 minutes and then tumbled for 3 days (only fibers present). The diameter and composition of the fibers were the same as the unground fibers. However, like figure 57, the length of the fibers decreases and ranges from 1 µm to 20 µm, suggesting poor processing.

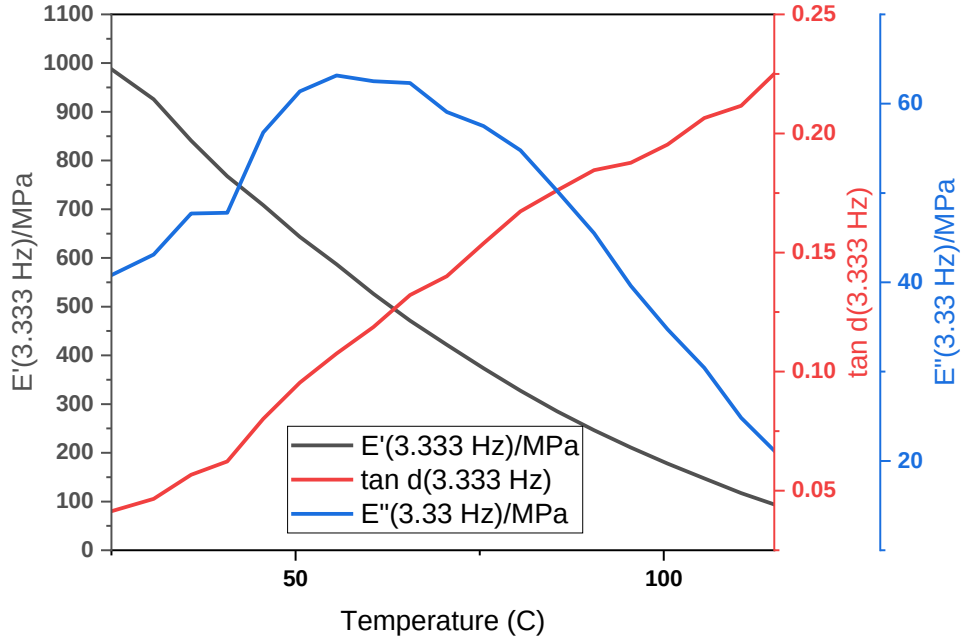

Figure 59: DMA Results of 7 wt % 800°C 120 min AMT Fibers

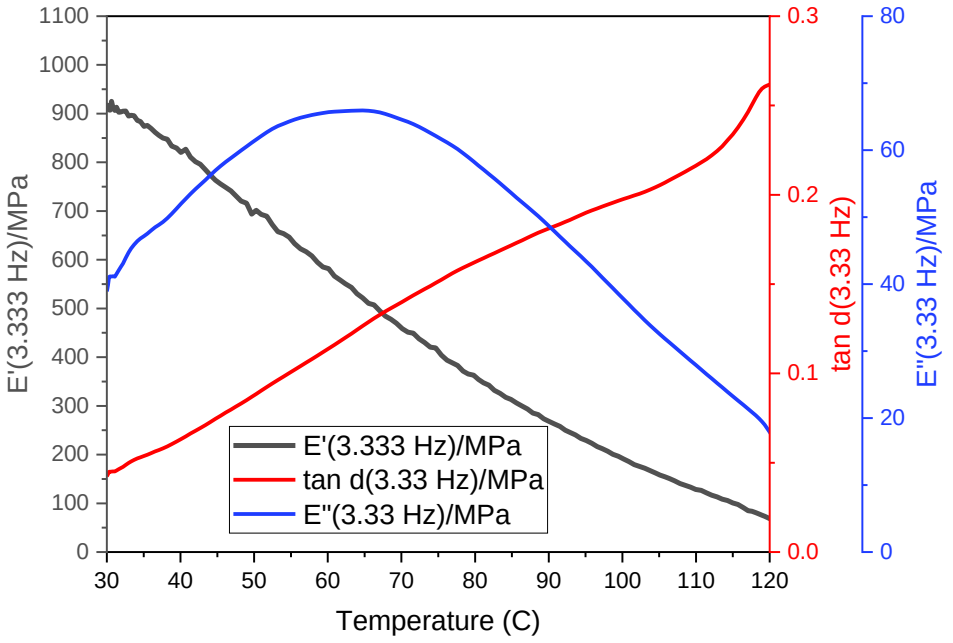

Figure 60: DMA Results of Control Sample

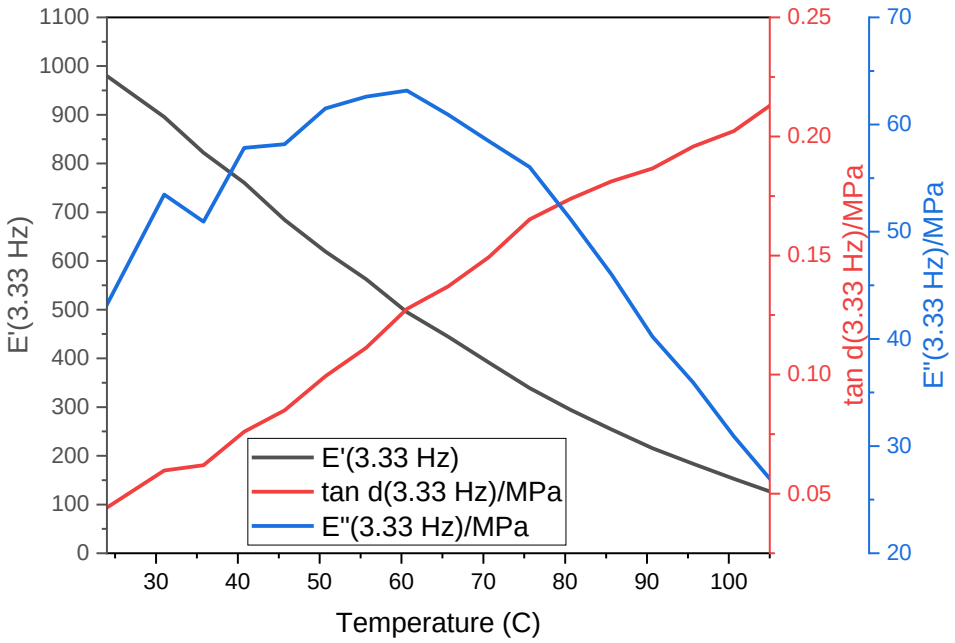

Figure 61: DMA results of 7 wt% 900°C 120 min AMT Fibers

Figures 59, 60 and 61 are the DMA results at 3.33 Hz of the control, 7 wt % composite of 800 °C fibers, and 7 wt% composite of 900 °C fibers. All samples exhibit the same viscoelastic behaviors, E' decreases with temperature while E" initially increases before reaching a peak and declining, resulting in a positive slope for tan (δ). The addition of fibers into the UHMWPE matrix slightly reduced the mechanical properties in the 900 °C fiber sample while barely increasing them in the 800 °C sample. Suggesting poor wetting as the matrix is unable to transfer the load of the DMA test to the added fibers. To overcome this, additional samples with a higher weight percentage of fibers can be made. Also, the effect sieving the material through a sieve that will remove the micro particles should be investigated.

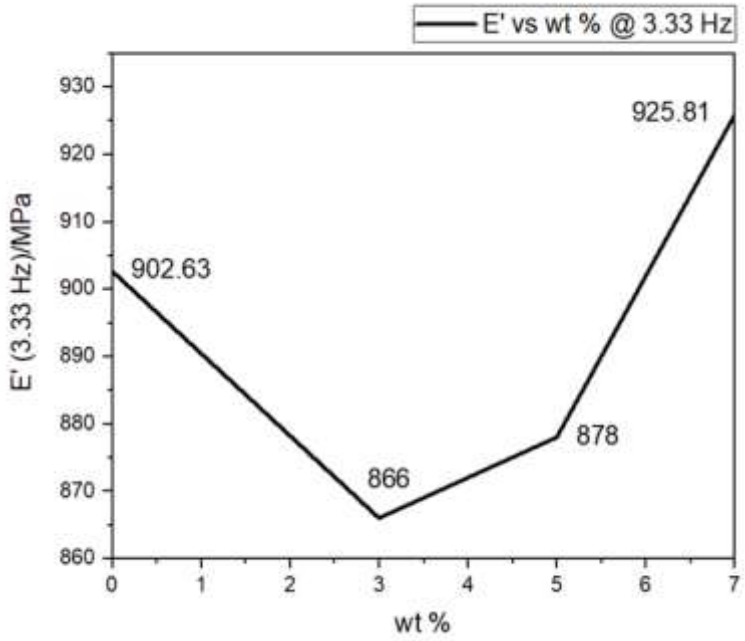

Figure 63: Effect of Fiber wt % for 800°C 120 min Fibers

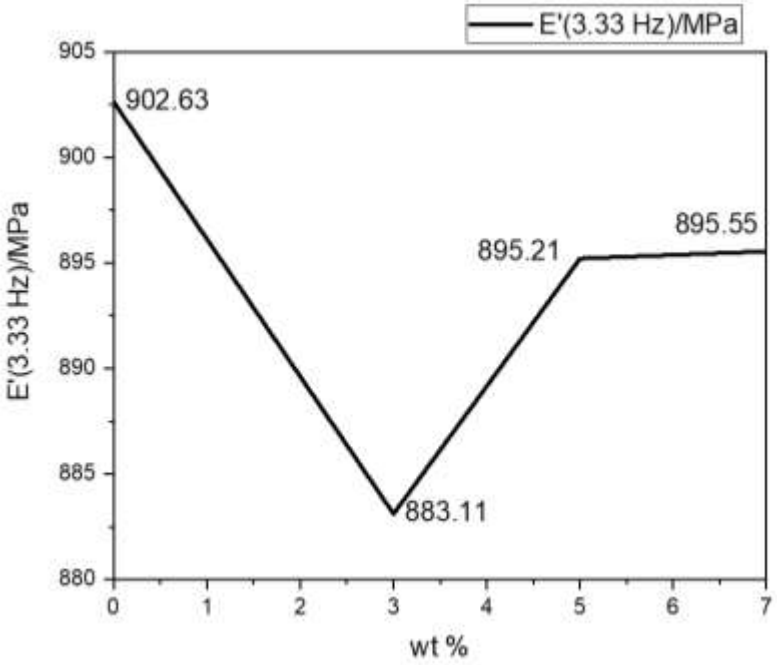

Figure 62: Effect of Fiber wt % 900°C 120 min Fibers

Figures 62 and 63 show the effect of the weight percentage of fibers in the DMA composite samples. The control, 0 wt%, performs better than both samples when they're composed of 3 and 5 wt% of AMT fibers. However, in Figure 62, the 800 °C sample shows an

increase in mechanical performance at 7 wt% fiber composition. The positive correlation between fiber wt% and an increase in composite performance (compared to composites with fibers) suggests that the addition of more fibers past 7wt % should increase the mechanical properties more. However, figure 63 shows no change between 5 wt% and 7 wt% of fibers. The tests need to be repeated to ensure that a mistake was not made during the measurement of components when developing the composite powders. To check the DMA results the sample data was compared to the work done in a similar setup using UHMWPE as well [21], the results yielded in this research were similar to the results mentioned in that paper - at 27 °C the storage modulus is 843 (3.33 Hz)/MPa compared to the 902.63 (3.33 Hz)/MPa at 30 °C in this study. Thus it can be concluded that the DMA tests were performed correctly and that the poor composite performance is due to another reason.

CHAPTER IV

CONCLUSION

This goal of this study was to develop silicon nitride, silicon carbide, and tungsten carbide polymer-derived ceramic nanofibers via Forcespinning©, understanding the mechanisms for polymer-ceramic conversion to set the groundwork for future ceramic fibers synthesized this way, and testing of the reinforcement properties of tungsten carbide fibers in a polymer matrix. Based on the experiments and data gathered during this research the resulting conclusions can be derived from this thesis.

The crosslinking mechanisms for a new preceramic fiber were derived using TGA in conjunction with TGA. Silicon carbide fibers with no oxygen presence and a near 1:1 silicon to carbon ratio were synthesized using Forcespinning© technology and the appropriate heat treatments using a new material for fiber development and cheap active material, polyphenymethylsiloxane. Heat-treated fibers derived from polyphenymethylsiloxane also exhibited signs of silicon nitride phase in FTIR analysis for fibers heat dwelled at 1300 °C and 1400 °C under a 20 mL/min flow rate.

Ammonium metatungstate hydrate fibers were transformed into tungsten carbide nanofibers at temperatures 800, 900, and 1000 °C as confirmed by EDS and FTIR. Fibers heat-

treated below 800 °C still had nitrogen content. The preceramic to ceramic transformation process for AMT fibers is completed within 60 minutes as shown by EDS and FTIR analysis.

Tungsten carbide fibers derived from AMT can be used as reinforcement fibers in a polymer matrix. UHMWPE and tungsten carbide composite material showed an increase in mechanical properties when a minimum of 7 wt % tungsten carbide fibers was added. A positive correlation between the weight percentage of fibers and mechanical strength suggests that additional fibers added to the matrix will increase mechanical properties further.

Further work will be to perform XRD analysis on the fibers to confirm the crystal phases. Adjusting the PPS solution to form higher silica content fibers and reduce the brittleness of the formed ceramic fibers to allow the fibers to be tested for EMI shielding properties. Sieving the tungsten carbide ground fibers and repeating the completed DMA tests while also performing additional DMA tests of samples with a higher weight percentage.

REFERENCES

1. Advanced Ceramics Market Size, Share & Trends Analysis Report By Material (Alumina, Titanate), By Product (Monolithic, Coatings), By Application, By End Use, By Region, And Segment Forecasts, 2019-2025. 2019: p. 168.

2. Abadikhah, H., et al., Morphological engineering of silicon nitride hollow fiber membrane for oil-field-produced-water treatment. Ceramics International, 2019. 45(8): p. 10541-10549.

3. Andrzejewski, J., et al., The influence of processing conditions on the mechanical properties and structure of poly(ethylene terephthalate) self-reinforced composites. Journal of Thermoplastic Composite Materials, 2016. 29(9): p. 1194-1209.

4. Barsoum, M.W., Fundamentals of Ceramics. Series in Material Science and Engineering. 2002: Taylor & Francis

5. Becher, P.F., et al., Microstructural design of silicon nitride with improved fracture toughness: I, Effects of grain shape and size. Journal of the American Ceramic Society, 1998. 81(11): p. 2821-2830.

6. Benítez, R., A. Fuentes, and K. Lozano, Effects of microwave assisted heating of carbon nanofiber reinforced high density polyethylene. Journal of Materials Processing Technology, 2007. 190(1-3): p. 324-331.

7. Bernardo, E., et al., Advanced Ceramics from Preceramic Polymers Modified at the Nano-Scale: A Review. Materials (Basel), 2014. 7(3): p. 1927-1956.

8. Boris Molthig, C.P., <Chapter 5 - Silicon Carbide Fibers Inorganic and Composite Fibers>. Elsevier, 2018: p. 87-103.

9. Cappi, B., et al., Cytocompatibility of high strength non-oxide ceramics. J Biomed Mater Res A, 2010. 93(1): p. 67-76.

10. Chang, H.W., et al., Wettability of Reinforcing Fibers, in Molecular Characterization of Composite Interfaces, H. Ishida and G. Kumar, Editors. 1985, Springer Berlin Heidelberg: Berlin, Heidelberg. p. 413-421.

11. Chaudhari, S. and M. Srinivasan, 1D hollow α-Fe2O3 electrospun nanofibers as high performance anode material for lithium ion batteries. Journal of Materials Chemistry, 2012. 22(43).

12. Colombo, P., et al., Polymer-Derived Ceramics: 40 Years of Research and Innovation in Advanced Ceramics. Journal of the American Ceramic Society, 2010: p. no-no.

13. Ekabutr, P., et al., Carbonized electrospun polyvinylpyrrolidone/metal hybrid nanofiber composites for electrochemical applications. Journal of Applied Polymer Science, 2018. 135(1).

14. Fan, J., et al., Electrochemical synthesis of nano-metallic carbides from the mixtures of metal oxide and graphite. Journal of the Electrochemical Society, 2017. 164(7): p. E144-E150.

15. Flores, D., et al., Production of carbon fibers through Forcespinning® for use as anode materials in sodium ion batteries. Materials Science and Engineering: B, 2018. 236-237: p. 70-75.

16. G Motz, R.K.B., Processing Structure and Properties of Ceramic Fibers, in Handbook of textile fibre structure. 2009. p. 378-424.

17. Gebru, K.A. and C. Das, Effects of solubility parameter differences among PEG, PVP and CA on the preparation of ultrafiltration membranes: Impacts of solvents and additives on morphology, permeability and fouling performances. Chinese Journal of Chemical Engineering, 2017. 25(7): p. 911-923.

18. Greil, P., Advanced Engineering Ceramics.pdf. Advanced Materials, 2002. 14(10): p. 8.

19. Gu, J., et al., Synthesis, densification, and microstructure of TaC-TaB2-SiC ceramics. Journal of the American Ceramic Society, 2018. 101(12): p. 5400-5410.

20. Guan, Z., et al., Novel zinc/tungsten carbide nanocomposite as bioabsorbable implant. Materials Letters, 2020. 263.

21. Guedes, R.M., Analysis of temperature and aging effects on biomedical ultra-high molecular weight polyethylene's grades using a viscoelastic model. Polymer Testing, 2011. 30(6): p. 641-650.

22. Guo, A., et al., Preceramic polymer-derived SiOC fibers by electrospinning. Journal of Applied Polymer Science, 2014. 131(3).

23. Hong, E., et al., Tribological properties of copper alloy-based composites reinforced with tungsten carbide particles. Wear, 2011. 270(9-10): p. 591-597.

24. Hosseinian, H., et al., Determining the effect of centrifugal and electrical forces on the jet behaviors, the nanofiber structure, and morphology. Polymers for Advanced Technologies, 2019. 30(4): p. 941-950.

25. Howlett, C.R., E. McCartney, and W. Ching, The effect of silicon nitride ceramic on rabbit skeletal cells and tissue. An in vitro and in vivo investigation. Clinical Orthopaedics and Related Research, 1989(244): p. 293-304.

26. Hu, H. and Y. Liu, 11 - High modulus, high tenacity yarns, in Technical Textile Yarns, R. Alagirusamy and A. Das, Editors. 2010, Woodhead Publishing. p. 329-386.

27. Ichikawa, H. and T. Ishikawa, 1.6 Silicon Carbide Fibers (Organometallic Pyrolysis), in Comprehensive Composite Materials II, P.W.R. Beaumont and C.H. Zweben, Editors. 2018, Elsevier: Oxford. p. 127-166.

28. J., B.E., Introduction to Composite Materials Design, Third Edition. 2018: CRC Press - Taylor & Francis. 1-150.

29. Jalaly, M., F.J. Gotor, and M.J. Sayagués, Mechanochemical combustion synthesis of vanadium carbide (VC), niobium carbide (NbC) and tantalum carbide (TaC) nanoparticles. International Journal of Refractory Metals and Hard Materials, 2019. 79: p. 177-184.

30. Kamimura, S., T. Seguchi, and K. Okamura, Development of silicon nitride fiber from Si-containing polymer by radiation curing and its application. Radiation Physics and Chemistry, 1999. 54(6): p. 575-581.

31. Katoh, Y. and L.L. Snead, Silicon carbide and its composites for nuclear applications – Historical overview. Journal of Nuclear Materials, 2019. 526: p. 151849.

32. Li, Q., et al., Facile and Scalable Synthesis of “Caterpillar-like” ZnO Nanostructures with Enhanced Photoelectrochemical Water-Splitting Effect. The Journal of Physical Chemistry C, 2014. 118(25): p. 13467-13475.

33. Maitra, S. and J. Roy, 3 - Nanoceramic matrix composites: Types, processing, and applications in Advances in Ceramic Matrix Composites (Second Edition)I.M. Low, Editor. 2018 Woodhead Publishingp. 27-48

34. Mali, S.S., et al., Synthesis of SnO2 nanofibers and nanobelts electron transporting layer for efficient perovskite solar cells. Nanoscale, 2018. 10(17): p. 8275-8284.

35. Medvecká, V., et al., Atmospheric pressure plasma assisted calcination by the preparation of TiO 2 fibers in submicron scale. Applied Surface Science, 2018. 428: p. 609-615.

36. Miele†, P., et al., Recent Developments in Polymer-Derived Ceramic Fibers (PDCFs): Preparation, Properties and Applications – A Review. Soft Materials, 2007. 4(2-4): p. 249-286.

37. Mishra, A.K., Sol-gel based nanoceramic materials: Preparation, properties and applications 2016 1-297

38. Mistry, J.M. and P.P. Gohil, Experimental investigations on wear and friction behaviour of Si3N4p reinforced heat-treated aluminium matrix composites produced using electromagnetic stir casting process. Composites Part B: Engineering, 2019. 161: p. 190-204.

39. Nasouri, K., A.M. Shoushtari, and M.R.M. Mojtahedi, Effects of polymer/solvent systems on electrospun polyvinylpyrrolidone nanofiber morphology and diameter. Polymer Science Series A, 2015. 57(6): p. 747-755.

40. Nasouri, K., A.M. Shoushtari, and M.R.M. Mojtahedi, Thermodynamic Studies on Polyvinylpyrrolidone Solution Systems Used for Fabrication of Electrospun Nanostructures: Effects of the Solvent. Advances in Polymer Technology, 2015. 34(3): p. n/a-n/a.

41. Obregon, N., et al., Effect of Polymer Concentration, Rotational Speed, and Solvent Mixture on Fiber Formation Using Forcespinning®. Fibers, 2016. 4(4).

42. Ohji, T.S., Mrityunjay, Engineered ceramics current status and future prospects. 2015: Wiley.

43. Peng, Z., et al., Growth and Mechanism of Network-Like Branched Si3N4 Nanostructures. Journal of the American Ceramic Society, 2010. 93(8): p. 2264-2267.

44. Phiri, R.R., O.P. Oladijo, and E.T. Akinlabi, Tungsten carbide thin films Review: Effect of deposition parameters on film microstructure and properties. Procedia Manufacturing, 2019. 35: p. 522-528.

45. Qiao, W.M., et al., Synthesis of crystalline SiC nanofiber through the pyrolysis of polycarbomethylsilane coated platelet carbon nanofiber. Applied Surface Science, 2007. 253(10): p. 4467-4471.

46. Rahaman, M. and W. Xiao, Silicon nitride bioceramics in healthcare. International Journal of Applied Ceramic Technology, 2018. 15(4): p. 861-872.

47. Šajgalik, P., J. Dusza, and M.J. Hoffmann, Relationship between Microstructure, Toughening Mechanisms, and Fracture Toughness of Reinforced Silicon Nitride Ceramics. Journal of the American Ceramic Society, 1995. 78(10): p. 2619-2624.

48. Salinas, A., M. Lizcano, and K. Lozano, Synthesis of β-SiC Fine Fibers by the Forcespinning Method with Microwave Irradiation. Journal of Ceramics, 2015. 2015: p. 1-5.

49. Sani, E., et al., Compositional dependence of optical properties of zirconium, hafnium and tantalum carbides for solar absorber applications. Solar Energy, 2016. 131: p. 199-207.

50. Santibenchakul, S., S. Chaiyasith, and W. Pecharapa, Effect of PVP concentration on microstructure and physical properties of electrospun SnO2nanofibers. Integrated Ferroelectrics, 2016. 175(1): p. 130-137.

51. Sarkar, K., et al., Electrospinning to Forcespinning™. Materials Today, 2010. 13(11): p. 12-14.

52. Selvarajan, L., et al., Investigation on spark electrical discharge machining of Si3N4 based advanced conductive ceramic composites. Materials Today: Proceedings, 2019.

53. Sharma, N., et al., FTIR and absorption edge studies on tungsten oxide based precursor materials synthesized by sol–gel technique. Journal of Non-Crystalline Solids, 2002. 306(2): p. 129-137.

54. Shrivastava, A., 3 - Plastic Properties and Testing, in Introduction to Plastics Engineering, A. Shrivastava, Editor. 2018, William Andrew Publishing. p. 49-110.

55. Tam, T. and A. Bhatnagar, 1 - High-performance ballistic fibers and tapes, in Lightweight Ballistic Composites (Second Edition), A. Bhatnagar, Editor. 2016, Woodhead Publishing. p. 1-39.

56. Tan, T.L., et al., High-Throughput Survey of Ordering Configurations in MXene Alloys Across Compositions and Temperatures. ACS Nano, 2017. 11(5): p. 4407-4418.

57. Ul-Hamid, A., Components of the SEM, in A Beginners' Guide to Scanning Electron Microscopy, A. Ul-Hamid, Editor. 2018, Springer International Publishing: Cham. p. 15-76.

58. W.R. Matizamhuka, W.R., Advanced ceramics - the new frontier in modern-day technology: Part I. Journal of the Southern African Institute of Mining and Metallurgy, 2018. 118(7).

59. Wang, P., et al., Flexible SiC/Si3N4 Composite Nanofibers with in Situ Embedded Graphite for Highly Efficient Electromagnetic Wave Absorption. ACS Appl Mater Interfaces, 2017. 9(34): p. 28844-28858.

60. Wang, Y. and S. Lim, Tribological behavior of nanostructured WC particles/polymer coatings. Wear, 2007. 262(9-10): p. 1097-1101.

61. Yang, X., et al., High-temperature properties and interface evolution of silicon nitride fiber reinforced silica matrix wave-transparent composite materials. Journal of the European Ceramic Society, 2019. 39(2-3): p. 240-248.

62. Zhang, J.-W., et al., Preparation and characterization of silicon nitride hollow fiber membranes for seawater desalination. Journal of Membrane Science, 2014. 450: p. 197-206.

63. Zhang, Z., et al., Tribology characteristics of ex-situ and in-situ tungsten carbide particles reinforced iron matrix composites produced by spark plasma sintering. Journal of Alloys and Compounds, 2017. 704: p. 260-268.

64. Zhou, W., et al., SiC nanofibers modified Si 3 N 4 ceramics for improved electromagnetic interference shielding in X-band. Ceramics International, 2018. 44(2): p. 2249-2254.

65. Zhou, X., et al., Tungsten carbide nanofibers prepared by electrospinning with high electrocatalytic activity for oxygen reduction. International Journal of Hydrogen Energy, 2011. 36(13): p. 7398-7404.

APPENDIX A

APPENDIX A

TUNGSTEN CARBIDE FIBER DISTRIBUTIONS

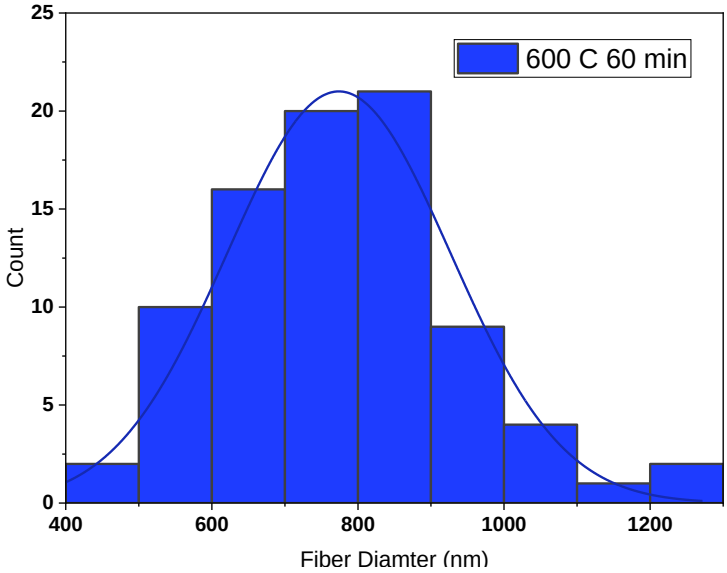

Figure 64: 600 °C 60 min AMT Fiber Distribution

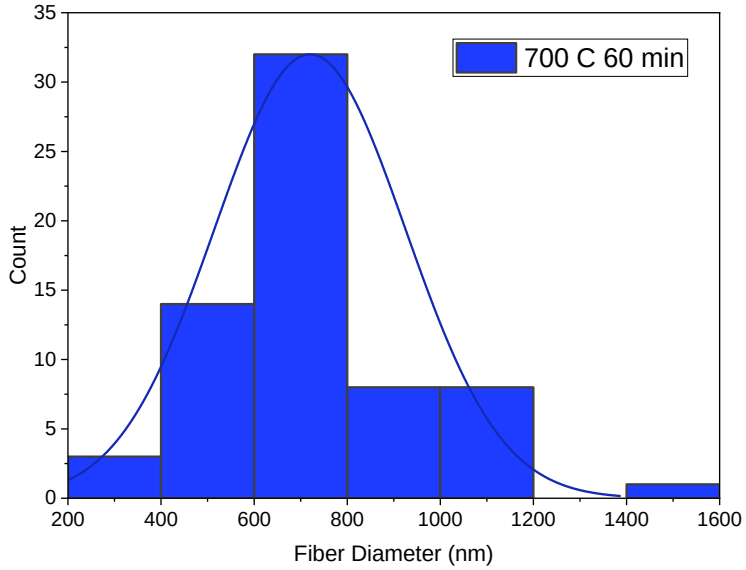

Figure 65: 700° C 60 min AMT Fiber Distribution

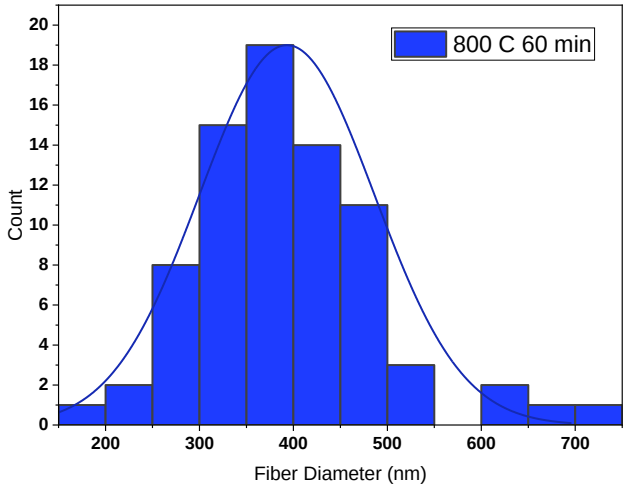

Figure 66: 800° C 60 min AMT Fiber Distribution

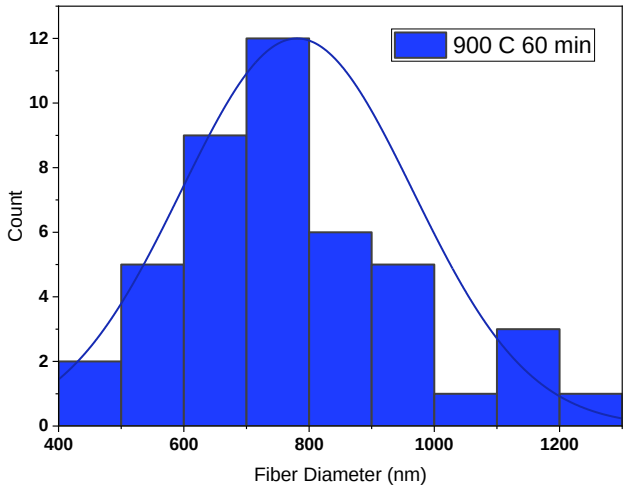

Figure 67: 900° C 60 min AMT Fiber Distribution

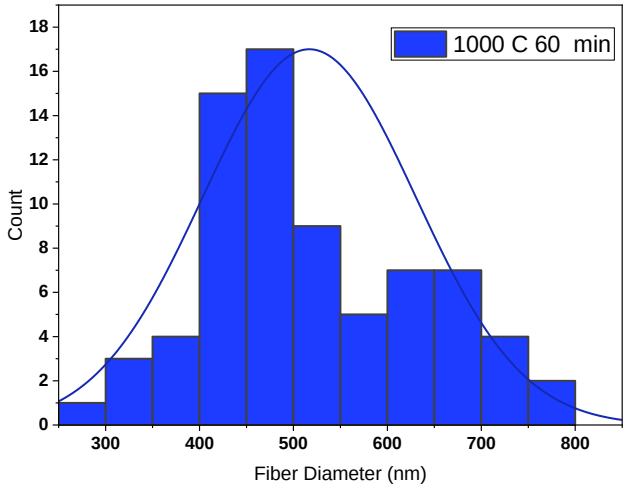

Figure 68: 1000° C 60 min AMT Fiber Distribution

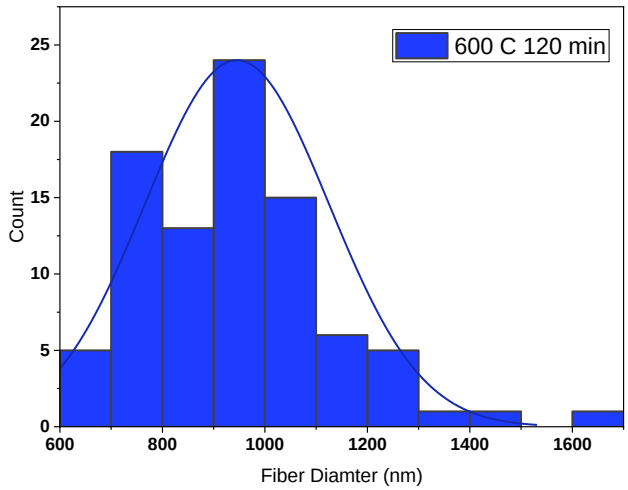

Figure 69: 600° C 120 min AMT Fiber Distribution

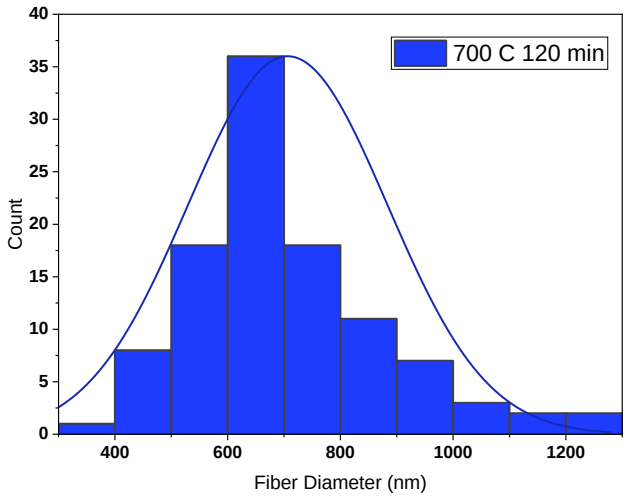

Figure 70: 700° C 120 min AMT Fiber Distribution

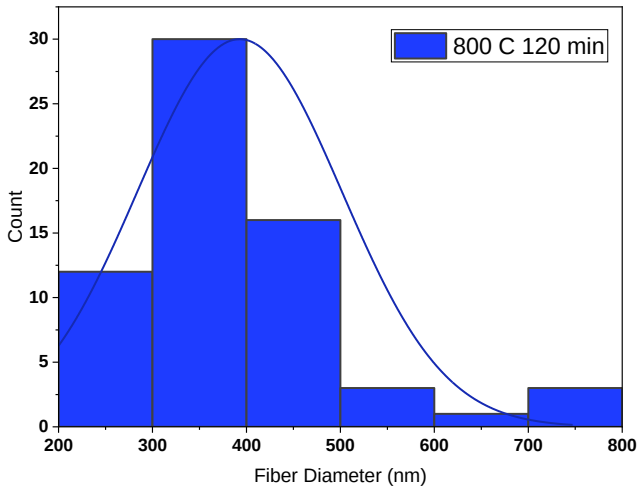

Figure 71: 800° C 120 min AMT Fiber Distribution

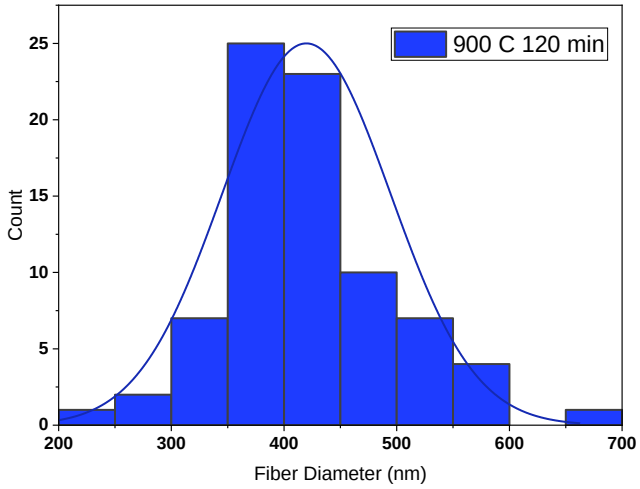

Figure 72: 900° C 120 min AMT Fiber Distribution

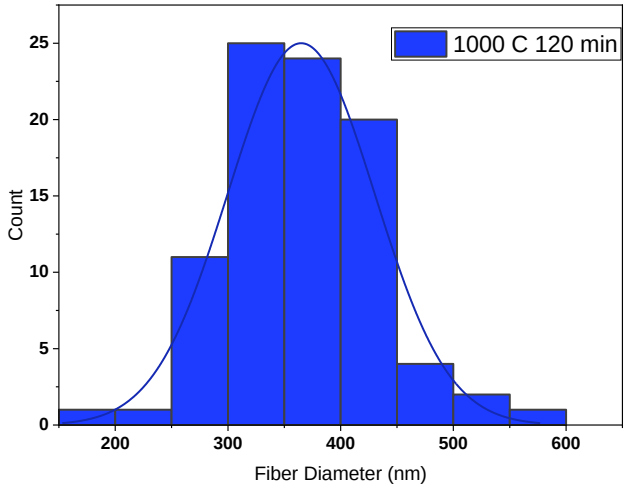

Figure 73: 1000° C 120 min AMT Fiber Distribution

APPENDIX B

APPENDIX B

STATE OF THE ART EQUIPMENT AND SOFTWARE

Table 7: State-of-the-Art Equipment

Equipment	Purpose	Results Obtained
SEM – Zeiss Sigma |VP SEM	Microscope to measure fiber diameter	SiC and WC fibers were visualized and images are included in Chapter 5 of the thesis.
EDS – EDAX Octane Super	SEM attachment used to identify elemental composition of fibers	The composition of SiC and WC fibers were identified and results are presented in chapter 5 of the thesis.
TGA – TG 209 F3 Tarsus	Material characterization equipment used to perform thermal analysis on fibers	Thermal analysis was performed on SiC and WC fibers and results are presented in chapter 5 of the thesis.
FTIR – Bruker Invenio	Material characterization technique used to identify the bonds present in a material.	SiC and WC fibers were analyzed using FTIR and results are included in Chapter 5 of the thesis.
DMA – DMA 242 E Artemis	DMA is a material characterization technique that provides information on the viscoelastic mechanical properties of a material.	UHMWPE/WC composite samples were analyzed using the DMA under a tensile configuration. DMA results are presented in chapter 5 of the thesis.
Forcespinning®	Equipment that uses centrifugal force to form fibers.	PVP/PPS and PVP/AMT green fibers were formed. The fibers were then heat treated and analyzed using the equipment above, results are in chapter 5 of the thesis.

Table 8: State-of-the-Art Software

Equipment	Purpose	Results Obtained
Excel	Excel was used to store and organize characterization data before processing into origin.	Data was organized then further processed in ORIGIN for all characterization techniques whose results are shown in chapter 5 of the thesis.
OPUS	Convert FTIR signals into raw .dpt data files.	FTIR data was further processed in ORIGIN and results for SiC and WC fibers are shown in chapter 5 of the thesis.
ORIGIN 2020	Analyze data from characterization and form useful figures ranging from standard line plots to statistical box plots.	All data was processed using ORIGIN where various techniques were applied, including peak analysis, distribution plots, box plots, Gaussian smoothing, baseline adjustment, etc. All figures shown in chapter 5 of the thesis (excluding SEM images) are from ORIGIN.

BIOGRAPHICAL SKETCH

Christian Garcia was born in McAllen Texas and has lived in the Rio Grande Valley his entire life where he attended the University of Texas Rio Grande Valley as an undergraduate student to pursue a Bachelor of Science in Mechanical Engineering, completed May 2018. During his undergraduate years, Christian worked as a student mentor and participated in student orgs such as Material Advantage and SHPE. Christian served as president of Material Advantage during his senior undergraduate year. Christian was also a Mickey Leland Fellow and conducted research on the creep life of superalloys under his work with the National Energy Technology Laboratory, together he co-authored 3 papers there.

After entering graduate school Christian began working as a research assistant and continued to participate in student orgs. He received his Masters of Science in Mechanical Engineering in May 2020. In July 2020 Christian began work as a hardware engineer with Northrop Grumman. Should the reader wish to contact Christian they may me use the following information: email: christiang7777@gmail.com